POLITECNICO DI TORINO

Facoltà di Ingegneria
Corso di Dottorato in Ingegneria Elettronica e delle Comunicazioni

Tesi di Dottorato

Wavelet based design of digital multichannel communications systems

Tutore:
Prof. Letizia Lo Presti

Coordinatore:
Prof. Ivo Montrosset

Fabio Dovis

XII Ciclo

Summary

The huge penetration of the personal communications systems in the market is constantly presenting new challenges to the research, aimed at satisfying people's needs and requirements for effective communication systems. At present, the cellular telephone network is perhaps the most evident example of communication system that has had a great impact on the lives of ordinary people and, at the same time, is the subject of interest of many researchers both at academic and industrial level. For the future, one of the main challenges in telecommunications will be the provision of ubiquitous broadband tetherless integrated services to mobile users. Such a pretentious goal cannot be achieved without a continuous research facing such problems as service quality, complete mobility support, and affordable complexity that are still open problems.

However, present telecommunication problems are not only a matter of implementation or development of new services, exploiting a totally assessed doctrine. In order to respond to the mobility of the users personal communication systems have to deal with the wireless communication channel whereby mobility and non-stationarity of the propagation conditions require a stochastic description of the channel parameters. While this fact can be viewed as strong limitation to the development of a solid theory whose validity can be assesed in practice, on the other hand allows for an investigation and study of novel communication schemes, sometimes encompassing basic aspects of digital communications.

This thesis, is the result of a research work that has investigated one of the basic building block of every communication systems, the modulation scheme, and the design of the pulse shape carrying the digital information. We have studied the design of multichannel communication scheme exploiting the mathematical theory of wavelets. Such a theory, developed recently, has had a great impact in many fields of engineering and of other scientific disciplines. In particular, wavelet theory has become very popular in the signal processing area; in fact it is a flexible toolbox for signal analysis allowing effective representation of signals for features extraction purposes.

The main features that make wavelet waveforms suitable to be used as shaping pulses for modulation are their substantial compact support both in the time and frequency domains, and the fact that they are ISI-free pulses over frequency flat channels. The study presented in this thesis is focused on application of wavelet theory to design high-efficiency multichannel communication schemes and to the performance evaluation over linear and non-linear channels. We present a general method to design wavelet based multichannel communication schemes that we denoted *Wavelet Orthogonal Frequency Division Multiplexing (WOFDM)*. We show that such schemes, having a larger spectral efficiency for a small number of channels, are a valid alternative to the classical OFDM. Potential advantage of wavelet modulation are shown presenting other applications examined in this thesis: a joint use of WOFDM and Trellis Coded Modulation to shape the power spectrum in order to match a frequency selective channel and minimize distortion, and application to spread spectrum modulation.

Particular attention has been devoted to the timing recovery problem in multichannel communication schemes, exploiting the timing information of the different subchannels to improve the error variance in estimation of the sampling instant leading to a reduction of the adjacent channels interference.

Contents

List of Tables

List of Figures

Chapter 1

Wavelets theory

1.1   Introduction

Among all the disciplines of the engineering science, telecommunications has had a great impulse in the past few years, leading to a phenomenon sometimes called the "telecommunication revolution", because of the great impact it has had in the ordinary lives of common people. In fact, everyday life has been deeply changed by the diffusion of personal communication systems, modifying people's habits, and creating a need for "communications". Theoretical results achieved many years ago are being implemented exploiting a mature electronic technology that allows for the realization of personal communications systems capable of giving voice, video and multimedia connections between users. At the same time these devices are becoming always more user friendly, lighter, more cost-effective, less power consuming, and smaller.

The huge penetration of the developed systems in the market is constantly presenting new challenges in the research front, to satisfy people's needs and requirements for effective communication systems. At present, cellular telephone networks are among the most evident examples used by many people everyday and that is the subject of interest of many researchers both at academic and industrial level. For the future, one of the main challenges in telecommunications will be the provision of ubiquitous broadband tetherless integrated services to mobile users. Such a pretentious goal cannot be achieved without continuous research facing such problems as service quality, complete mobility support, affordable complexity, and other open problems.

However, present telecommunication problems are not only a matter of implementation or development of new services, exploiting a totally assessed

doctrine. In order to respond to the mobility of the users, Personal communication systems, have to deal with the wireless communication channel whereby the mobility and non-stationarity of the propagation conditions require a stochastic description of the channel parameters. The stochastic nature of the channel makes it difficult to find an optimal definition of all the parameters defining a telecommunication system both at the transmitter and the receiver side. While this fact can be viewed as strong limitation to the development of a solid theory, on the other hand allow for an investigation and study of novel communication schemes, sometimes encompassing basic aspects of digital communications.

This thesis, is the result of a research work that has investigated one of the basic building blocks of every communication systems, the modulation scheme, and the design of the pulse shape carrying the digital information. The pulse shape design for multichannel communication schemes has been studied. Multichannel modulation has gained interest because it is robust to non-linear channel distortions and is suitable for transmission of pieces of information with different signalling rates, a feature that is extremely important in modern communications systems where voice, video, and data have to share the same mo-demodulator system.

In particular we have tried to tie together one of the most significant mathematical theories of the recent times, at least for the impact that it had on the engineering science, with the design of digital communication systems. Such a theory is known as the theory of *wavelets*, (because it involves short oscillating waveforms), and it is a complete framework with both digital and continuous aspects that are particularly suitable to be applied to classical telecommunications problems. The study presented in this thesis has always had the perspective of the possible application to modern personal communication systems, so that the effectiveness of the results has always involved typical propagation scenarios, interesting for the applications. Theoretical and simulation results have been obtained, for the largest part, on satellite non-linear channel or for the wireless fading channel.

1.2   Structure of the thesis

Wavelet theory is complex and sometime cumbersome, so it is not possible to provide an exhaustive presentation of all the theoretical results and properties within this thesis; the remainder of the chapter deals with some theoretical basic aspects limiting the presentation to the results that will be used in the following chapters and that have a direct application to the telecommunication system design. Chapter 2 will explain how such a theory is useful and

can be exploited in the telecommunications field. Some results useful in the following chapters are presented. In particular, a technique suitable to the design of high efficiency wavelet based communications schemes, is presented along with a novel wavelet waveform for communications. Chapter 3 is essentially based on performance evaluation of wavelet waveforms over linear and non-linear channels, presenting theoretical and simulation results. Two different applications of wavelet based design of multichannel systems for power spectrum shaping and spread spectrum communications are presented in chapter 4. Finally, chapter 5 deals with the timing signal recovery in wavelet based multichannnel systems.

1.3   Wavelet theory

The theory of wavelets stands at the intersection of the frontiers of mathematics, scientific computing, and signal processing. Its goal is to provide a coherent set of concepts, methods and algorithms that are suitable to many applications in different scientific fields. Due to this fact, the mathematical theory is very rich and sometimes cumbersome because of the many aspects involved. Moreover, being developed in different scientific fields, different approaches to the theoretical description are possible. Meyer in [32] enumerates at least seven sources of the wavelet theory, some of them developed back in the years around 1930 and that only few years ago have been collected together with new results under a common scientific perspective to generate the wavelet theory as we know it nowadays.

It is alien to the objective of these thesis to provide a complete explanation of the overall wavelet theory, but in this chapter we will recall only the basics of the wavelet transform, of the orthonormal wavelets theory and the properties that will be useful for the devised application of wavelets to digital modulation. Moreover we will essentially follow a "signal processing approach" connecting the wavelets to the digital filter theory of multiresolution analysis.

Many books and articles cover the subject of wavelets in depth [25, 27, 29], and we refer the interested reader to such references for the details of the material presented here.

1.4 The wavelet transform

The easiest way to introduce wavelets is as kernels of a signal transform defined as

$$CWT_f(a,b) = \frac{1}{\sqrt{a}} \int_{\mathcal{R}} \psi^* \left(\frac{t-b}{a} \right) f(t)dt, \qquad (1.1)$$

where $a \in \mathcal{R}^+$ and $b \in \mathcal{R}$. Moreover the function ψ must satisfy the admissibility condition:

$$\int_{-\infty}^{+\infty} \psi(t)dt = 0. \qquad (1.2)$$

The transform (1.1) measures the similarity between the function $f(t)$ and shifts and scaled versions of an elementary function,

$$\psi_{a,b}(t) = \frac{1}{\sqrt{a}} = \psi \left(\frac{t-b}{a} \right)$$

denoted as wavelet function. The set of functions obtained considering all the possible values of the parameters a and b is an overcomplete basis. The features of the representation of signals onto such a redundant basis are exploited for signal processing purposes Time-scale representation has become very popular for the analysis of nonstationary signals or for signal with self-similarity properties. Further details on the CWT can be found in [29].

Special choices for $\psi(t)$ and the discretization of the parameters

$$a = a_0^j, \quad b = k a_0^j b_0$$

lead to a reduction of the redundancy of the set of basis functions. In particular, choosing

$$a = 2, \quad b = 1$$

the orthonormal bases or wavelet series can be obtained, as Daubechies demonstrated in [33]; such a choice for the parameters yields to a *dyadic* set of orthonormal functions. In the following section we will focus primarily on these sets of orthonormal functions.

1.5 Orthonormal wavelets and Multiresolution Analysis

In a dyadic [25] multiresolution analysis, the scaling function $\psi(t)$ satisfies the *scaling equation*

$$\phi(t) = 2^{1/2} \sum_{n \in \mathcal{Z}} h[n]\phi(2t-n), \qquad (1.3)$$

where $\mathcal{Z}$ is the set of integers. Similarly, the wavelet can be expressed as

$$\psi(t) = 2^{1/2} \sum_{n \in \mathcal{Z}} g[n]\phi(2t - n). \qquad (1.4)$$

The sequence $h[n]$ is called the *scaling vector*, while the sequence $g[n]$ is denoted as the *wavelet vector*. The scaling function and wavelet are shift-orthogonal and span orthogonal subspaces of the $L^2(\mathcal{R})$ space.

A ladder of subspaces of $L^2(\mathcal{R})$ can be constructed using the dilated versions of the scaling function and wavelet as shift-orthogonal basis. In particular, the subspace V_i is spanned by

$$\{2^{i/2}\phi(2^i t - n) \ \ \forall n \in \mathcal{Z}\},$$

while the orthogonal complement of V_i in V_{i+1}, the subspace W_i, is spanned by

$$\{2^{i/2}\psi(2^i t - n) \ \ \forall n \in \mathcal{Z}\}.$$

From the orthogonality properties of the subspaces spanned by the scaling function and wavelet, the scaling and wavelet vectors must be individually shift-orthogonal and orthogonal to each other, with period two:

$$\sum_{n \in \mathcal{Z}} h[2m + n]h[2l + n] = \delta_{m,l},$$

$$\sum_{n \in \mathcal{Z}} g[2m + n]g[2l + n] = \delta_{m,l},$$

$$\sum_{n \in \mathcal{Z}} h[2m + n]g[2l + n] = 0 \ \ \forall \ m,l,$$

where δ is the Kronecker delta function. If we denote the Z-transforms of the sequences $h[n]$ and $g[n]$ by $H(z)$ and $G(z)$, respectively, and we add two additional normalization conditions $\sum_n h[n] = \sqrt{2}$, and $\sum_n g[n] = 0$, the orthogonality and normalization conditions require that the filters $H(z)$ and $G(z)$ be a Quadrature Mirror Filter (QMF) pair [28], and that they be power complementary. If these filters are paraunitary (or lossless) [28], all the desired conditions are met.

It is interesting to observe the subspaces spanned by scaling functions and wavelets in the Fourier transformed domain. In the frequency domain the space spanned by the scaling function is a lowpass channel,while the space spanned by the wavelet is a bandpass channel. In what follows we shall use the terms subspace and frequency channel interchangeably.

Consider the subspace V_i defined above. In the dyadic decomposition case this channel is *split* into two subchannels V_{i-1} and W_{i-1} each having

roughly half the bandwidth of space V_i (in practice there is an overlap between the band of frequencies occupied by V_{i-1} and W_{i-1}). W_i can be also split into two subchannels. The sequences relating the basis in the new subspaces to the basis spanning the mother spaces are precisely the scaling and wavelet vectors. This splitting procedure can be iterated further. The use of the two-channel split provides a binary decomposition of the subspaces. An M-ary decomposition is possible using the multiplicity-M paraunitary filter bank impulse responses [28] as coefficient systems in the scaling equations. The set of scaling functions and wavelets generated are called M-band scaling functions and wavelets. Further decomposition yields M-band wavelet packets.

The general recursion formulas that may be used to generate the wavelet packets are [91]:

$$\mu_{2n}(t) = \sum_k h[k]\mu_n(2t - k), \ \ \mu_{2n+1}(t) = \sum_k g[k]\mu_n(2t - k),$$

where $n = 0,1,2,...$ and the basic scaling and wavelet functions are, respectively, $\phi(t) = \mu_0(t)$ and $\psi(t) = \mu_1(t)$. The following notation is used: $\Omega_n = clos_{L^2(\mathcal{R})}\{\mu_n(t - k)|k \in \mathcal{Z}\}$, $n = 0,1,2,...$ define the subspaces of $L^2(\mathcal{R})$ at resolution one ($clos_{L^2(\mathcal{R})}$ means closure in $L^2(\mathcal{R})$). Similarly, $\Delta^k\Omega_n = clos_{L^2(\mathcal{R})}\{2^{k/2}\mu_n(2^k t - l)|l \in \mathcal{Z}\}$ denote the subspaces at resolution 2^k. It can be shown that given the binary expansion of $n = \sum_{j=1}^{+\infty} \epsilon_j 2^{j-1}, \epsilon_j \in 0,1$, the Fourier transform of $\mu_n(t)$ is $M_n(f) = \prod_{k=1}^{+\infty} P_{\epsilon_k}(e^{j\omega/2^k})$, where $P_0(z) = 0.5 \sum_k h[k]z^{-k}$ and $P_1(z) = 0.5 \sum_k g[k]z^{-k}$ are the Z-transforms of the scaling and wavelet vectors.

The splitting of the subspace W_i, $\forall i \in \mathcal{Z}$ embedded in the multiresolution analysis can be seen as generation in the frequency domain of sets of orthogonal subchannels, as depicted in figure 1.1.
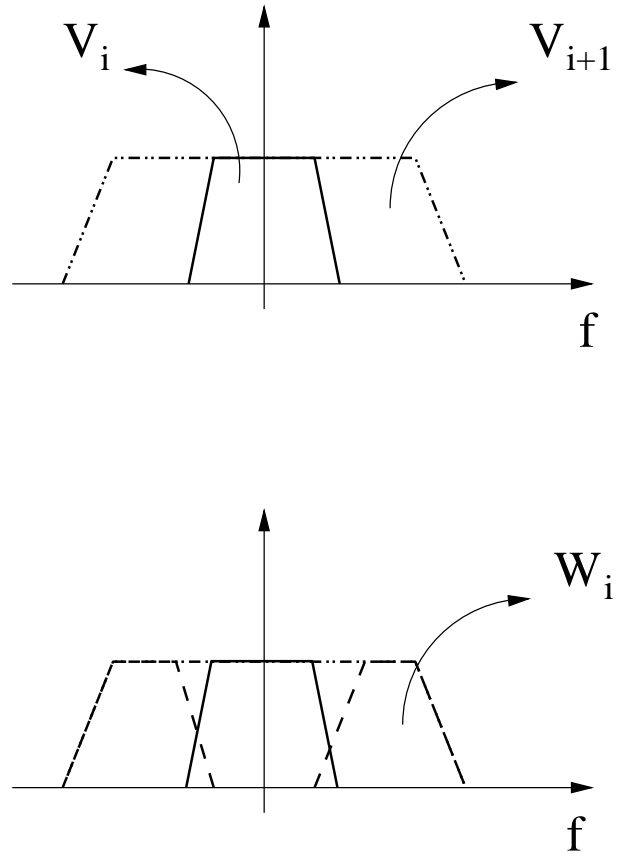
Figure 1.1. Representation in the Fourier transformed domain of the subspaces V_i and W_i of a multiresolution analysis

Chapter 2

Use of wavelet waveforms for modulation

2.1   Introduction

In this chapter, after a presentation of the state of the art concerning the use of wavelets for modulation purposes, a connection between wavelet theory and the principles of digital communications will be presented. Sections will be devoted to the introoduction of general techniques to generate wavelet based multichannel modulation schemes and to increase the number of signalling dimensions at the modulator. Finally a novel wavelet designed to be suitable for digital modulation applications will be discussed.

2.2   State of the Art

Perhaps the first evidence that wavelets could be used for modulation appeared in connection with the use of Transmultiplexers [45]. Indeed, the structure of a Transmultiplexer is that of a modulator-demodulator bank. Subsequently, Wornell and Oppenheim [46] proposed the use of self-similar signals for fractal modulation. Such signals are essentially non-smooth wavelets. Following this work, Tzannes and Tzannes [47] proposed the use of discrete wavelet sequences for channel coding. The use of wavelets for modulation and coding has appeared in several works. Looking at the different proposals we can distinguish some different classes of application of wavelet to digital modulation. The use of wavelet based waveforms as shaping pulses for multicarrier modulation was proposed because of the link between wavelet orthogonality properties and the first Nyquist criterion [1, 49, 48]. We mention in particular the works of Jones [50] and Lindsey [51, 52, 53, 54]; other

studies can be found in [80, 55, 57]. Cioffi and others discussed implementation of digital mo-demodulators through wavelet filterbanks in [100, 92]. As far as the design of wavelet based shaping pulses is concerned results can be found in [9, 56, 84].

Particular interest has been devoted to the application of wavelets to spread spectrum communications and CDMA systems [2, 51, 58, 59, 60, 83]. Common denominator of such works is the exploitation of the filterbank structure of the modulator to implement the spreading of the information signal over the available bandwidth. Performance results for transmission over wireless channels are presented in [61, 62]. Recently an application of wavelet waveforms to optical communications has also been proposed [63].

2.3 Connection to Nyquist I Criterion, WOFDM and Spectral Shaping

It is possible to link the orthonormal wavelets to the Nyquist I criterion for ISI removal [1]. In particular, let $Q(f)$,$C(f)$, and $U(f)$ denote the shaping pulse, the channel, and the receiver filter transfer functions respectively. Let us define $S(f) = Q(f)C(f)R(f)$. The Nyquist I criterion for ISI elimination requires that the overall system impulse response $s(t) = \mathcal{F}^{-1}[S(f)]$ sampled at integer multiples of the symbol period Δ be zero except at $t = m\Delta$ [22] (we are assuming that there is a delay of $m\Delta$ seconds). For a linear phase channel with a flat transfer function, the optimum receiver is a matched filter $R(f) = Q^*(f)e^{-j2\pi fm\Delta}$. Hence, in the frequency domain the Nyquist condition reduces to

$$\sum_{k=-\infty}^{\infty} |Q(f - k/\Delta)|^2 = \Delta. \tag{2.1}$$

In the digital domain with sampling interval Δ/M, the condition (2.1) can be expressed as

$$\sum_{k=0}^{M-1} |Q(e^{j2\pi(f-k/M)})|^2 = C_0 \tag{2.2}$$

for some integer M and constant C_0. If we interpret each term $Q(e^{j2\pi(f-k/M)})$ as a filter in a filter bank, we conclude that the discrete filter satisfying the ISI free condition is power complementary. The M-channel analysis filter banks whose polyphase component matrix are paraunitary [28], obey such a property. More precisely, if $H_k(z)$ denotes the k-th analysis filter in a

paraunitary filter bank, then

$$\sum_{k=0}^{M-1} |H_k(e^{j2\pi f})|^2 = C_0. \tag{2.3}$$

In such a case the synthesis filters can be written as $F_k(z) = C_1 z^{-L} \tilde{H}_k(z)$, where $\tilde{H}(z) = H^*(z^{-1})$ (i.e., the synthesis filter is a matched filter to the analysis filter). Note that the basic distinction between the ISI free condition (2.2) in the discrete case and that in the general filter bank case (2.3) is that in the former, the filter banks are obtained via modulation from a single prototype filter, while this is not necessarily the case in the latter.

The connection between the discrete filters and wavelets comes about because the discrete filter impulse response values can be used as coefficient systems in equations (1.5) and (1.5). Such wavelets are the spectral factors [28] of the system transfer functions satisfying the Nyquist I criterion.

2.4   The splitting procedure

We recall that a set of M shift orthogonal sequences $\{s_k[n]\}_{k=0}^{M-1}$ with periods $\{I_k\}_{k=0}^{M-1}$ satisfy the orthogonality conditions:

$$\begin{aligned}
\sum_{n \in \mathcal{Z}} s_k[I_k m + n] s_k[I_k l + n] &= \delta_{m,l}, k = 0,..,M-1 \\
\sum_{n \in \mathcal{Z}} s_k[I_k m + n] s_{k'}[I_{k'} l + n] &= 0 \quad \text{if } k \neq k', \ \forall m,l,
\end{aligned}$$

where, $\delta_{m,l}$ is the Kronecker delta function which is zero except for $m = l$ where it assumes a value of one. The splitting sequences are the impulse responses of a Perfect Reconstruction (PR) filter bank [28]. Given a set $\{s_k[n]\}_{k=0}^{M-1}$ and a shift orthogonal function $q(t)$ with shift orthogonality period $L\Delta$ where L is a positive integer, M shift orthogonal functions $q_k(t), k = 0, \ldots, M - 1$ can be obtained by forming the linear combinations of shifted versions of $q(t)$

$$q_k(t) = \sum_n s_k[n] q(t - nL\Delta) \quad k = 0, \ldots, M - 1 \ . \tag{2.4}$$

The resulting functions $q_k(t)$ have shift orthogonality periods $I_k L\Delta$, and are orthogonal to each other with periods $min(I_k, I_h)L\Delta$, such that

$$\langle q_k(t), q_h(t - nI_h LT) \rangle = \langle q_k(t - nI_k L\Delta), q_h(t) \rangle = 0 \text{ if } k \neq h \ ,$$

for each n, where $\langle ., . \rangle$ is the scalar product in $L^2(\mathcal{R})$. Equation (2.4) can be interpreted as the filtering of the analog waveform $q(t)$ with M tapped

delay line filters with coefficients $\{s_k[n]\}_{k=0}^{M-1}$ and transfer functions $S_k(f) = \sum_n s_k[n]e^{-j2\pi fn\Delta}$. This operation corresponds to the subdivision of the original space (channel) spanned by translates of $q(t)$ into M orthogonal subspaces (subchannels) spanned by translates of $\{q_k(t)\}_{k=0}^{M-1}$. The spectral characteristics of the various subchannels from a communication point of view depend on the choice of the *splitting* sequences $\{s_k[n]\}_{k=0}^{M-1}$.

Since the orthogonality periods I_k of the various splitting sequences may be different and we can iterate on the splitting operation, a very flexible tiling of the time-frequency plane can be obtained [29]. Indeed the desired filtering operations enjoy the computational efficiency of filter banks [28].

For modulation purposes, the *synthesis* filter bank whose inputs are the possibly complex data symbols, followed by the shaping filter, is implemented at the transmitter, while the *analysis* filter bank follows the sampled matched filter at the receiver. The shaping filter itself is a root-Nyquist filter. The *continuous time* shaping filter at the transmitter receives as input the *discrete sequence* generated by the synthesis filter bank and having a period equal to the shift-orthogonality period of the shaping pulse. The cascade of the continuous time shaping filter at the transmitter, with the corresponding matched filter at the receiver, has a pulse response that is full-Nyquist with periodic zero crossings that allows detection of the input sequence without intersymbol interference at the receiver. Thus, the transmitter shaping filter converts the input sequence to a time waveform, and the receiving filter and sampler recovers this input sequence.

As an example, Fig. 2.1 illustrates a general transmitter-receiver structure based on the 2-ary synthesis-analysis tree of depth-2 whereby various subspaces are represented by distinct frequency channels. The synthesis filter bank would be used at the transmitter to form the discrete sequence that modulates the *continuous time* root-Nyquist pulse $q(t)$ which is shift-orthogonal with shift period Δ. The analysis filter bank would follow the sampled matched filter at the receiver. Note that different levels of the tree may use different QMF pairs [92]. Even within a given level different QMF filter pairs may be used, although this is not common in practice. Note that in general instead of a binary synthesis we may perform an M-ary synthesis. The analysis filter bank is matched to the synthesis filter bank.

In Fig. 2.3 we show the transition from an all digital synthesis filter bank to an analog interface representing the continuous time shaping pulse $q(t)$. This is done for the purposes of associating Fig. 2.3 with the splitting procedure which may be considered to be the unifying thread in the generation of multidimensional signals presented in this chapter. Obviously, an all digital implementation can be obtained by replacing the analog interface of the synthesis filter bank, by the FIR filter whose coefficients are the samples of the
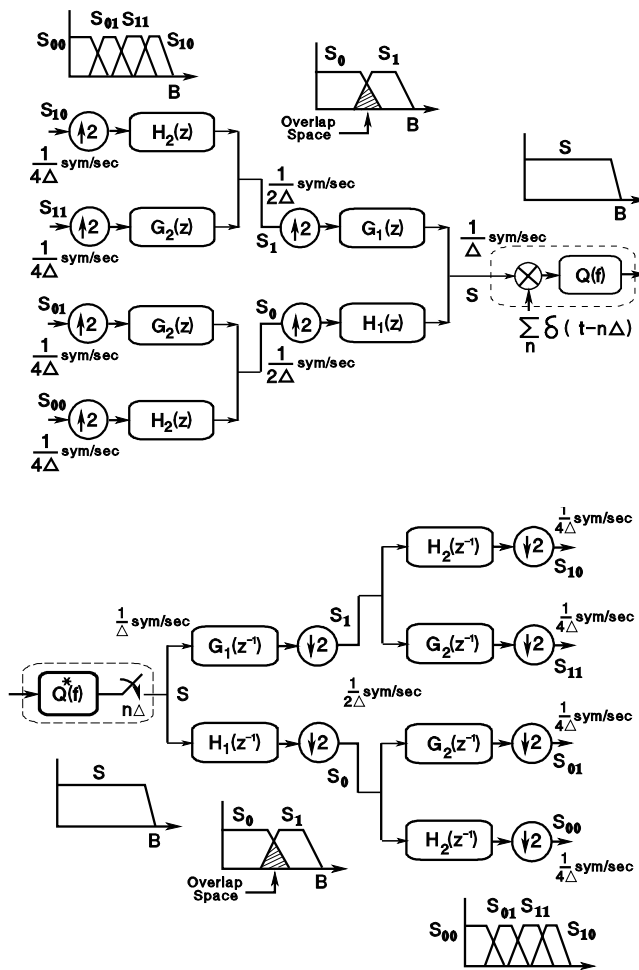
Figure 2.1.   The synthesis and analysis filter banks used at the transmitter
and receiver respectively for the WOFDM

root-Nyquist pulse $q(t)$. The resulting digital output can then be converted
to an analog waveform suitable for transmission over the channel. Similarly,
the analog interface of the analysis filter bank can be replaced by a FIR filter
whose inputs are the samples of the down converted received signal, leading
to a purely digital receiver.

2.4.1   The overlap space

Consider a low pass channel spanned by integer translates of an orthonor-
mal scaling function. The fact that the frequency channel spanned by the

corresponding wavelet overlaps this lowpass space yet is orthogonal to it, motivates us to consider deriving a basis for the space whose frequency occupancy lies in this overlap region (henceforth called the *overlap space*) in terms of the basis spanned by the wavelet. Doing so would provide us with additional basis to use for modulation at no cost in bandwidth.

The space W_n spanned by the mother wavelet is in general bandpass and overlaps the space V_n in frequency. Let this overlap occur in the frequency interval (f_1, f_2). We can *improve* the spectral efficiency of our modulation scheme by performing a partition of the space W_n with the aim of deriving a subspace of W_n with concentration in the frequency interval (f_1, f_2) [1]. We should in practice derive a basis for this subspace in terms of the basis in W_n. This is possible using the wavelet packets. The crucial point is that the overlap space is spanned by shift orthogonal basis that are automatically orthogonal to the basis in V_n. These added basis can be used to carry additional information within the same bandwidth spanned by subspace V_n. In the following sections we will show that the use of the overlap space as shaping pulse is a mean to increase the dimensionality of the modulation scheme, and we will provide performance of such modulations schemes over satellite non-linear channels.

2.4.2 Wavelet Orthogonal Frequency Division Multiplexing

Application of wavelets to orthogonal frequency division multiplexing is quite natural in light of the discussion on multiplicity-M wavelets and wavelet packets (indeed, WOFDM [2] may be considered a generalization of the standard OFDM [64]). Different information could be frequency multiplexed on overlapping adjacent frequency channels using multiplicity-M wavelets and/or wavelet packets as envelope functions [2]. Note that by definition this modulation scheme requires clock synchronization among all the channels. Such an approach would be useful in radio relay link and broadcast applications. This multiplexing scheme enjoys the efficiency of the wavelet decompositions in general, since the maximal decimation property of the filter banks is retained (the literature on this subject is vast, we refer the interested reader to [28]).

The use of multiple frequency subchannels in WOFDM allows a natural and simple scheme of embedding unequal error protection in the modulation process. In particular, for a fixed total available power, we can offer different degrees of protection to the transmitted data by controlling the SNR of the different subchannels. Given the enormous flexibility of the frequency

channelization in WOFDM, it is evident that we can precisely control the different fractions of the total data rate that are to receive different degrees of protection.

Spectral shaping (with or without TCM coding) and line coding are other natural applications of wavelet modulation [3]. Consider a narrowband system whereby the channel is modeled as a linear filter with AWGN. The channel transfer function imposes restrictions on the form of the shaping pulse to be used for modulation. Clearly, we can form a piece-wise constant approximation of the channel transfer function $C(f)$ with whatever degree of accuracy desired. In this way, the available bandwidth for modulation is partitioned into many not necessarily equal sized non-overlapping cells, where within each cell the channel transfer function has constant gain and delay. Consider forming wavelet packets tailored to this piece-wise constant approximation of $C(f)$, such that in the i-th cell we have a wavelet packet with bandwidth equal to the cell bandwidth. Assuming that the tail of the spectrum of each wavelet packet so generated only influences the adjacent cells significantly, and that the group delay is almost constant among neighboring cells, the effect of the channel on the wavelet packets is a simple multiplication by a complex constant, which based on our assumption should not cause excessive cross talk between the information carried by the wavelet packets in adjacent cells. Given this formulation, it should be evident that the effective spectral shape of the transmitted signal can be modified in whatever way desired. The important thing to note is that each wavelet packet spans a subspace of the space of functions with spectral occupancy in the available transmission bandwidth. This form of modulation is indeed a special case of WOFDM introduced above, and its counterpart in connection with source coding, is subband coding. Once again it is evident that we can easily offer unequal error protection to the data when needed.

2.5   Multidimensional signaling using wavelets

It is a well known fact that the number of dimensions (orthogonal waveforms) available in a given rectangular region of the time-frequency plane is proportional to the area of the region in this plane. Using heuristic arguments one can conclude that in a T sec interval and B Hz of bandwidth we can generate at most $2BT$ dimensions. Throughout the rest of this chapter, by basis functions we mean orthogonal waveforms spanning a function space. Slepian, Pollak, and Landau in [69, 70, 71, 72] demonstrated that this heuristic argument is indeed valid for the best basis functions, namely, the

prolate spheroidal wave functions. Even though one is tempted to generalize this notion to non-rectangular regions of the time-frequency plane, this generalization is by no means trivial [25].

Throughout the rest of the section we use the following terminology and definitions:

1. the pulse duration is denoted by T, and *bandwidth* by B. Since, in this section we are primarily interested in root-Nyquist pulses, we are more interested in the *shift-orthogonality period* Δ. Note that normally $T/\Delta >> 1$ for shift-orthogonal pulses (for time division multiplexing, normally $T = \Delta$);

2. *dimensional rate* for a root-Nyquist pulse that is shift-orthogonal with shift period Δ is defined to be $1/\Delta$. If complex modulation is used, this dimensional rate is defined to be $2/\Delta$;

3. *dimensional rate* and *symbol rate* mean the same thing. When dealing with subspaces of a function space it is more natural to use dimensional rate. These subspaces essentially correspond to frequency subchannels, in which case, it is more natural to talk about symbol rate;

4. if each symbol carries M-bits, the *data rate* is M/Δ bits per second;

5. when sampling *analog* waveforms, the *sampling rate* in samples per second used *for simulation* is assumed to be significantly above the Nyquist sampling rate of $2B$

By different distribution of dimensions we mean the following; take a rectangular region of the Time-Frequency (TF) plane say $0 \le t \le NT$ and $0 \le f \le LB$ for some large integers N and L, and populate this region by a set of TF tiles (examples are shown in Fig. 2.8). Each tile in the TF plane corresponds to a signaling dimension. The width of each tile is generally some multiple of the basic shift period Δ, and its height equals the bandwidth of the subchannel associated with that tile. Consider placing a dot at the center of each tile in the TF plane. Next, project the dots along the time axis. The resulting distribution of the dots on the time axis, is what we refer to as the *distribution of dimensions* in time. In the context of the material presented in this section, a given distribution of dimensions in time corresponds to a given channelization of the available frequency band into a set of not necessarily equal bandwidth frequency subchannels.

In the usual definition of the TF tile (see for instance [29] pp.72-73), the width of the tile along the time axis I_t, and that along the frequency axis I_w, are chosen such that a certain percentage of the total signal energy

17

(e.g., 90%) is contained in I_t and I_w respectively. For shift-orthogonal basis functions, the pulses stretch over the time axis and localization based on I_t leads to overlapping tiles. However, focusing on the shift period directly, we eliminate this possibility and that is why we have adopted it here.

Given the connection between bandwidth B and the shift parameter Δ for root-Nyquist pulses of duration T (i.e., $2B\Delta > 1$), we focus on a closely related issue of *distribution* of dimensions in time. Note that the quantity $(2B\Delta - 1)$ is the *excess bandwidth* often presented in percentage and assumed to be less than 100%. To motivate the concept, suppose we have B Hz of bandwidth available for modulation. The maximum number of dimensions we could generate *per unit time* (i.e., the symbol rate) using this bandwidth is $2B$. A question of interest is how are these dimensions distributed in time? Classically we have had two options: 1) if $\Delta = T$, the best basis functions to use are prolate spheroidal wave functions [72], although such basis functions are not used in practice and often a simple rectangular window is used instead; and 2) if $\Delta << T$, it is natural to use a root-Nyquist pulse such as the square root raised-cosine shaping pulse. The case $\Delta > T$ is of no practical interest.

One of our goals here is to present systematic methods based on the theory of wavelets and filter banks to generate other distributions of dimensions in time. Our approach will be primarily based on root-Nyquist pulses yielding the desired distributions [8].

Recently, several authors have addressed the problem of pulse shape design for multidimensional signaling over a bandlimited AWGN channel [89, 90]. Since the symbol rate in time cannot be above the Nyquist limit, their work could best be described as *redistribution* of dimensions in time using shift-orthogonal envelope functions. In [90], Saha and Birdsall described a four-dimensional signal basis, called Q^2PSK, whereby the four orthogonal signals $x(t)cos2\pi f_c t$, $y(t)cos2\pi f_c t$, $x(t)sin2\pi f_c t$ and $y(t)sin2\pi f_c t$, with $0 \le t \le T$, $x(t) = cos(\pi t/T)$, and $y(t) = sin(\pi t/T)$ are used to transmit a four-dimensional vector (a_1, a_2, a_3, a_4). The baseband shaping pulses $x(t)$ and $y(t)$ co-exist in the same bandwidth and are orthogonal. This work was later extended in [89] by setting up an optimization problem whose solution yields two root-Nyquist pulses satisfying three constraints: (1) the shaping pulses individually satisfy the first Nyquist criterion; (2) the shaping pulses and their shifts span orthogonal channels; (3) the fraction of out-of-band power is minimized. Once again this setup is seen to be another attempt at redistribution of dimensions in time with the objective function of maximizing spectral efficiencies. The procedure outlined here generalizes these results and provides much richer and broader families of shift-orthogonal basis functions with high spectral efficiencies, in addition to providing a very

18

large number of possible distribution of dimensions in time.

The basic ingredients needed in our work are:

1. shift-orthogonal functions. These include scaling functions (baseband), wavelets (passband), or in general any other root-Nyquist pulse;

2. multiplicity-M discrete shift-orthogonal sequences;

3. scaling and wavelet vectors to be used for the partitioning of the space spanned by the scaling function and wavelet, for the formation of the wavelet packets;

4. a variety of lowpass and bandpass filters.

To provide examples of the proposed techniques we use the Daubechies compactly supported wavelets, and the square root raised-cosine shaping pulse with roll-off greater than $1/3$ (the square root raised-cosine pulse with roll-off less than $1/3$ is in fact a Meyer scaling function).

2.5.1   Generation of arbitrary distributions of dimensions in time

In general, the multidimensional signal spaces presented in this section are efficiently implemented using filter banks.

Root-Nyquist pulses spanning orthogonal frequency channels that define the multidimensional signal space are obtained via a *splitting* procedure outlined below and exemplified by wavelet packets of the previous section. In general, they are obtained using an *analysis* filter bank via splitting the spectrum of a root-Nyquist pulse at the root of the tree.

In the methods presented here, the spectrum of the multidimensional signals generated can have two split sidebands. Note that it is not possible to send QAM signals over narrowband filters that overlap unless the bands are split. This may be undesirable in certain applications where the channel may effect the split sidebands of a given signal differently. If this is the case, to remedy the problem, Single SideBand (SSB) or Vestigial SideBand (VSB) transmission may be employed. Clearly, regardless of whether quadrature modulation, or SSB transmission is employed, the spectral efficiency of the modulation is unaffected.

In general the spectrum of the scaling function and wavelet overlap in the frequency domain. The space of functions whose spectrum lies in this region (henceforth referred to as the *overlap space*) is spanned by a wavelet packet. Strictly speaking, wavelet packets result from the *iterated use* of scaling and

wavelet vectors as splitting sequences. In the rest of the section, with a slight abuse of notation we use the word wavelet packet even when the same QMF filter-pairs are not used as splitting sequences at every level of the tree. As an example, we show this overlap space qualitatively in Fig. 2.2 as the cross hatched region at the first level of the tree. Later we shall obtain the basis of the overlap space for general shaping pulses that may not satisfy the dyadic scaling equation.

To achieve high spectral efficiencies, especially in connection with the use of wavelets for modulation, it is necessary to use the basis functions of this wavelet packet. This is because it may be desirable to start with a given scaling function with a certain excess bandwidth β, and use it with an additional shaping pulse in a composite multicarrier modulation scheme achieving a higher spectral efficiency. Another motivation for the generation of a basis for the overlap space is in connection with the design of optimal pre-filters eliminating pattern dependent jitter [7]. In particular, it can be shown that such a filter lies entirely in the overlap space.

In light of the above, in the methods presented below, our first step is to generate this wavelet packet (or its equivalent). Such basis functions are generated when wavelet packets are obtained, and they are often very useful in applications. We may *independently* split these spaces into subchannels and generate a very large number of possible distribution of dimensions in time, should it be necessary to do so.

2.5.2   Multidimensional signaling using wavelets

On the basis of the concepts described in Section 2, we can partition the frequency channel spanned by a scaling function $q(t)$ according to the following procedure.

Method 1:

Step 1.1: The wavelet is filtered in a filter bank corresponding to a wavelet packet tree to generate a wavelet packet with a frequency occupancy in the region of overlap between the spectra of the scaling function and wavelet [1, 2];

Step 1.2: The space spanned by the scaling function can be split into orthogonal frequency channels using a set of splitting sequences. The overlap space due to the overlap of the spectra of the scaling function and wavelet separated in Step 1.1 above, can be similarly and independently partitioned
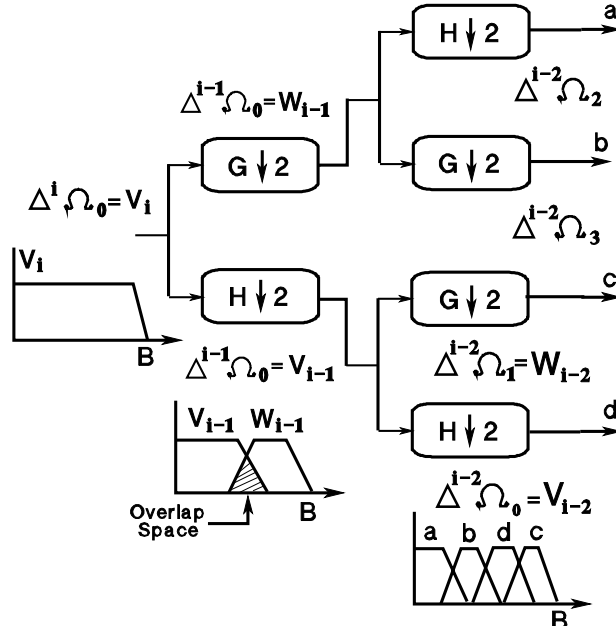
Figure 2.2. Two level binary ($M = 2$) wavelet packet decomposition tree. The subspaces at different levels of the tree are represented as distinct frequency channels. The $\Delta^k \Omega_n$ denotes the closure in the $L^2(\mathcal{R})$ of $\{2^{k/2} \mu_n (2^k t - l) | l \in \mathcal{Z}\}$ which are subspaces of the $L^2(\mathcal{R})$ at resolution 2^k. Decomposition starts at temporal resolution 2^i. The V_k and W_k denote subspaces spanned by the scaling function and wavelet at temporal resolution 2^k. The symbols $H \downarrow 2$ and $G \downarrow 2$ represent analog TDL filtering using the scaling and wavelet vectors respectively, used as the splitting sequences, followed by decimation by two. In a fully digital implementation, we may use FIR realization of the TDL filters operating on samples of the scaling function.

This orthogonal frequency channelization is extremely flexible. An example of the spectra of a scaling function $q(t)$ and overlap function $o(t)$ generated with this method is shown in Fig. 2.4. In all of the examples presented in this section we represent the continuous time functions using their samples with a sampling rate significantly above the Nyquist rate, and we obtain the FIR realization of the continuous time signals. Hence, the simulation bandwidth is large enough to obtain accurate estimates of the signal spectra. In the example of Fig. 2.4, we used the Daubechies length 39 scaling function [25] with its shift period Δ normalized to one. The number of samples per shift

period Δ is $N_s = 8$. The horizontal axis in Fig. 2.4 represents continuous frequency in Hertz. The analog TDL analysis filter bank generating $q(t)$ and $o(t)$ is depicted in Fig. 2.5-(a), whereas a general digital filter bank implementation of the transmitter and receiver associated with method 1 is depicted in Fig. 2.6-(a). The basis for the overlap space is shift-orthogonal with shift period $4\Delta = 4$. Performing a four way split of the space spanned by the scaling function using the Daubechies splitting sequences we obtain five subchannels as depicted in Fig. 2.7 (in this example we did not split the overlap space).

The splitting sequences $h[n]$ and $g[n]$ used in this example are length 40 Daubechies scaling and wavelet vectors. The resulting five subspaces (i.e., subchannels) are spanned by orthonormal basis with shift period four. When used simultaneously to support quadrature modulation, they generate a 10 dimensional space every four time units. This is because there are a total of five orthogonal subchannels over a shift period of $4\Delta = 4$ each supporting quadrature modulation (yielding two dimensions per subchannel). Hence, in four time units we generate 5 dimensions per quadrature component (i.e., the symbol rate per quadrature component is $5/4$). This symbol rate is within 11% of the Nyquist limit (relative to the 45 dB bandwidth). Not using the basis of the overlap space amounts to a loss of 20% in the symbol rate. The tilings of the time-frequency plane corresponding to the channelizations of Fig. 2.4 and Fig. 2.7 are shown in Fig. 2.8. In Fig. 2.8, B is the 3 dB bandwidth of the overall modulation scheme, the height of each tile corresponds to the 3 dB bandwidth of each subchannel, while the width of the tiles is a multiple of the elementary shift period Δ, which corresponds to the shift-orthogonality periods of the shaping pulses associated with different subchannels. Note that while the width of the tiles are clearly defined in terms of the shift-orthogonality period, the height of the tiles is dependent on how the bandwidth is defined. We used the 3 dB bandwidth in Fig. 2.8 to show more clearly the distinction between the different tilings that can be obtained.

The generalization of the above procedure to other shift-orthogonal envelope functions is of interest and will be described in the next section.

2.5.3 Multidimensional signaling using a general Root-Nyquist pulse

Let $q(t)$ be a shift-orthogonal envelope function that is either even or odd about the point $L\Delta$, where L is a positive integer, and Δ is the shift-orthogonality parameter (later we shall generalize the results to the case

the shaping pulse may not have any temporal symmetry). Then the minimum bandwidth of such a shaping pulse would be $1/2\Delta$ and any spectral components beyond this value leads to excess bandwidth. Let the bandwidth of this envelope function be $(1 + \beta)/(2\Delta)$. For practical applications generally $0 < \beta < 1$ and this is what we shall assume here. Then it is possible to prove that $w(t) = \sqrt{2}q(t)sin(2\pi t/\Delta)$ (the sine modulation is crucial) spans a bandpass space that is orthogonal to the lowpass space spanned by translates of $q(t)$ by integer multiples of Δ. Furthermore, $w(t)$ is shift-orthogonal with shift parameter Δ. Note that for any nonzero β the spectra of the functions $q(t)$ and $w(t)$ overlap. It is possible to obtain a function $o(t)$ which is shift-orthogonal with shift period Δ and orthogonal to $q(t)$, by filtering $w(t)$ with a filter having the following characteristics: (1) impulse response $h_N(t)$ with even symmetry in the time domain around $t = K\Delta$, where K is a positive integer; (2) transfer function $H_N(f)$ constant in the frequency range $-\frac{1+\beta}{2\Delta} \leq f \leq \frac{1+\beta}{2\Delta}$ and Nyquist-symmetrical about $1/\Delta$ (i.e., satisfying the first Nyquist criterion with period $\Delta/2$). In analogy with wavelets this process may be viewed as one of generating a wavelet packet from the wavelet itself.

To prove that $o(t)$ and $q(t)$ span orthogonal frequency channels, let us recall that $H_N(f)$ must satisfy the condition $\sum_n |H_N(f - 2n/\Delta)|^2 = K_1$, where K_1 is a constant.
We can write:

$$\langle o(t), q(t - n\Delta) \rangle = \int_{-\infty}^{+\infty} O(f)Q^*(f)e^{j2\pi n\Delta f} df =$$

$$= \int_{-\infty}^{+\infty} H_N(f)W(f)Q^*(f)e^{j2\pi n\Delta f} df = \qquad (2.5)$$

$$= \frac{\sqrt{2}}{2j} \left[\int_{\frac{1-\beta}{2\Delta}}^{\frac{1+\beta}{2\Delta}} H_N(f)Q\left(f - \frac{1}{\Delta}\right) Q^*(f)e^{j2\pi n\Delta f} df - \right.$$

$$\left. - \int_{-\frac{1+\beta}{2\Delta}}^{-\frac{1-\beta}{2\Delta}} H_N(f)Q\left(f + \frac{1}{\Delta}\right) Q^*(f)e^{j2\pi n\Delta f} df \right]$$

$$= \sqrt{2} \left[\int_{\frac{1-\beta}{2\Delta}}^{\frac{1+\beta}{2\Delta}} H_N(f)Q\left(f - \frac{1}{\Delta}\right) Q(f) \sin\left(2\pi(n - K)\Delta f\right) df \right] = 0 \ (2.6)$$

where $W(f)$ and $O(f)$ are the Fourier transforms of $w(t)$ and $o(t)$, equality (2.5) follows since $Q(f)$ is assumed to have frequency support in $(-(1 + \beta)/(2\Delta),(1 + \beta)/(2\Delta))$ and equality (2.6) follows because the function

$$H_N(f)Q(f - 1/\Delta)Q(f) \sin\left(2\pi(n - K)\Delta f\right)$$

is odd around $f = 1/(2\Delta)$. Because of the limited support of $Q(f)$ we

can write

$$
\begin{aligned}
T(f) &= \sum_n \left| H_N\left(f - \frac{n}{\Delta}\right) \right|^2 \left| W\left(f - \frac{n}{\Delta}\right) \right|^2 = \\
&= \frac{1}{2} \sum_n \left| H_N\left(f - \frac{n}{\Delta}\right) \right|^2 \left[\left| Q\left(f - \frac{n}{\Delta} - \frac{1}{\Delta}\right) \right|^2 + \left| Q\left(f - \frac{n}{\Delta} + \frac{1}{\Delta}\right) \right|^2 \right] \ .
\end{aligned}
$$
(2.7)

To prove that $o(t)$ satisfies the Nyquist criterion we have to prove that equation (2.7) is equal to a constant K_2. If this condition is satisfied for $0 \le f \le 1/\Delta$, then it is satisfied everywhere. Since $Q(f) = 0$ for $|f| > 1/\Delta$, we can write (for $0 \le f \le 1/\Delta$):

$$
\begin{aligned}
T(f) &= \frac{1}{2} \left\{ \left| H_N\left(f + \frac{1}{\Delta}\right) \right|^2 |Q(f)|^2 + |H_N(f)|^2 \left| Q\left(f - \frac{1}{\Delta}\right) \right|^2 + \right. \\
&\quad \left. + \left| H_N\left(f - \frac{1}{\Delta}\right) \right|^2 |Q(f)|^2 + \left| H_N\left(f - \frac{2}{\Delta}\right) \right|^2 \left| Q\left(f - \frac{1}{\Delta}\right) \right|^2 \right\} = \\
&= \frac{1}{2} |Q(f)|^2 \left\{ \left| H_N\left(f + \frac{1}{\Delta}\right) \right|^2 + \left| H_N\left(f - \frac{1}{\Delta}\right) \right|^2 \right\} + \\
&\quad + \frac{1}{2} \left| Q\left(f - \frac{1}{\Delta}\right) \right|^2 \left\{ |H_N(f)|^2 + \left| H_N\left(f - \frac{2}{\Delta}\right) \right|^2 \right\} = \\
&= \frac{K_1}{2} \left\{ |Q(f)|^2 + \left| Q\left(f - \frac{1}{\Delta}\right) \right|^2 \right\} = \frac{K_1 \Delta}{2} \quad \text{for} \quad 0 \le f \le \frac{1}{\Delta} \ .
\end{aligned}
$$

The above equality follows since $Q(f)$ and $H_N(f)$ individually satisfy the Nyquist criterion with periods Δ and $\Delta/2$, respectively (in particular, we have $\sum_n |Q(f - n/\Delta)|^2 = \Delta$ since $q(t)$ is a unit-energy root-Nyquist pulse). Hence $o(t)$ satisfies the first Nyquist criterion and is shift-orthogonal with shift parameter Δ.

The restriction to the case of temporally symmetric pulses is not necessary for the previous orthogonality relations to hold valid. In particular, write $q(t + L\Delta) = q_{ev}(t) + q_{od}(t)$ where, $q_{od}(t)$ is the odd part of $q(t + L\Delta)$ and $q_{ev}(t)$ is the even part of $q(t + L\Delta)$. Form $q(-t + L\Delta) = q_{ev}(t) - q_{od}(t)$ and let $q_1(t) = q_{ev}(t - L\Delta) - q_{od}(t - L\Delta)$. The functions $q_{ev}(t - L\Delta)$ and $q_{od}(t - L\Delta)$ individually satisfy the orthogonality relations above. It can be easily verified that the *combination* $q_1(t) = q_{ev}(t - L\Delta) - q_{od}(t - L\Delta)$ also satisfies *all* the orthogonality relations above. In particular, at the transmitter we can use the shaping filters $Q_1(f)$ and $O(f) = H_N(f)[Q(f - 1/\Delta) - Q(f + 1/\Delta)]/2j$ for data transmission, while at the receiver we can use the matched filters $Q_1^*(f)$ and $O^*(f)$ for data detection. In the rest of this subsection we focus

on symmetric root-Nyquist pulses since these are among the most commonly used shaping pulses in applications, with the understanding that we could apply the methods to any root-Nyquist pulse with the modification noted.

Given this setup, the frequency channel spanned by a symmetric baseband root-Nyquist pulse $q(t)$ can be partitioned according to the following procedure.

Method 2:

Step 2.1: The function $o(t)$ spanning the overlap space is generated by filtering $w(t)$ using a filter with transfer function $H_N(f)$ satisfying the following conditions: (1) $H_N(f) = |H_N(f)|e^{-j2\pi K\Delta f}$ where K is a positive integer; (2) $|H_N(f)|^2$ is Nyquist-symmetrical around $f = 1/\Delta$ and is constant for $-(1+\beta)/(2\Delta) \leq f \leq (1+\beta)/(2\Delta)$;

Step 2.2: This step is totally analogous to Step 1.2 of Method 1 presented above. The spectrum of the shift-orthogonal functions $q(t)$ and $o(t)$ can be individually channelized using multiplicity-M splitting sequences.

Among all the possible filters, the one leading to the highest spectral efficiency is the ideal lowpass filter with cut-off frequency $1/\Delta$ (in effect, ideal brick-wall filtering creates a wavelet packet using a $sinc(.)$ scaling function as L^2 filter).

As an example, we used the FIR realization of a square root raised-cosine shaping pulse with 100% roll-off and generated the function $o(t)$, whose spectrum is shown in Fig 2.9. The shift period of the square root raised-cosine pulse is normalized to $\Delta = 1$, the number of samples per symbol period is $N_s = 10$, and the overall length of the pulse was set to 40Δ. The FIR almost ideal LowPass Filter (LPF) used to generate $o(t)$ was obtained via frequency sampling. The stopband attenuation was set to 60 dB, the transition band to 0.01 Hz, and Kaiser windowing was used in the filter design. The number of taps in this FIR filter is 365. The resulting Peak Distortion (PD) of $o(t)$ is 4.6% and the PD due to cross-talk between the two subchannels is 0.9%. The PD of $o(t)$ is defined as follows. Let $r_o(t)$ be the time autocorrelation of $o(t)$ shifted along the time axis so that it has its peak value at the origin, then $PD = \{\frac{100}{r_o(0)}((\sum_{m=-\infty}^{\infty}|r_o(m\Delta)|) - |r_o(0)|)\}\%$, where Δ is the shift-orthogonality period of $o(t)$. The PD due to cross-talk is obtained as follows. Let $r_{q,o}(t)$ be the time cross correlation of $o(t)$ and $q(t)$ shifted along the time axis so that its center of symmetry is at origin. Then, the PD due to cross-talk between the subchannel spanned by $o(t)$ and that spanned by $q(t)$ is $PD = \{\frac{100}{r_o(0)}\sum_{m=-\infty}^{\infty}|r_{q,o}(m\Delta)|\}\%$.

The block diagram of the signal processing generating $o(t)$ based on analog TDL filtering is depicted in Fig. 2.5-(b). In this figure, we also show the transition into an analog analysis filter bank structure that may be used to generate the multidimensional signal space. The function $o(t)$ and the square root raised-cosine shaping pulse used simultaneously for modulation yield spectral efficiencies near the Nyquist limit. In Fig. 2.6-(b), we show a general digital filter bank implementation of the transmitter and receiver associated with method 2.

Notice that one drawback of Method 2 is that for very high spectral efficiency, a very steep filter is required in Step 2.1. As an alternative, when the value of $\beta < 1$, the function $o(t)$ can be generated by filtering the function $w(t)$ with a TDL filter with elementary delay Δ, having coefficients that form a shift-orthogonal sequence with period P, followed by lowpass filtering of the resulting function, which we denote by $\hat{o}(t)$. The resulting shift-orthogonality period of $\hat{o}(t)$ is $P\Delta$. Let us write $\hat{o}(t)$ as the sum of two functions with disjoint frequency supports, $\hat{o}(t) = o(t) + o_h(t)$, where $o(t)$ contains the low frequency components of $\hat{o}(t)$ and $o_h(t)$ contains the high frequency components of $\hat{o}(t)$, such that: $O(f) = 0$ for $|f| \geq \frac{1}{\Delta}$, and $O_h(f) = 0$ for $|f| < \frac{1}{\Delta}$ or $|f| \geq \frac{2}{\Delta}$ (the equality to zero for $|f| \geq \frac{2}{\Delta}$ arises because $q(t)$ has a bandwidth less than $1/\Delta$, hence its sine modulated version $w(t)$ has a bandwidth less than $2/\Delta$. Since $\hat{o}(t)$ is obtained via TDL filtering of $w(t)$, it cannot have any frequency components above $2/\Delta$-Hz). As a consequence of the above equations we have $\left|\hat{O}(f)\right|^2 = |O(f)|^2 + |O_h(f)|^2$. It is possible to prove that $o(t)$ and $o_h(t)$ *individually* satisfy the first Nyquist criterion and can be used for modulation. To prove this, note that since $q(t)$ is real then $|Q(f)|^2$ is an even function of frequency. Consider $|W(f)|^2$ and note that $|Q(f - 1/\Delta)|^2$ is even around $1/\Delta$ and $|Q(f + 1/\Delta)|^2$ is even around $-1/\Delta$. Let us normalize Δ to equal one for convenience. The squared magnitude of the transfer function of the splitting sequence is periodic and even around $f = \pm 1$. Let the discrete filter used to separate the overlap space have transfer function $A(e^{j2\pi f\Delta})$. Then, recalling equation (2.4), we have $\left|\hat{O}(f)\right|^2 = |W(f)|^2 \left|A(e^{j2\pi f\Delta})\right|^2$. By design $\hat{o}(t)$ is shift-orthogonal with shift period $\Delta' = P\Delta = P$ (a positive integer). Hence we can write:

$$\langle\hat{o}(t),\hat{o}(t - nP)\rangle = \int_{-\infty}^{+\infty} \left|\hat{O}(f)\right|^2 cos(2\pi nPf)df = \delta_{0,n} \qquad (2.8)$$

$$= 2\int_{0}^{+\infty} |O(f)|^2 cos(2\pi nPf)df + 2\int_{0}^{+\infty} |O_h(f)|^2 cos(2\pi nPf)df \qquad (2.9)$$

$$= 2(-1)^{nP}\left[\int_{-0.5}^{+0.5} |O(f + 0.5)|^2 cos(2\pi nPf)df + \right.$$

$$\int_{-0.5}^{+0.5} |O_h(f+1.5)|^2 \, cos(2\pi n P f) df \Big] \qquad (2.10)$$

where equation (2.9) follows since $|\hat{O}(f)|^2$ is even, equation (2.10) is obtained via two different shifts of the variable of integration of the two parts of equation (2.9) and using the fact that the frequency support of $|O(f)|^2$ and $|O_h(f)|^2$ is limited as stated before. Now, we have the following: 1) $|Q(f-1)|^2$ is even around $f=1$ and $|Q(f+1)|^2$ is even around $f=-1$; 2) $|\hat{O}(f)|^2 U(f)$ where $U(f)$ is the unit step function in frequency is even around $f=1$ since TDL has a periodic transfer function around $f=1$. Hence,

$$|\hat{O}(f+1)|^2 U(f+1) = [|O(f+1)|^2 + |O_h(f+1)|^2] U(f+1)$$

is even around $f=0$ and

$$|\hat{O}(-f+1)|^2 U(-f+1) U(-f) = |\hat{O}(f+1)|^2 U(f+1) U(-f); \qquad (2.11)$$

3) since $O(f)=0$ for $|f| \geq 1/\Delta = 1$, $|O(f+1)|^2 U(f+1) U(f) = 0$ and

$$|\hat{O}(f+1)|^2 U(f+1) U(f) = |O_h(f+1)|^2 U(f+1) U(f) = |O_h(f+1)|^2 U(f). \qquad (2.12)$$

Similarly, since $O_h(f)=0$ for $|f| < 1/\Delta = 1$ or $|f| \geq 2/\Delta = 2$,

$$|O_h(f+1)|^2 U(f+1) U(-f) = 0$$

$$|\hat{O}(f+1)|^2 U(f+1) U(-f) = |O(f+1)|^2 U(f+1) U(-f). \qquad (2.13)$$

From equations (2.11)-(2.13) we conclude that

$$|O_h(-f+1)|^2 U(-f) = |O(f+1)|^2 U(f+1) U(-f).$$

Multiplying both sides of this last equality by $U(f+1)$ and replacing f by $(f-0.5)$ leads to

$$|O_h(-f+1.5)|^2 U(f+0.5) U(-f+0.5) = |O(f+0.5)|^2 U(f+0.5) U(-f+0.5)$$

which can be written as:

$$|O(f+0.5)|^2 = |O_h(-f+1.5)|^2 \quad \text{for} \quad |f| \leq 0.5 \ . \qquad (2.14)$$

Since $cos(2\pi n P f)$ is even around $f=0$ we have that

$$\int_{-0.5}^{+0.5} |O(f+0.5)|^2 \, cos(2\pi n P f) df = \int_{-0.5}^{+0.5} |O_h(f+1.5)|^2 \, cos(2\pi n P f) df \ . \qquad (2.15)$$

27

From equations (2.8), (2.10), (2.14), and (2.15), we conclude that $o(t)$ and $o_h(t)$ individually satisfy the first Nyquist criterion and can be used for modulation.

Since it is the spectrum of $o(t)$ that overlaps that of $q(t)$, we can filter out $O(f)$ and obtain a shift-orthogonal basis for the overlap space. Note that for values of β close to 1 the requirements on the filter needed to separate $O(f)$ are less stringent than those of Method 2. This is because the sharp filtering of the overlap space is achieved by the TDL, and the low pass filter that is needed to separate $O(f)$ from $\hat{O}(f)$ can have a much larger transition bandwidth and hence many fewer coefficients in comparison to the filter that would be needed in method 2.

We can now summarize the steps required to perform this channelization.

Method 3:

Step 3.1: In this step the function $\hat{o}(t)$ is generated by filtering $w(t)$ with a TDL filter whose coefficients form a shift-orthogonal sequence (an example is given below). This is analogous to Step 1.1 of Method 1;

Step 3.2: The function $o(t)$ containing the low frequency components of $\hat{o}(t)$, is separated from $\hat{o}(t)$ by means of a non ideal lowpass filter with group delay $K\Delta$ for some integer K (by non ideal, we mean a lowpass filter that has a nonzero transition bandwidth);

Step 3.3 This step is identical to the Step 1.2 of Method 1.

As an example of the application of this procedure, consider the square root raised-cosine shaping pulse (denoted by $q(t)$) with 35% roll-off. The shift period is normalized to one. For the FIR realization of this pulse, the number of samples per symbol is $N_s = 10$ and the pulse length is set to 40Δ. The overlap space occupies the frequency interval 0.325 Hz to 0.675 Hz. The splitting sequence used to generate $\hat{o}(t)$ is obtained at the second level of the tree structure generating the Daubechies discrete wavelets [25]. We used the Daubechies length 40 sequences (this is the sequence length at the first level of the tree). In particular, let $h[n]$, $n = 0,1,...,39$ denote the scaling sequence and $g[n]$, $n = 0,1,...,39$ denote the corresponding wavelet sequence; then, the splitting sequence used to generate the overlap space is $c[n] = \sum_{k=0}^{39} g[n - 2k]h[k]$.

Fig. 2.10 shows all the various frequency channels (i.e., subspaces) defined previously collected in one place. From this figure, it is evident that a portion of the high frequency component of the spectrum of $w(t)$ is also filtered in the process; hence, we used a lowpass filter to separate $O(f)$ (i.e., the component

of the spectrum in the overlap space). This LPF was realized via frequency sampling and Kaiser windowing and has a stopband attenuation of 50 dB, and transition bandwidth of 0.06 Hz. The number of taps of this FIR filter is 51. The signal processing block diagram based on analog TDL filtering for this example is depicted in Fig. 2.5-(c). In Fig. 2.6-(c), we show a general digital filter bank implementation of the transmitter and receiver associated with method 3.

The overlap space has a symbol rate of 2/4 using quadrature modulation (i.e., two dimensions every four time units). We performed a four-way split of the spectrum of $q(t)$ using the Daubechies splitting sequences obtained at the second level of the tree structure generating the discrete wavelet packets. The resulting spectrum is depicted in Fig. 2.11. The symbol rate of each one of the four subspaces is 2/4 using quadrature modulation. When used with the basis of the overlap space we generate a 10-dimensional space every four time units. The subspaces of Fig. 2.11 generated in the tree structure of Fig. 2.5-(c) are denoted, in order of increasing center frequency, as channels C_0,C_1,C_3 and C_2. The subchannels at the first level of the tree of Fig. 2.5-(c) are denoted as B_0 (lowpass) and B_1 (bandpass). The symbol rate of each of these subchannels is 2/2 using quadrature modulation. This multidimensional scheme is used in an example below.

2.5.4 Example of application

To test the performance of the proposed schemes on real channels, we consider transmission of a multidimensional signal over a stationary fading channel with nulls in the transmission band. The channel is modeled as a linear filter with transfer function depicted in Fig. 2.12 whose output is corrupted by additive white Gaussian noise. The transfer function of Fig. 2.12 has been obtained as a possible realization of a multipath channel in an urban environment with 20 reflections and at bit-rate of 500 Kbit/s [78].

We used a temporally symmetric square root raised-cosine pulse with 35% roll-off and utilized the following transmission schemes in our simulations (in all the schemes we use the QPSK modulation format): (A) the square root raised-cosine shaping pulse $q(t)$ whose spectrum is shown in Fig. 2.10 (denoted as channel A) is used at a rate of 1 symbol per second; (B) the two shift-orthogonal waveforms spanning the subchannels B_0 and B_1 of Fig. 2.5-(c) are used at a rate of 1 symbol per 2 seconds per subchannel; and (C) the four shift-orthogonal waveforms whose spectra are shown in Fig. 2.11, spanning the subchannels C_0,C_1,C_3 and C_2 of Fig. 2.5-(c) are used at a rate of 1 symbol per 4 seconds per subchannel.

The value of E_b/N_0 required to obtain a bit error probability of 10^{-5}

at the receiver has been measured via simulation and the following results were obtained: 17.7 dB for subchannel A; 11.6 dB for subchannel B_0 and more than 30 dB for subchannel B_1 (i.e., the channel has introduced an irreducible error rate for subchannel B_1); 12.3, 15.8, 12.5 dB for subchannels C_0,C_1,C_3 respectively, and more than 30 dB for subchannel C_2 (i.e., the channel has introduced an irreducible error rate for subchannel C_2). Note that for scheme (B), there is a gain of 6.1 dB on one of the subchannels while there is a significant loss on the other subchannel in comparison to scheme (A). In scheme (C) on the other hand, three of the subchannels show gains of 5.4 dB, 1.9 dB, and 5.2 dB in comparison to scheme (A), while there is a significant loss on the fourth subchannel.
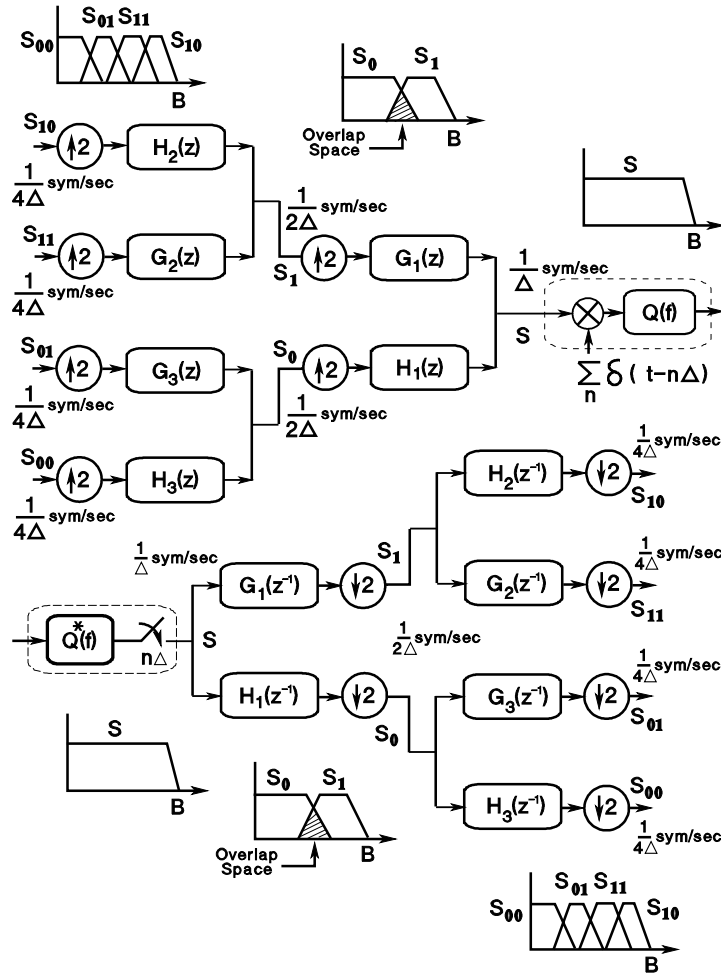
Figure 2.3.   Two level binary ($M = 2$) synthesis and analysis filter bank tree. The synthesis bank would be used at the transmitter, the analysis bank at the receiver. The inputs to the synthesis filter bank are all digital. The dashed boxes contain the analog interfaces of the digital filter banks. The data rates at various nodes of the tree are specified in symbols per second (sym/sec). The shaping pulse $q(t)$ is shift-orthogonal with period Δ. The Gray code labeling of the subchannels S_{ij} ensures that the subchannels are in order of increasing center frequencies.

31
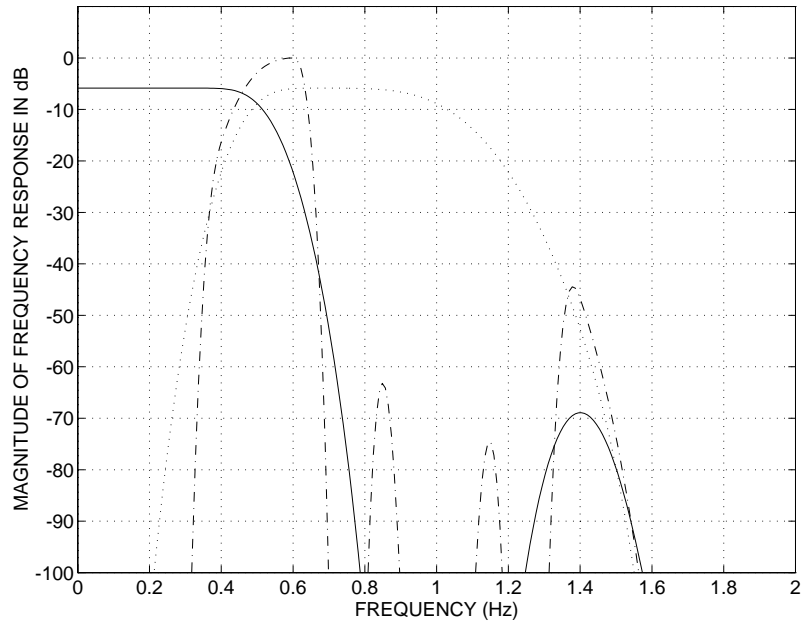
Figure 2.4.   Magnitude (in dB) of the Fourier transform of the Daubechies scaling function of length 39 $q(t)$ (solid line), the wavelet (dotted line), and the "overlap space function" $o(t)$ (dash-dot line) generated with Method 1.
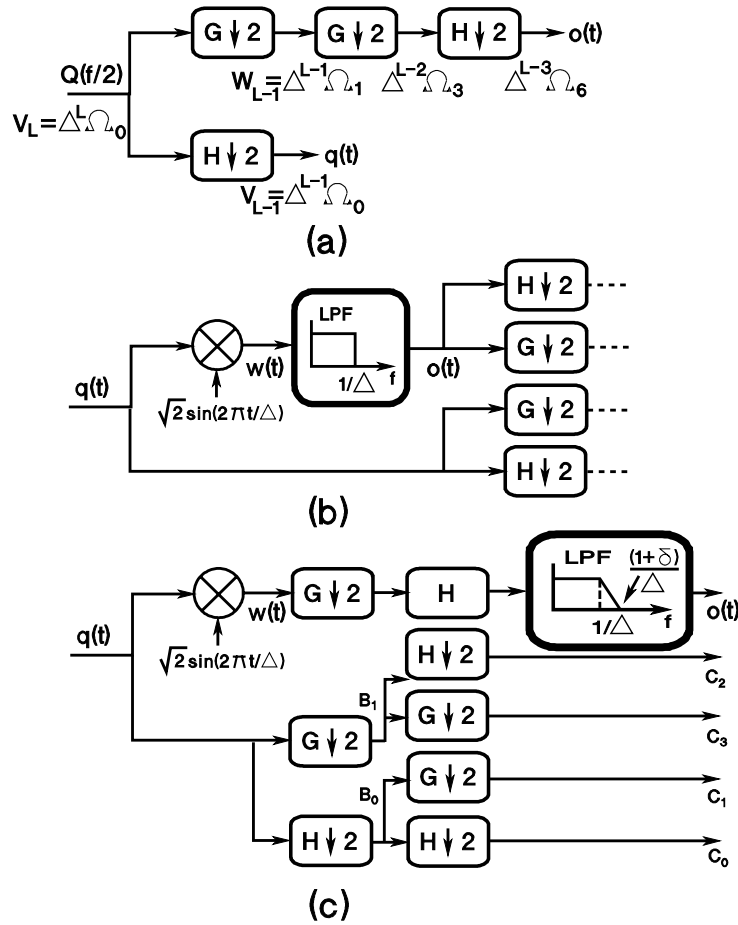
Figure 2.5. Block diagrams of signal processing associated with different splitting techniques, (a) for Method 1, (b) for Method 2, and (c) for Method 3. $H_k(e^{nj\omega\Delta})$ and $G_k(e^{nj\omega\Delta})$ are transfer functions of analog TDL filter-pairs with elementary tap delay of $n\Delta$. In the examples of the section, the TDL filter-pairs used are the same and independent of the level of the tree. In (a), we show the subspaces that would result at various levels of the wavelet packet decomposition tree if the scaling and wavelet vectors were used as splitting sequences at every level. In part (a), the subspaces spanned by shifts of $q(t)$ and $o(t)$ may be split further, but this is not shown in the figure. Similarly in part (c), the subspace spanned by shifts of $o(t)$ may be split further. The delays needed to obtain causal filters are not shown in the figures.
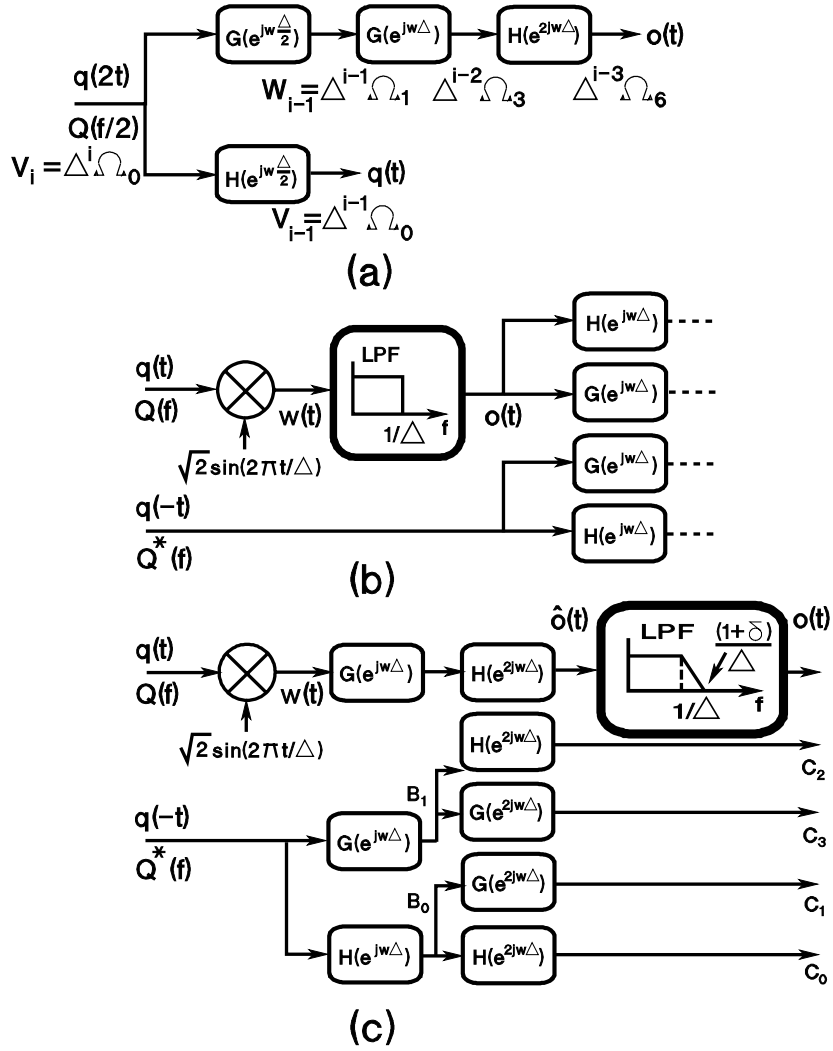
Figure 2.6. One level analysis and synthesis filter bank trees associated with different splitting techniques, (a) for method 1, (b) for method 2, and (c) for method 3. The synthesis bank would be used at the transmitter, the analysis bank at the receiver. The dashed boxes in the analysis and synthesis trees contain the analog interfaces of the digital filter banks. The signal processing for generation of the shaping pulse $o(t)$ for all three methods are also depicted in the figure. The different methods are essentially distinguished based on how $o(t)$ is generated.
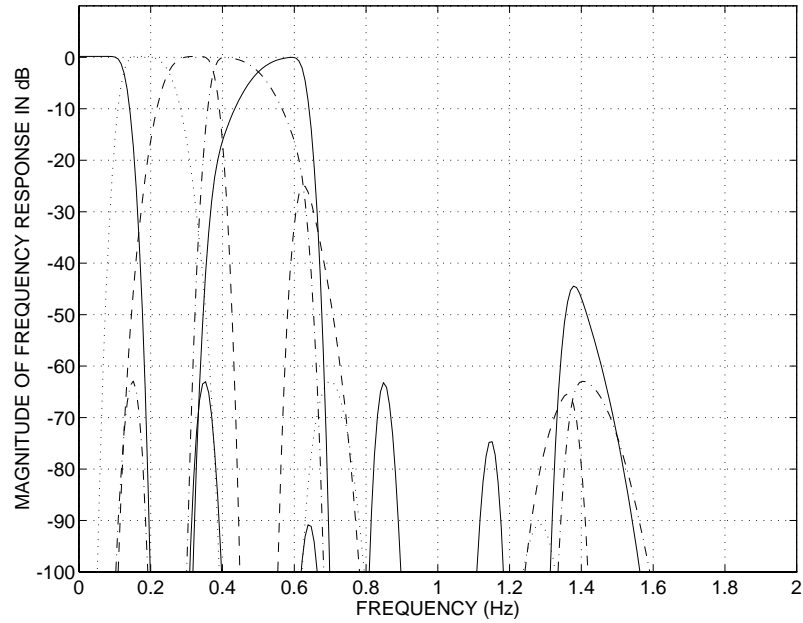
Figure 2.7. Magnitudes of the frequency responses (in dB) of the four subspaces obtained from the split of the spectrum of the Daubechies scaling function of Fig. 2.4, and the overlap space. The subspaces are spanned by shift-orthogonal basis with dimensional rate (or symbol rate) 2/4 using quadrature modulation, using method 1.
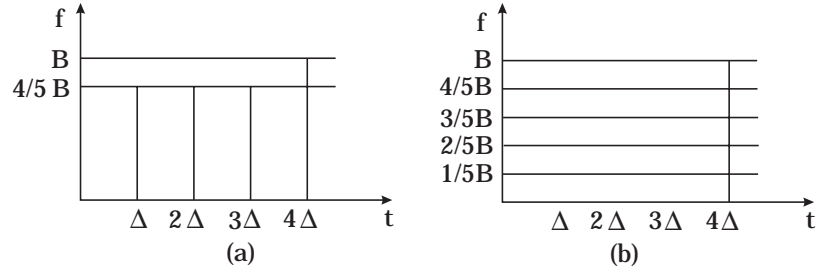
Figure 2.8.   Tiling of the time-frequency plane corresponding to the channelizations of Fig. 2.4 and Fig. 2.7.
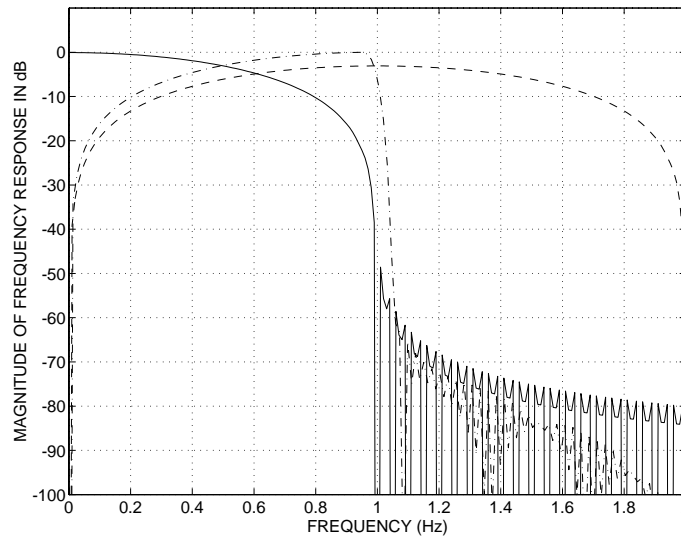
Figure 2.9.   Magnitudes of the frequency responses (in dB) of the square root raised-cosine shaping pulse $q(t)$ with 100% roll-off (solid line), the function $w(t)$ (dash line), and the overlap function $o(t)$ (dash-dot line), using method 2.

36
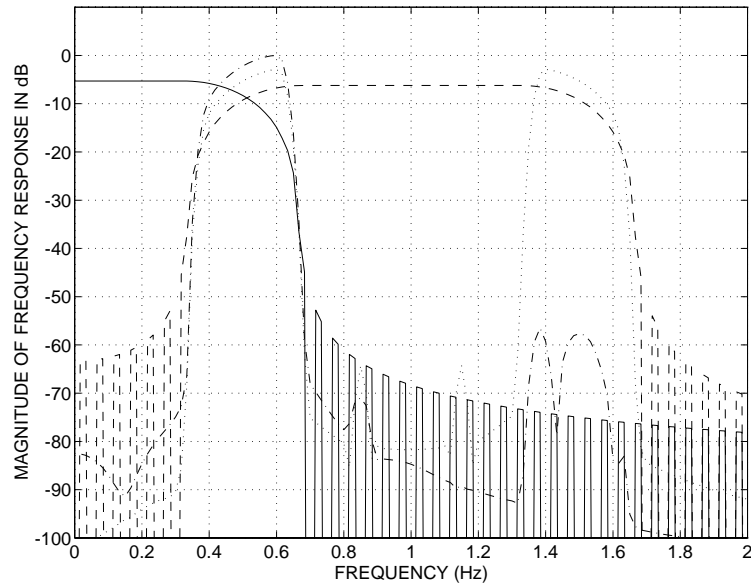
Figure 2.10.   Magnitudes of the frequency responses (in dB) of the square root raised-cosine shaping pulse $q(t)$ (solid line) with 35% roll-off, the function $w(t)$ (dashed line), the output $\hat{o}(t)$ of the TDL filter using the splitting sequence $c[n]$ (dotted line), and output of the lowpass filter used to separate the overlap space $o(t)$ (dash-dot line), using method 3.
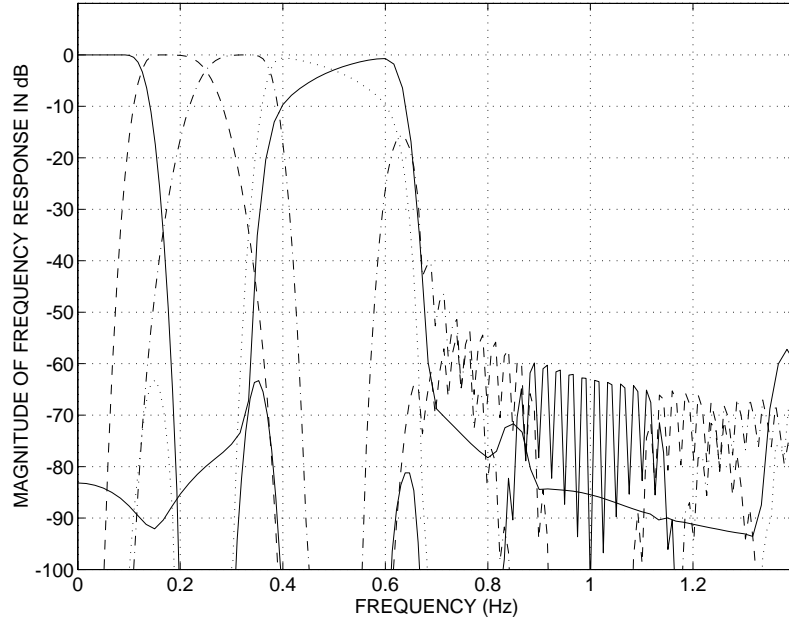
Figure 2.11.   Magnitudes of the frequency responses (in dB) of the four subchannels generated from the split of the spectrum of the square root raised-cosine shaping pulse with 35% roll-off, and the overlap space. The five subspaces are, in order of increasing center frequency, the channels C_0,C_1,C_3 and C_2 of section 2.5.4, and the overlap subchannel, using method 3.

Figure 2.12.   Magnitude (in dB) and group delay of the channel transfer function considered in Section 2.5.4.

2.6   A novel wavelet for modulation: the Modified Gaussian

In this section we present a wavelet with very low sidelobes whose spectral occupancy in the frequency domain is controlled by a parameter that can assume any positive real value. The associated scaling function is derived from the Gaussian waveform. Due to its good spectral characteristics, this function is well suited as an elementary shaping pulse for digital modulation.

An undesirable feature commonly observed in wavelets found in the literature in connection with their use as elementary shaping pulses for modulation is that their spectral occupancy is not parametrically defined, and can vary from one wavelet family to another. Hence, when selecting a suitable wavelet shaping pulse in a communication system, it is necessary to examine a particular family of wavelets to determine its suitability given the available bandwidth. It would be desirable to have a parametrically defined wavelet, having a feature like the square-root raised-cosine shaping pulse, whose spectral occupancy and excess bandwidth are controlled (although to a limited extent) by the roll-off parameter.

In fact, the square-root raised-cosine pulse satisfies the Dyadic scaling equation and is therefore a scaling function, but only for values of the roll-off parameter less than $1/3$. To the best of our knowledge, there are no parametrically defined wavelets with good spectral characteristics with a parameter whose value can vary over the entire positive real axes.

2.6.1   The Modified Gaussian

The wavelet presented here is obtained by applying the *orthogonalization trick* [25] to a Gaussian waveform. It is known that this trick preserves some properties of the original function and, if successful, allows the creation of a new family of wavelets in the multiresolution analysis toolbox.

The use of the Gaussian waveform as a starting point in the application of the orthogonalization trick is motivated by the fact that this function has excellent Time-Bandwidth product near the uncertainty bound [72], in addition to being parametrically defined with the parameter being the variance of the pulse.

Note that the original Gaussian waveform is not shift-orthogonal and its use as an elementary pulse in a coherent modulation scheme causes inter-symbol interference even on a channel with flat spectrum.

In what follows, we describe the construction of the modified Gaussian wavelet using the procedure presented in [25]:

1. choose a function $s(t)$ with good decay characteristics in both the time and frequency domains satisfying the two relations

$$s(t) = \sum_{n \in \mathcal{Z}} c_n s(2t - n\Delta)$$

$$0 < \alpha \leq \sum_{l \in \mathcal{Z}} \left| S\left(f + \frac{l}{\Delta}\right) \right|^2 \leq \beta < \infty$$

and having a nonzero integral. We chose the Gaussian waveform

$$s(t) = \frac{1}{2\sigma\Delta\sqrt{\pi}} e^{-\frac{t^2}{4\sigma^2\Delta^2}}$$

where Δ denotes the eventual shift orthogonality period of the or-thonormal pulse to be derived, and $4\sigma^2\Delta^2$ is the pulse variance in time. It can be verified that this pulse satisfies all the required properties;

2. if necessary, perform the orthogonalization trick

$$\Phi(f) = S(f) \left[\sum_{l \in \mathcal{Z}} \left| S\left(f + \frac{l}{\Delta}\right) \right|^2 \right]^{-1/2} .$$

on the Gaussian waveform, which is not shift orthogonal. The Fourier transform of $s(t)$ is

$$S(f) = e^{-\sigma^2\Delta^2(2\pi f)^2} .$$

Applying the orthogonalization trick to $S(f)$ we obtain the function

$$\Phi(f) = \frac{e^{-\sigma^2\Delta^2(2\pi f)^2}}{\sqrt{\sum_{l \in \mathcal{Z}} e^{-8\sigma^2\Delta^2\pi^2(f+l/\Delta)^2}}} \tag{2.16}$$

whose inverse Fourier transform $\phi(t)$ can play the role of a scaling function in the Dyadic multiresolution analysis;

3. determine the corresponding wavelet $\psi(t)$ according the following pro-cedure:

a) find $M_1(f) = M_0(f)W_{2/\Delta}(f) = \frac{\Phi(f)}{\Phi(f/2)}W_{2/\Delta}(f)$ where the window function $W_{2/\Delta}(f)$ is 1 in the interval $-1/\Delta \leq f < 1/\Delta$ and zero outside. $M_0(f)$ itself is periodic and the above expression gives the value of the function in its principal period;
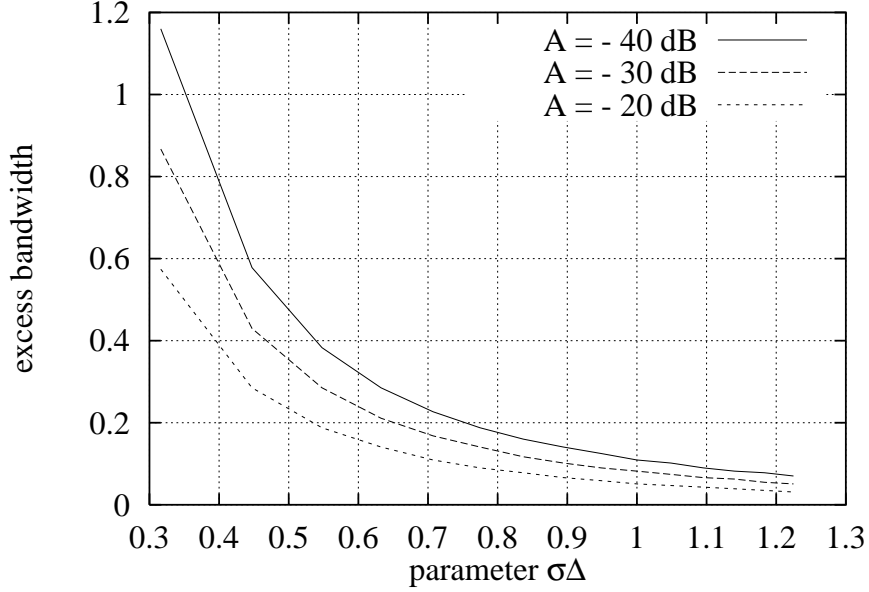
Figure 2.13.   Excess bandwidth of $\phi(t)$ vs. $\sigma\Delta$ for $A = -20, -30, -40$ dB.

b) the Fourier transform of the wavelet is given by

$$\Psi(f) = \Phi(f/2) \sum_{n \in \mathcal{Z}} M_1^*(f + (2n + 1)/\Delta)$$

where $M^*(.)$ denotes complex conjugate of M.

From equation (2.16) it should be evident that the spectral occupancy of the scaling function and the associated wavelet is dependent on the parameter $\sigma\Delta$, which can assume any positive real value and directly controls the spectral characteristics of the shaping pulses. We define the *excess bandwidth* γ of $\phi(t)$ as the value that satisfies the relation

$$20 \log \left| \Phi \left(\frac{1}{2\Delta} + \frac{1}{2\Delta}\gamma \right) \right| = A \ dB \ .$$

A plot of γ versus the parameter $\sigma\Delta$ for $A = -20, -30, -40$ dB is reported in figure 2.13.

The good decay of the derived scaling function in both the time and frequency domains suggest that this waveform is an excellent candidate as a shaping pulse for modulation purposes. In practical applications, the shaping

42
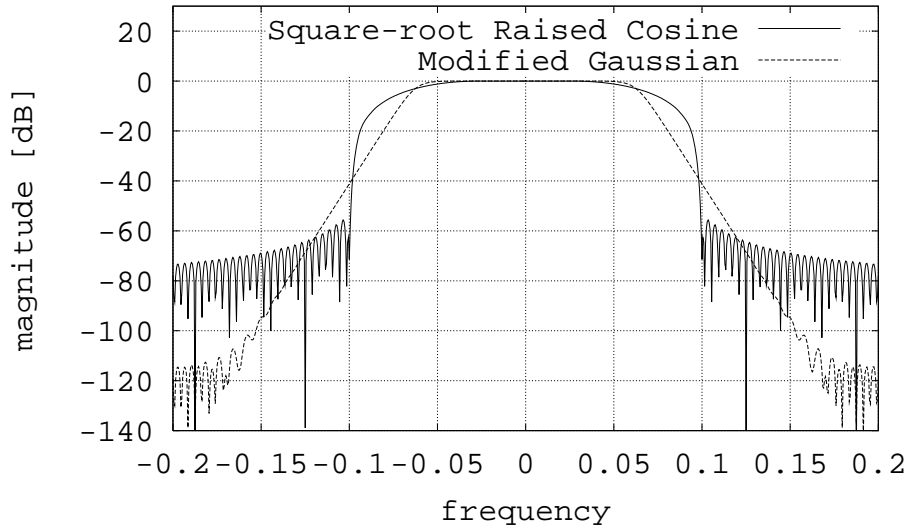
Figure 2.14.   Magnitude of the Fourier transform of $\phi(t)$ with $\sigma\Delta = 0.447$ and the square-root raised-cosine with roll-off $\beta = 0.29$ and the same excess bandwidth $\gamma = 0.30$ measured at a level of -40 dB ($\Delta = 1$). Both waveforms implemented as FIR filters with 256 taps.

pulse must be sampled to provide a FIR implementation. The good time domain decay characteristic of $\phi(t)$ allows us to approximate the shaping pulse with a FIR filter with relatively small number of taps, and the good decay of the magnitude of $\Phi(f)$ in the frequency domain guarantees that practical realizations of $\phi(t)$ provide very low sidelobes. Figure 2.14 depicts the magnitude of the Fourier transform of $\phi(t)$ with $\sigma\Delta = 0.447$ ($\gamma = 0.57$ for $A = -40$ dB) and the square-root raised-cosine waveform with the same excess bandwidth. Both waveforms have unit energy and are implemented as FIR filters with 256 taps. Figure 2.15 depicts the scaling function $\phi(t)$ with $\sigma\Delta = 0.447$ and the corresponding wavelet $\psi(t)$.
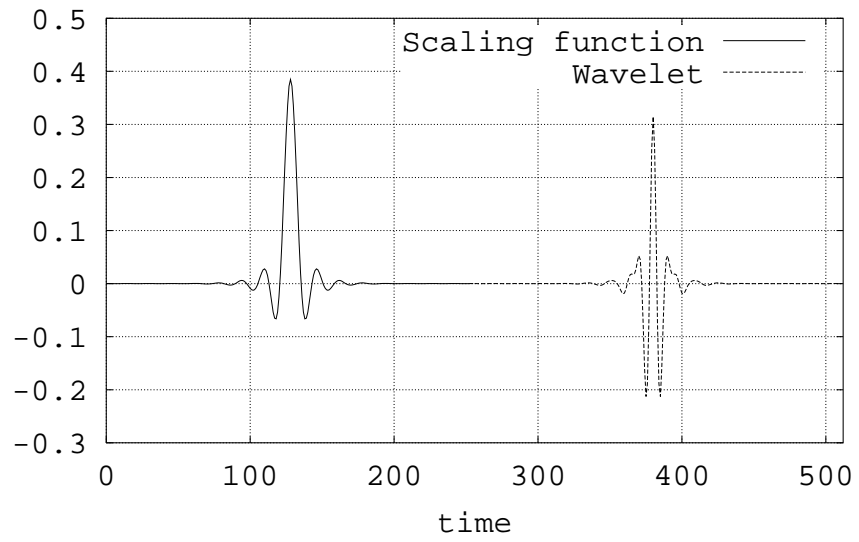
Figure 2.15.   The scaling function $\phi(t)$ with $\sigma\Delta = 0.447$ and the corresponding wavelet $\psi(t)$.

Chapter 3

Comparative study of wavelet waveforms over linear and non-linear channels

3.1 Introduction

At this point it is interesting to compare the performance of different wavelet families with classic waveforms like square-root raised cosine with roll-off β [22] on different channels, including non-linear channels and channels affected by multipath propagation. It should be recalled, however, that the square-root raised cosine with roll-off $\beta \leq 1/3$ is a Meyer scaling function [25] itself with $\nu(x) \in \mathcal{C}^1$, where $\mathcal{C}^1$ is the class of once differentiable continuous functions of compact support. We also recall that the roll-off β is the *theoretical excess bandwidth*, and is generally different from the actual excess bandwidth γ which depends on the actual filter implementation and the selected $X-$dB bandwidth.

3.2 Wavelet Waveforms over Linear Channels

3.2.1 Single Pulse Modulation

Wavelet families provide a set of shift-orthogonal pulses that can be used as elementary waveforms for modulation. As seen in the previous sections, the shift orthogonality implies the satisfaction of the Nyquist I criterion, so that on AWGN channel no ISI is present. This is true for the transmission of a single pulse (e.g. the scaling function).

Aside from spectral efficiency, another goal of multiple waveform design for modulation is sensitivity to timing errors. As far as the symbol timing

synchronization performance of scaling functions is concerned, the normalized timing jitter of Meyer scaling function and square-root raised cosine with roll-off $\beta = 0.29$ and the same excess bandwidth of $\gamma = 0.3$ at a level of -40 dB is shown in Fig. 3.1. The results are obtained by simulating a Maximum Likelihood symbol timing recovery [65] scheme with oversampling factor of 32. A gain of roughly a factor 3 of the Meyer scaling function with respect to the square-root raised cosine can be observed for SNR values greater than 10.

It can also be observed that the use of scaling functions as waveforms for modulation allows the implementation of jitter-free timing synchronization schemes [5], exploiting the information contained in the orthogonal space, spanned by the associated wavelet waveform.

3.2.2 Double Pulse Modulation

In connection with the procedure outlined in section 2.3 for improving the spectral efficiency, let us consider two possible scenarios employing double pulse modulation.

Case-study 1

Consider the Daubechies scaling function and wavelet of length 39 (i.e., with $N = 20$) and $\Delta = 1$. It can be verified that the overlap space with orthogonality period of wavelet and scaling function set to $\Delta = 1$, occupies the frequency band (0.3 Hz, 0.7 Hz) [1]. We would like to generate an orthogonal basis for this overlap space by filtering the continuous wavelet $\psi(t)$ with a proper orthonormal sequence. We consider using the sequences $h[n]$ and $g[n]$ that were used to generate the scaling function and wavelet as the coefficient system for generating the desired basis. A possible basis for this subspace is given by

$$b(t) = \sum_n \sum_k h[n]g[k]\psi(t - 2n - k). \tag{3.1}$$

with Fourier transform

$$B(f) = H(e^{j4\pi f})G(e^{j2\pi f})\psi(f)$$

where $H(e^{j2m\pi f}) = \sum_n h[n]e^{-j2nm\pi f}$. The basis for the overlap space derived above are orthonormal with shift period of four. Hence, together with the scaling function we can generate 1.25 dimensions per unit time. The composite magnitude response has a -40 dB bandwidth of 0.68 Hz and excess bandwidth equal to 0.087.

47

$\diamond$

Case-study 2

For the second case-study of this section we use the Meyer wavelet with Fourier transform

$$\Psi(f) = e^{j\pi f}[\Phi(f+1) + \Phi(f-1)]\Phi(f/2), \tag{3.2}$$

where, $\Phi(f)$ is the Fourier transform of the Meyer scaling function $\phi(t)$ and we have chosen $\nu(x) = 0.5[1 + cos(\pi(x-1))]$ for $0 \le x \le 1$, for the construction of this scaling function [25], i.e. the $\nu(x) \in \mathcal{C}^{\infty}$ case. Following our normalization (i.e., $\Delta = 1$), the Meyer scaling function when used as a shaping pulse by itself generates one dimension per unit time using a bandwidth of 0.666 Hz. The excess bandwidth of this scheme is therefore 0.33. The spectra of the Meyer scaling function and wavelet overlap in the frequency range $1/3 \le |f| \le 2/3$, thus defining the overlap space. The highpass optimized multiplicity-3 Perfect Reconstruction filter in [67] can be used to produce the filtering effect desired to generate the basis of the overlap space. The impulse response $s_2[n]$ of this filter is shift orthogonal with shift period 3.

The basis function for the overlap space and the corresponding spectrum of this shaping pulse are depicted in Fig. 3.2. The basis for the overlap space in this case can be used at a rate of 1/3. The composite modulation rate when using the Meyer scaling function and the basis for the overlap space is therefore 4/3. The -40 dB bandwidth of this modulation scheme is 0.752 Hz and therefore the composite modulation scheme has an excess bandwidth equal to 0.128. The filter bank implementation of the transmitter and matched-filter receiver for the described modulation scheme is depicted in Fig. 3.3, where (a) is the scaling function channel and (b) is the overlap space channel.

$\diamond$

3.2.3 Multiple Pulse Modulation

Thanks to the orthogonality of the pulses at different scales and between scaling function and wavelet, it is also possible to generate wavelet-based signals spanning orthogonal subchannels of the frequency domain. On AWGN channel the orthogonal signals can be recovered using a bank of matched filters, which can also be implemented as decimated filter bank, as shown in Case-study 7 in what follows.
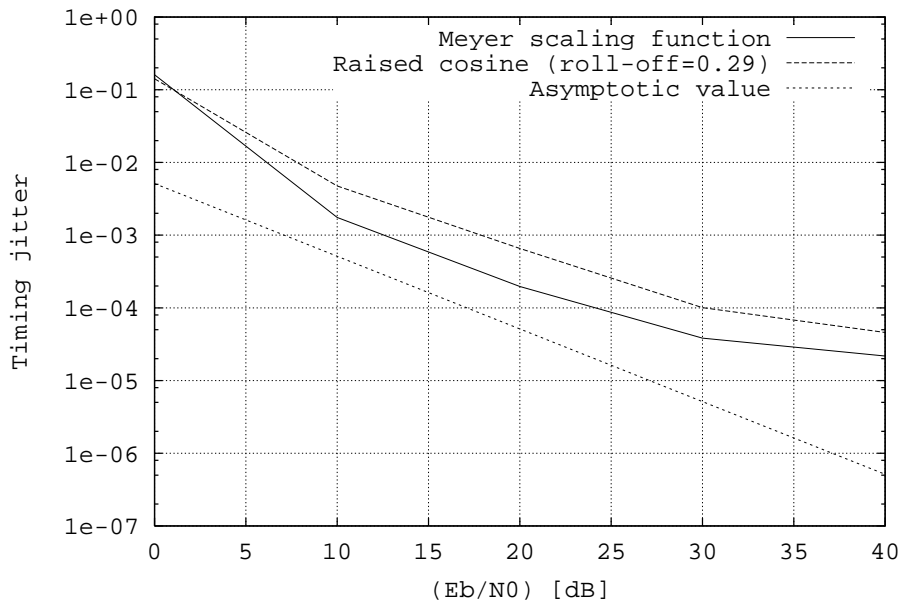
Figure 3.1.   Normalized timing jitter of Meyer scaling function and square-root raised cosine with roll-off $\beta = 0.29$ and the same excess bandwidth $\gamma = 0.3$. Both waveforms are generated using 256-taps FIR filters. The asymptotic lowerbound is also shown for comparison.

As far as the multichannel symbol timing synchronization is concerned, it is possible to show [4] that the splitting sequences used to split the spectrum of a shaping pulse to generate orthogonal frequency subchannels *do not effect* on the variance of the timing jitter in the tracking mode (at least, in a first order approximation). This variance is *totally determined* by the original shaping pulse whose spectrum is split and is critically dependent on its excess bandwidth.

3.3   Wavelet Waveforms over Non-Linear Channels

In this section we will present simulation results for wavelet based shaping pulses over satellite and multipath fading channels. In the case of satellite channel, we consider a scenario whereby the satellite acts purely as a transponder. The system scheme is depicted in Fig.3.4; we assume that the SNR on the uplink is high, so that the uplink noise may be insignificant and
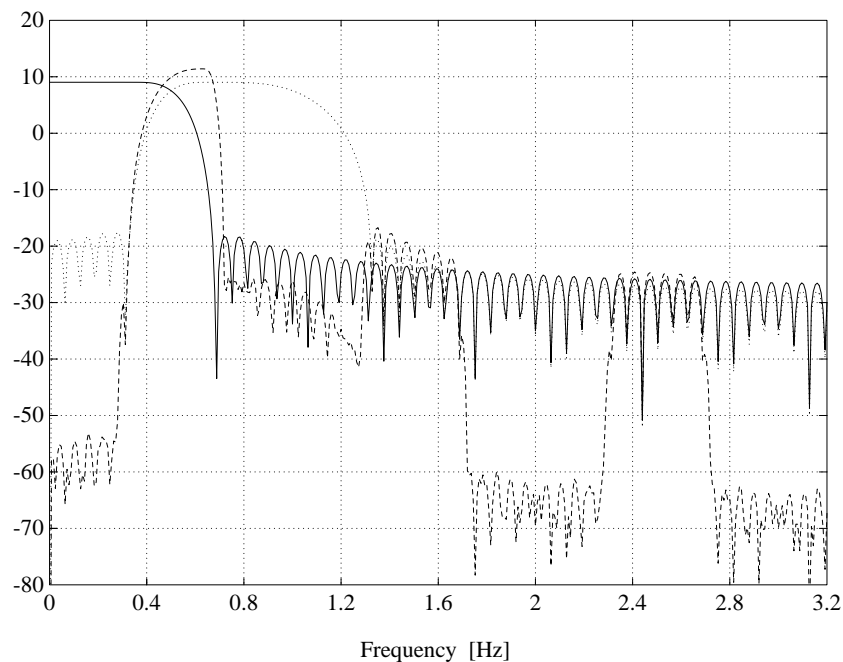
Figure 3.2.   Spectra of the Meyer scaling function, wavelet, and basis for
the overlap space of Case-study 2 ($\Delta = 1$).

therefore omitted from further consideration. Hence, the only noise present
in the system is the downlink noise. The frequency division multiplexed sig-
nals arriving at the satellite are amplified by a Traveling Wave Tube (TWT)
amplifier whose back-off parameter should be optimized in order to achieve
the highest possible SNR at the receiving station. The AM/AM and the
AM/PM characteristics of the considered TWT are reported in Fig.3.5. Due
to the complexity of the model, analytical performance evaluation of such a
system is practically impossible. Hence, we evaluate the performance of the
system using simulation.

Unless stated otherwise, the simulation results presented in the follow-
ing have been obtained by assuming ideal clock and carrier recovery. The
statistics of ISI and InterChannel Interference (ICI) have been derived by
Montecarlo simulation, and the bit error probabilities obtained by averaging
those statistics. All the filters used were simulated by 256-taps FIR filters
with an oversampling factor of 8. The measure used to compare the per-
formances is the required energy per bit versus noise power spectral density
at saturation $(E_b/N_0)_{sat}$ to have an error probability of $P(e) = 10^{-5}$ versus
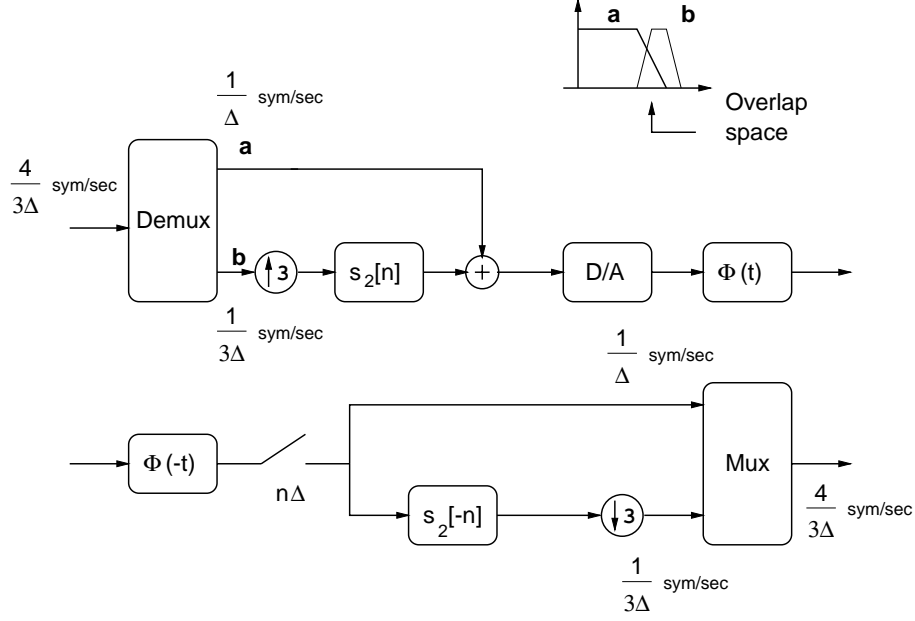
Figure 3.3.   The synthesis and analysis trees used at the transmitter and receiver for the double pulse modulation scheme of Case-study 2, based on Meyer scaling function and overlap space.
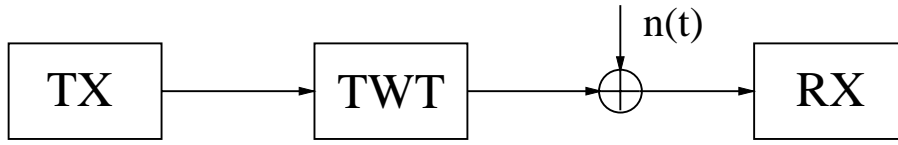
Figure 3.4.   Block Diagram of a satellite communication channel.

the input back-off of the non-linear amplifier. Minimization of the factor $(E_b/N_0)_{sat}$ corresponds to the minimization of the cost function:

$$10 \log_{10} \left[\left(\frac{E_b}{N_0} \right)_{sat} \right] = 10 \log_{10} \left[\left(\frac{E_b}{N_0} \right) \right] + 10 \log_{10} \left[\left(\frac{P_{out\_sat}}{P_{out}} \right) \right], \qquad (3.3)$$

where the terms in the right hand side of equation (3.3) are respectively the actual (E_b/N_0) required to obtain $P_b(e) = 10^{-5}$ and the *output backoff* of the non-linear amplifier. From a power efficiency point of view it is desirable to operate the TWT in saturation. However, this can cause severe signal distortion requiring a larger E_b/N_0 to offset the effect, given that $P_b(e)$ is

51
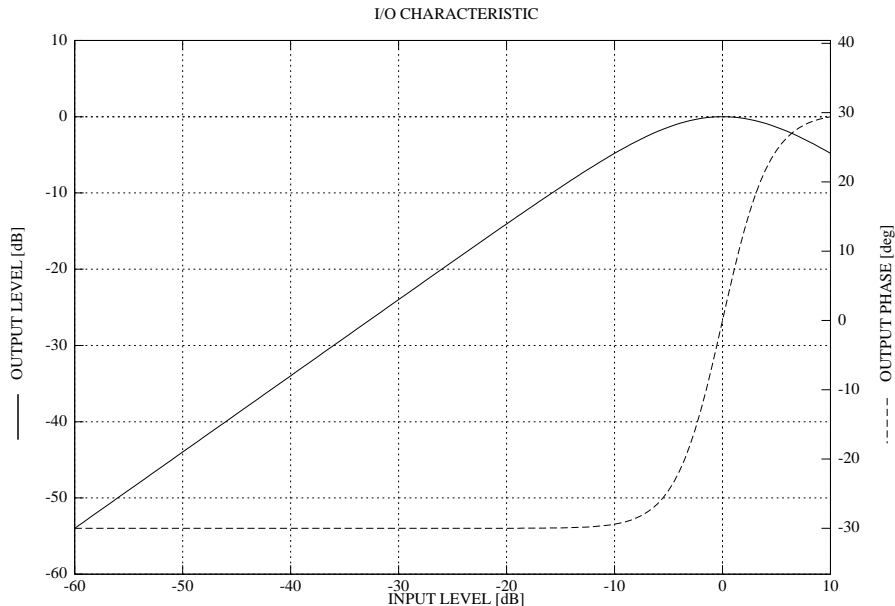
I/O CHARACTERISTIC

Figure 3.5.   The normalized AM/AM and the AM/PM charachteristics of the Travelling Wave Tube.

fixed. Hence, the joint minimization of the two terms is required because while minimization of the first term means to decrease the signal distortion fixing the working point on the linear part of the amplifier AM/AM characteristic, it is also required to efficiently exploit the amplifier itself minimizing the output power loss relative to the saturation point.

3.3.1   Single Pulse Modulation

In this section, we will be concerned with the transmission of a single pulse, the scaling function, on a satellite channel. We compared the performances of Daubechies with $N = 20$, Battle-Lemarié with different values of the degree N and Meyer scaling functions [25]. In particular, the Meyer scaling function with function $\nu(x) \in \mathcal{C}^\infty$ [25] has been considered. We also analyzed the new scaling function, the Modified Gaussian, that introduced in chapter 3. Its spectral efficiency is tuned by a parameter σ and it has good characteristics in the frequency domain (essentially low sidelobes). The magnitude of the Fourier transform of the Modified Gaussian scaling function with symbol period $\Delta = 1$ is depicted in Fig. 2.14, where it is compared to a square-root raised cosine with the same excess bandwidth $\gamma = 0.30$ (measured at a -40

dB level).

In Table 3.1, the losses of some scaling functions belonging to different wavelet families with respect to the square-root raised cosine with the same excess bandwidth γ measured at -40 dB are reported. As it can be observed, no scaling function by itself manages to outperform the square-root raised cosine on a non-linear channel, but the Modified Gaussian waveform scaling function shows very similar performances. Since the square-root raised cosine with roll-off $\beta \leq 1/3$ is a particular case of Meyer scaling function, some of the comparisons of Table 3.1 can be considered a comparison between different types of scaling functions. While the use of orthogonal scaling functions corresponds to a pair of matched transmit-receive filters, the use of a biorthogonal waveform allows the presence of non-matched transmit-receive filters still preserving the zero ISI property of the demodulated signals. One may wonder if a well chosen pair of transmit and receive filters could lead to better performances on a non-linear channel with respect to the orthogonal systems, since on this channel the optimum receiver filter is not a matched filter. To answer this question we examined biorthogonal spline scaling functions and obtained a loss of 0.97 dB with respect of the square-root raised cosine with the same spectral efficiency. If we deal with a more complex

Scaling function	loss vs. raised cosine	γ	β
Daubechies N=20	2.2 dB	0.37	0.37
Battle-Lemarié N=6	0.89 dB	0.31	0.31
Battle-Lemarié N=8	0.97 dB	0.26	0.25
Meyer	0.27 dB	0.30	0.29
Mod. Gaussian $\sigma\Delta = 1$	0 dB	0.072	0.070
biorthogonal spline	0.97 dB	0.5	0.5

Table 3.1. Comparison of scaling functions vs. square-root raised cosine with the same excess bandwidth γ on non-linear channel. Square-root raised-cosine has roll-off β and is implemented using a 256-taps FIR filter.

transmission scenario in which a useful channel suffers from interference due to neighboring channels, we can appreciate some advantages of wavelet based waveforms. In particular, we can verify if the substantial lack of sidelobes of the Modified Gaussian scaling function [9] can reduce the ICI due to the enlargement of the spectra after the non-linear amplifier.

`Case-study 3`

We considered a Frequency Division Multiplexed (FDM) system in which the available bandwidth has to be shared by many users, and a reduced guard band is desirable to increase the capacity of the overall system. We considered a Modified Gaussian waveform with $\sigma\Delta = 0.447$, which corresponds to an excess bandwidth $\gamma = 0.57$ measured at -40 dB. The separation between center frequencies of the channels is $0.575/T_b$, where T_b is the bit duration and QPSK modulation scheme is employed, with $\Delta = 2T_b$. The power spectra of the useful channel with the two interfering channels considered in this case study are depicted in Fig. 3.6 for $\Delta = 1$, where Δ is the symbol period. The actual gain in the signal-to-noise ratio necessary to achieve an error probability of 10^{-5} is roughly 4 dB as can be seen from Fig. 3.7 with respect to the square-root raised cosine with roll-off $\beta = 0.57$, having the same spectral occupancy and implemented with the same number of taps. The Modified Gaussian waveform allows a larger overlap between adjacent channels with reduced cross-talk after the non-linear amplifier. Using the Modified Gaussian waveform more channels can be allocated, increasing the overall capacity of a system in which the total available bandwidth is fixed to guarantee the compatibility with the preexistent systems.

A different result can be obtained if, instead of comparing waveforms with the same excess bandwidth, we separately optimize the spectral occupancy of each signal in terms of required signal power for a given error probability, given the available channel bandwidth. The result of this procedure is shown in Fig. 3.8, where the curves for the square-root raised cosine with roll-off $\beta = 0.5$ and for the Modified Gaussian waveform with $\sigma\Delta = 0.35$ are depicted, with frequency separation between channels of $0.65/T_b$. It can be observed that both the square-root raised cosine and the Modified Gaussian achieve practically the same performances, with different excess bandwidth values.

$\diamond$

3.3.2   Double pulse modulation

In this section we present the E_b/N_0 performance of double pulse modulation over single and multiple access non-linear channels. The proposed schemes present very high spectral efficiencies, and -33 dB bandwidth measures have been used for these particular cases.
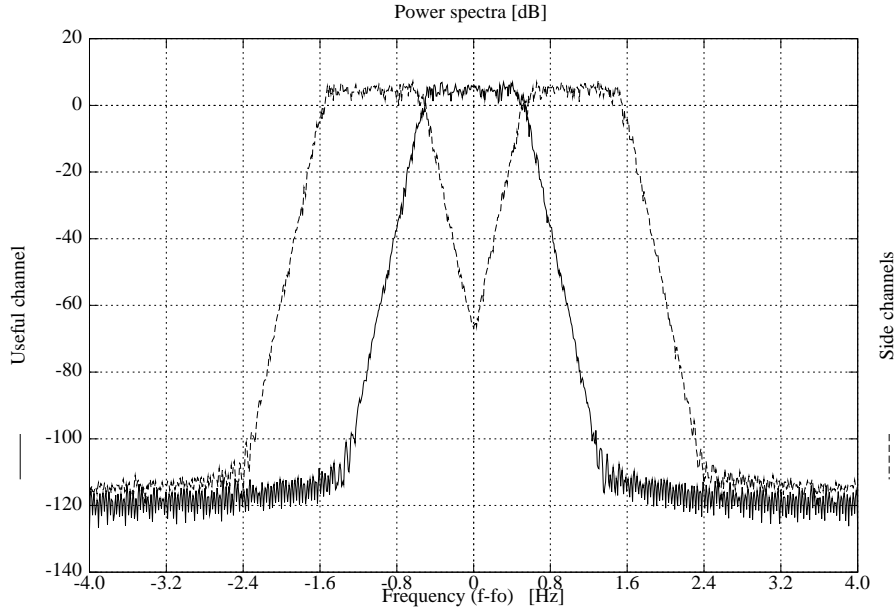
Figure 3.6.   Spectra of 3-channel FDM system with separation between channel center frequencies of $0.575/T_b$ and $\Delta = 1$, employing the Modified Gaussian shaping pulse with $\sigma\Delta = 0.447$ and $\gamma = 0.57$ measured at -40 dB (Case-study 3).

Case-study 4

As first case-study of double pulse modulation over non-linear satellite channel we present the comparison between the following schemes:

1. a QPSK scheme with bit duration T_b, using a square-root raised cosine shaping pulse with roll-off $\beta = 0.07$;

2. a *composite* scheme obtained as the superposition of two orthogonal subchannels employing QPSK constellations. The first subchannel operates at full rate (two bits every $\Delta = 3T_b$ seconds) and uses as shaping pulse an order-8 Battle-Lemarié scaling function, while the second subchannel operates at half rate (two bits every 2Δ seconds) and uses as shaping pulse the corresponding waveform spanning the overlap space.

   The basis for the overlap space has been obtained by filtering the order-8 Battle-Lemarié wavelet with an order-8 Battle-Lemarié wavelet vector.

55
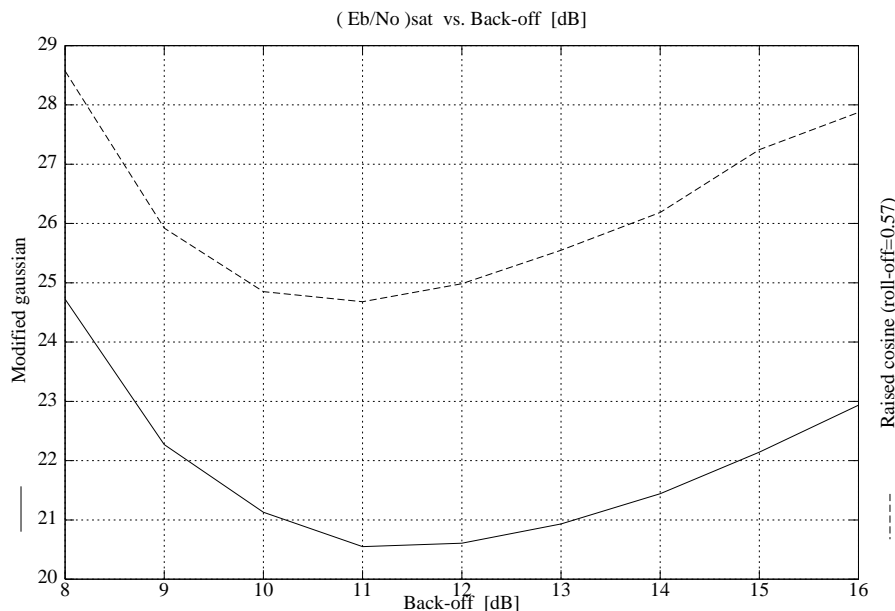
Figure 3.7. The required $(E_b/N_0)_{sat}$ versus the input back-off of the non-linear power amplifier for the Modified Gaussian waveform scaling function ($\sigma\Delta = 0.447$) and the square-root raised cosine ($\beta = 0.57$) with the same spectral efficiency in a FDM system with separation $0.575/T_b$ between center frequencies (Case-study 3).

These two schemes have the same -33 dB bandwidth requirement, and their excess bandwidth is 0.072. Simulations show a loss of roughly 1.5 dB of the composite scheme with respect to the single pulse scheme.

$\diamond$

The motivation for simultaneous use of the scaling function and overlap function subchannels in FDM systems with non-linearity is that it allows for a natural separation of the available spectrum into two parts. The first, is the scaling function subchannel which is less effected by ICI due to its smaller bandwidth; the second, is the overlap function subchannel which is more effected by ICI. Further subdivision of the part of the spectrum that is less effected by ICI is not necessarily desirable since such a subdivision would elongate the pulses in the time domain causing more distortions and cross-talk at the output of the non-linear amplifier.
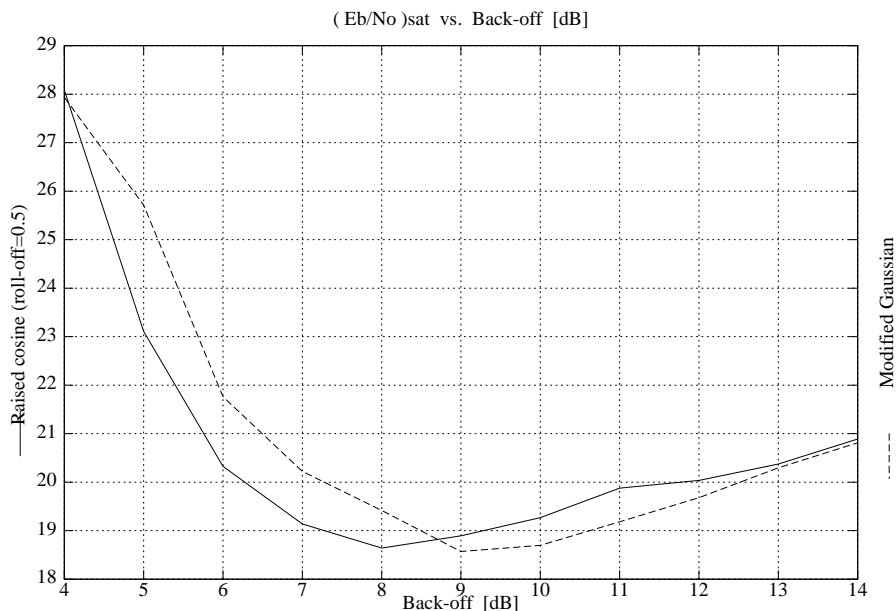
Figure 3.8.   The required $(E_b/N_0)_{sat}$ versus the input back-off of the non-linear power amplifier for the Modified Gaussian waveform scaling function ($\sigma\Delta = 0.35$, $\gamma = 1.054$ at -40 dB) and the square-root raised cosine ($\beta = 0.5$, $\gamma = 0.5$ at -40 dB). Both pulses are optimized to achieve the best performances in the FDM system with a separation between center frequencies of $0.65/T_b$ (Case-study 3).

Case-study 5

For our second double pulse case-study, in order to compare the performance of the wavelet-based shaping pulses with the standard techniques, we considered the following schemes:

1. a QPSK scheme with bit duration T_b, using a square-root raised cosine shaping pulse with roll-off $\beta = 0.072$;

2. a *composite* scheme obtained as the superposition of two orthogonal subchannels employing QPSK constellations. The first subchannel operates at full rate (two bits every $\Delta = 3T_b$ seconds) and uses as shaping pulse an order-6 Battle-Lemarié scaling function, while the second one operates at half rate (two bits every 2Δ seconds) and uses as shaping pulse the corresponding waveform spanning the overlap space. The basis for the overlap space has been obtained by filtering the order-6
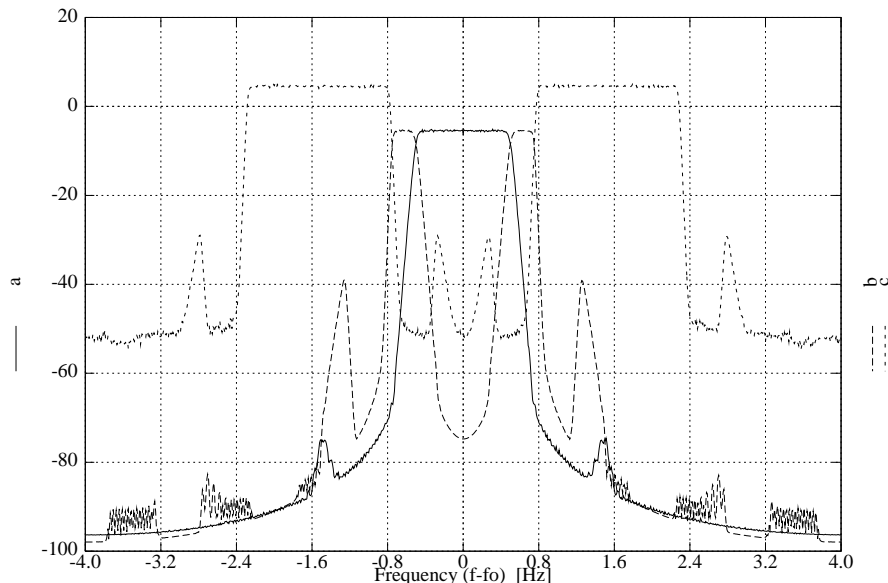
Figure 3.9.   Power spectral density of the overlap space (b) and the scaling function subchannel (a), that compose the useful channel of Case-study 5 (the center channel), and the interfering side channels (c).

Battle-Lemarié wavelet with an order-6 Battle-Lemarié wavelet vector.

These two schemes have the same -33 dB bandwidth requirement, and their excess bandwidth is 0.088.

The power spectra of the two subchannels that generate the composite scheme are shown in Fig. 3.9 for $\Delta = 1$. The two subchannels overlap in frequency, but their orthogonality is assured by the time-correlation properties of the scaling function and wavelet.

The individual FDM channels have a separation between center frequencies of $0.51/T_b$. In our simulations, we consider the useful channel plus two side interfering channels as shown in Fig. 3.9. In this environment, different channels may experience different propagation conditions. In order to examine a particularly critical condition, we assumed that the useful channel is attenuated by 10 dB relative to the interfering side channels. Fig. 3.10 shows the signal-to-noise ratio at saturation $(E_b/N_0)_{sat}$ needed to achieve a bit error probability of 10^{-5}, versus the input back-off of the amplifier. It can be observed that in this very critical condition, the wavelet-based shaping pulses outperform the square-root raised cosine by roughly 1.7 dB. The

58
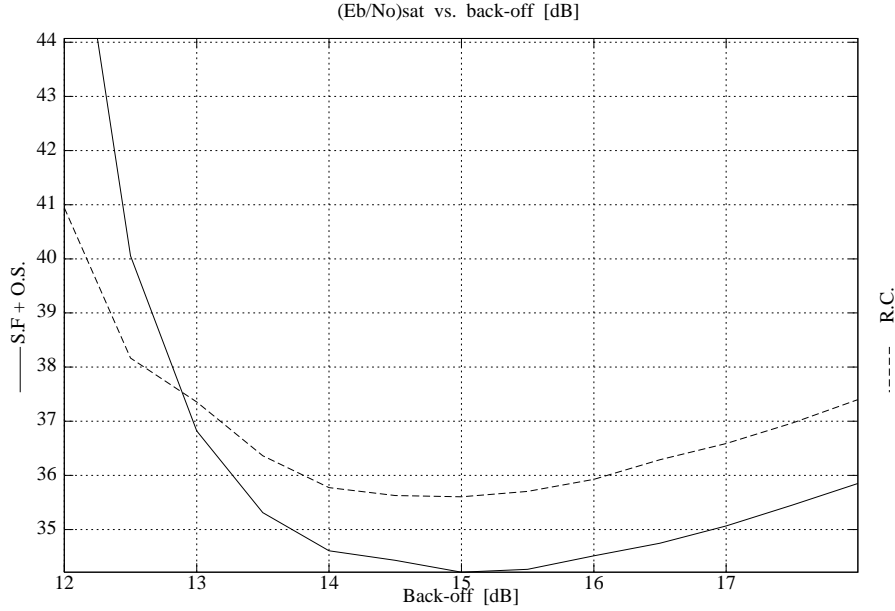
Figure 3.10. $(E_b/N_0)_{sat}$ in dB versus input back-off of the non-linear power amplifier for the channels considered in Case-study 5: composite channel, using the scaling function and overlap space function (S.F. + O.S.), and the channel based on the square-root raised cosine function (R.C.).

performance loss of the scheme employing the square-root raised cosine is mainly due to the sidelobes of the transfer function that are high because of the very small roll-off. It should also be noted that the performance of the wavelet-based waveforms are less encouraging on less critical channels.

◇

Case-study 6

For our third double pulse case-study, we considered the following schemes:

1. a QPSK scheme with bit duration T_b, using a square-root raised cosine shaping pulse with roll-off $\beta = 0.069$;

2. a *composite* scheme obtained as the superposition of two orthogonal subchannels employing QPSK constellations. The first subchannel operates at full rate (two bits every $\Delta = 2.5T_b$ seconds) and uses as

59

(Eb/No)sat vs. back-off [dB]
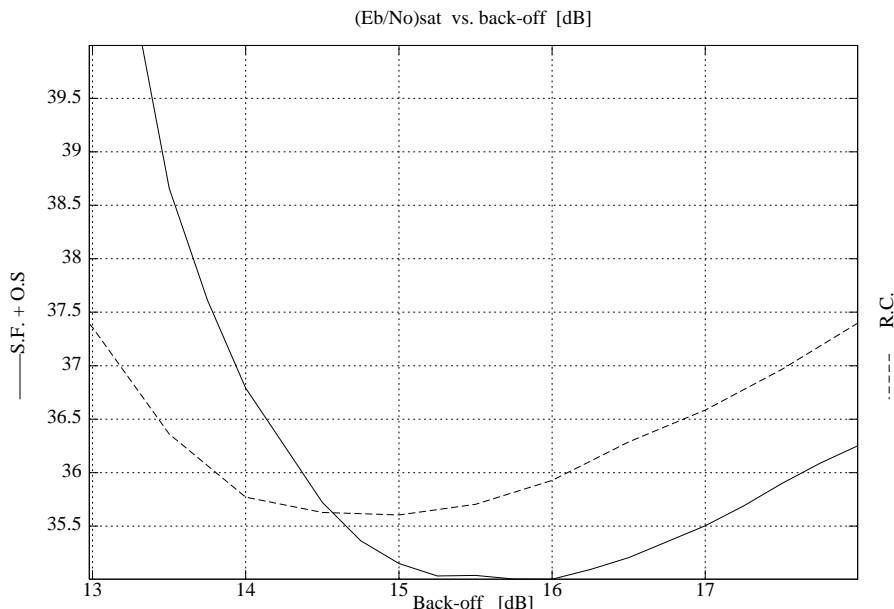
Figure 3.11. $(E_b/N_0)_{sat}$ in dB versus input back-off of the non-linear power amplifier for the channels considered in Case-study 6: composite channel, using the scaling function and overlap space function (S.F. + O.S.), and the channel based on the square-root raised cosine function (R.C.).

shaping pulse the order-20 Daubechies scaling function of Case-study 2, while the second one operates at one fourth the rate (two bits every 4Δ seconds) and uses as shaping pulse the corresponding waveform spanning the overlap space. The basis for the overlap space is expressed in equation (3.1).

These two schemes have the same -33 dB bandwidth requirement, and their excess bandwidth is 0.065. The individual FDM channels have a separation between center frequencies of $0.5125/T_b$ and, as in the previous example, the useful channel experiences an attenuation of 10 dB with respect to the two interfering side channels.

Fig. 3.11 shows the signal-to-noise ratio at saturation $(E_b/N_0)_{sat}$ needed to achieve a bit error probability of 10^{-5} versus the input back-off of the amplifier. From Fig. 3.11 it can be observed that the wavelet based scheme gains roughly 0.6 dB in comparison to the scheme employing a square-root raised cosine shaping pulse. It can be verified via simulation that for a given input back-off, the scaling function subchannel offers a lower bit error rate

60

in comparison to the overlap space subchannel. This behavior is mainly due
to the fact that the overlap space subchannel is more effected by ICI.

⬦
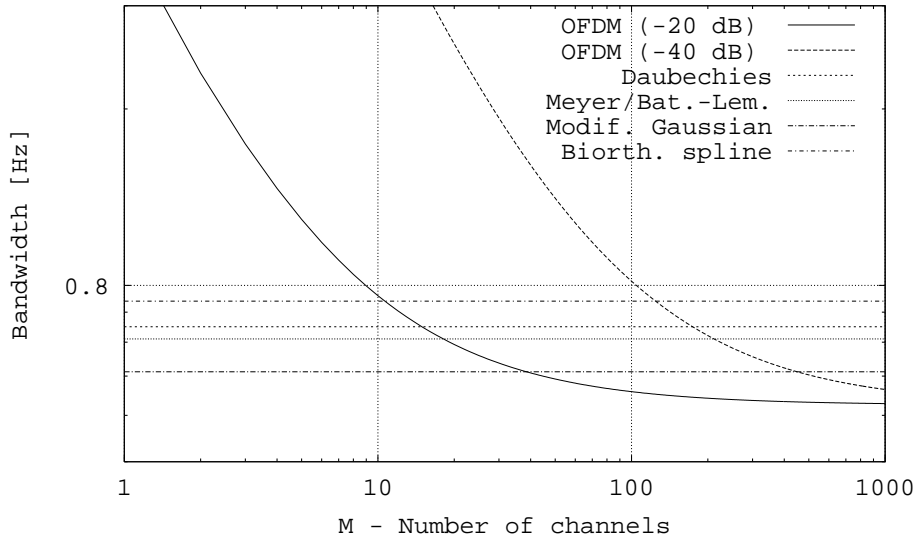
Figure 3.12.   -40 dB bandwidth occupation of the M-channel rectangular
pulse OFDM scheme and M-channel WOFDM schemes based on the fol-
lowing scaling functions: Daubechies ($N = 20$), Battle-Lemariè ($N = 6$
and $N = 8$) and Meyer, Modified Gaussian, and biorthogonal spline. The
-20 dB bandwidth of OFDM is also shown for comparison.

3.3.3   Multiple Pulse Modulation

Use of splitting sequences to obtain a new channel subdivision with the de-
sired spectral features can be generalized to more than two channels. The
resulting system can be considered a particular case of MultiCarrier Modu-
lation (MCM) that we denoted WOFDM [2].

It is well known that multicarrier systems have good properties on dis-
persive channels which exhibits great variations in gain across their available
bandwidth. In an ideal multicarrier system the effect of the fading channel
on each carrier can be accurately modeled as a different attenuation and
phase shift affecting each subchannel, thus allowing an easy equalization of
the various subchannels. In MCM systems it is also possible to optimize
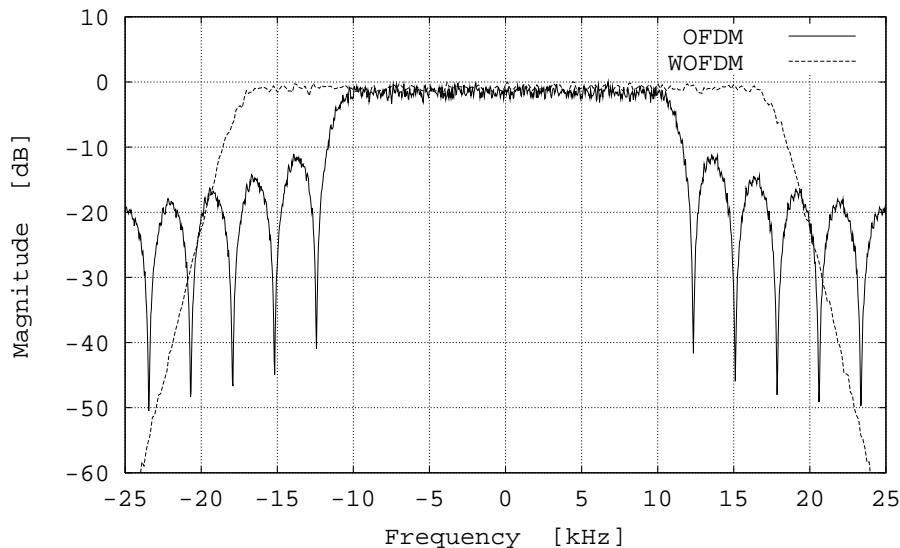
Figure 3.13.   Power spectral densities of the 8-channel OFDM (a) and WOFDM (b), with $\Delta = 227.56\mu s$ (Case-study 7).

the allocation of the data stream on the various channels. The most famous multicarrier system is the OFDM [64], which uses a set of orthogonal tones, and has been adopted as standard for the HDTV.

Use of different shaping pulses for multicarrier modulation on particular channels has been investigated in [68, 64].

The literature on the OFDM always considers a large number of carriers, because the spectral efficiency of the system increases with the number of channels. WOFDM can be considered an alternative to OFDM for a small number of channels, with a bandwidth occupation that is much smaller than OFDM. To give an idea of this phenomenon, we reported in Fig. 3.12 the -40 dB bandwidth occupation of the standard rectangular pulse used in the OFDM scheme together with various WOFDM schemes as a function of the number of channels M. A normalized symbol time $\Delta = 1$ is considered. As it can be observed from Fig. 3.12, because of the high side lobes of the $sinc(.)$ function, the OFDM scheme has high bandwidth occupation for low values of M, while its bandwidth decreases as M increases. The bandwidth occupation of WOFDM does not depend on M, since it is always the bandwidth of the original scaling function. The OFDM scheme becomes spectrally more efficient than WOFDM for values of M ranging between 100 and 400, depending on the type of scaling function. The -20 dB bandwidth of OFDM is

also shown for comparison.

Another difficulty that arises in using WOFDM with a large number of subchannels is due to the fact that it is difficult to find good splitting sequences for large values of M. Furthermore, for a large number of channels the lengths of the implulse responses increase also, leading to longer transmission filters and increasing the cross-talk between channels due to the non-linearity of the transmission media. The implementation complexity may be reduced with a decimated filter bank structure of the transmit and receive filters.

The choice of the splitting sequences is a delicate topic. Different shift-orthogonal sequences used on the same scaling function can lead to divisions of the bandwidth in which some channels have high sidelobes and are not suitable for transmission, or are not spectrally efficient. These effects are essentially due to the periodic nature of the discrete Fourier transform of the splitting sequences. The iterative splitting of the spectrum can produce catastrophic results if the residual sidelobes resulting from the previous splitting step, are amplified again by the splitting sequences at the current step.

However, an appropriate choice of the scaling function and of the splitting sequences can lead to efficient channelizations for a small number of channels. The total spectral occupancy depends on the original scaling function. Thanks to the availability of a very large number of possible wavelet functions, it is possible to choose a basic waveform whose spectral occupancy is lower than that of the OFDM system with the same number of subchannels. As an example, in Fig. 3.13 the total spectrum of a classical OFDM system with 8 tones (a) and the spectrum of a WOFDM using order-8 Battle-Lemarié wavelet packets with 8 subchannels (b) are reported in the case $\Delta = 227.56\mu s$.

Case-study 7

To demonstrate the effective advantage of the WOFDM, we chose the order-8 Battle-Lemarié wavelet packets, to obtain a system with 8 subchannels. This family of wavelet waveforms do not have compact support in the time domain, but their fast decay (exponential) allows an implementation with FIR digital filters with good approximation (i.e., the ISI and ICI due to the loss of orthogonality is negligible). The good time-frequency product of this family allows them to have good decay in the frequency domain with low sidelobes. These features imply that essentially each subchannel overlaps only with the two adjacent subchannels. Hence, the possibility of interchannel interference due to the non-linearity of the transmission channel is greatly reduced.

In Fig. 3.15 the synthesis and analysis filter banks used at the transmitter and receiver respectively, for the WOFDM scheme are depicted. The dashed boxes contain the analog interfaces of the digital filter banks, and the data rates at different nodes of the tree are specified in symbols per second. The order-8 Battle-Lemarié scaling function $\phi(t)$ is shift orthogonal with period Δ, and the sequences $h[n]$ and $g[n]$ represent the order-8 Battle-Lemarié scaling and wavelet vectors used as splitting sequences for each binary decomposition of the subspaces. The entry points of the data associated with the 8 subchannels that generate the overall signal spectrum are also shown. In Fig. 3.14 the results of the comparison of the OFDM and of the WOFDM schemes of Fig. 3.13 on the non-linear channel are reported. The OFDM scheme has an excess bandwidth of 1.26, while the WOFDM scheme has an excess bandwidth of 0.115 measured at -20 dB. Both schemes have a symbol period of $\Delta = 227.56\mu s$. The large saving in bandwidth requirement of the WOFDM scheme (which renders the technique suited for FDM applications) is counterbalanced by a loss of roughly 2.2 dB on the non-linear channel.

We also considered the transmission of a QPSK modulated signal on each frequency subchannel over a multipath fading channel in an urban environment. We assumed the presence of a direct path between the transmitter and the receiver; 4 groups of reflected rays are considered and each of them is composed of echoes whose delay τ_i is exponentially distributed between 0 and 7 μs. The phase shifts are uniformly distributed between $(0,2\pi)$. No coding or equalization is implemented. Table 3.2 reports the signal-to-noise ratio E_b/N_0 necessary to achieve a bit error probability $P(e) = 10^{-5}$ versus the variation A_g of the relative gain between the reflected rays and the direct ray for the OFDM and WOFDM schemes of Fig. 3.13, with $\Delta = 227.56\mu s$, and for an 8 channels WOFDM scheme with $\Delta = 112\mu s$ and the same bandwidth measured at -20 dB as the OFDM scheme. The E_b/N_0 is the mean value of the required E_b/N_0 for the 8 subchannels. The WOFDM system (C), with the same symbol period as the OFDM, shows a minimum gain of 1.8 dB, in addition to the much smaller bandwidth requirement. The WOFDM scheme (B), with a smaller symbol time and the same bandwidth occupation, shows a minimum gain of 4.6 dB plus allowing a larger transmission bit rate which again amounts to a larger bandwidth efficiency of the scheme. In general, the larger bandwidth efficiency of WOFDM for small number of channels allows, for a given fixed bandwidth occupation, the use of a smaller value of the symbol duration Δ, and a larger margin with respect to the channel coherence time.

◇

We should finally point out that the performances of OFDM can be improved using a guard interval in each symbol period, at a cost of reduced data rate. This is not possible for the WOFDM system in which the pulse extends over several symbol intervals.

A_g (dB)	OFDM (A)	WOFDM (B)	WOFDM (C)
-40	13.1	7.6	9.8
-30	12.0	7.0	10.0
-20	11.8	7.2	10.0
-10	47.5	34.0	34.5

Table 3.2. Required E_b/N_0 in dB for a $P(e) = 10^{-5}$ vs. A_g, the relative gain between the reflected ray and the direct ray, for the OFDM and WOFDM schemes of Case-study 7. Schemes (A) and (C) have $\Delta = 227.56\mu s$, scheme (B) has $\Delta = 112\mu s$. Schemes (A) and (B) have the same bandwidth, scheme (A) has $\gamma = 1.26$ and schemes (B) and (C) have $\gamma = 0.115$.

(Eb/No)sat vs. Back-off [dB]
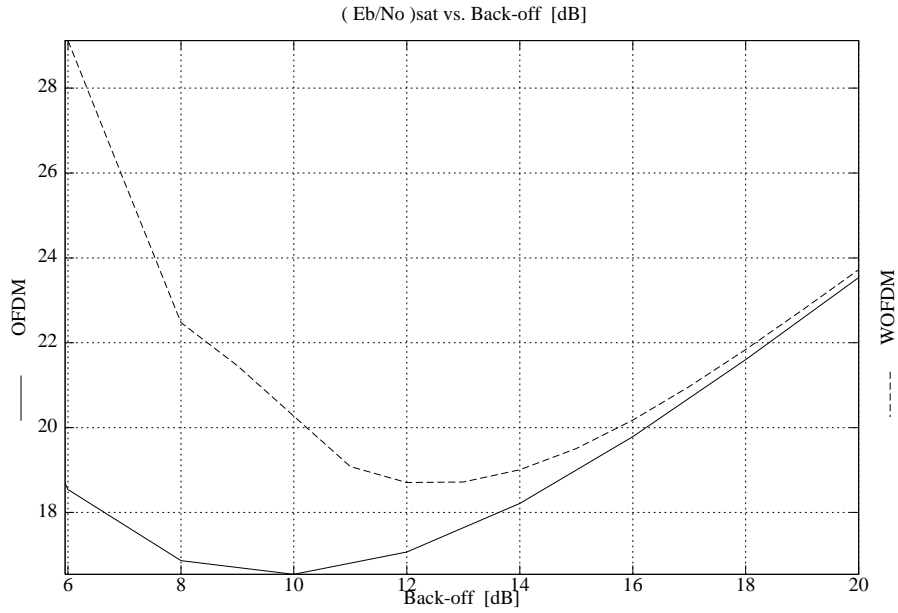
Figure 3.14. $(E_b/N_0)_{sat}$ in dB versus the input back-off of the non-linear power amplifier for the WOFDM and OFDM schemes with $\Delta = 227.56\mu s$ of Fig. 12 described in Case-study 7.
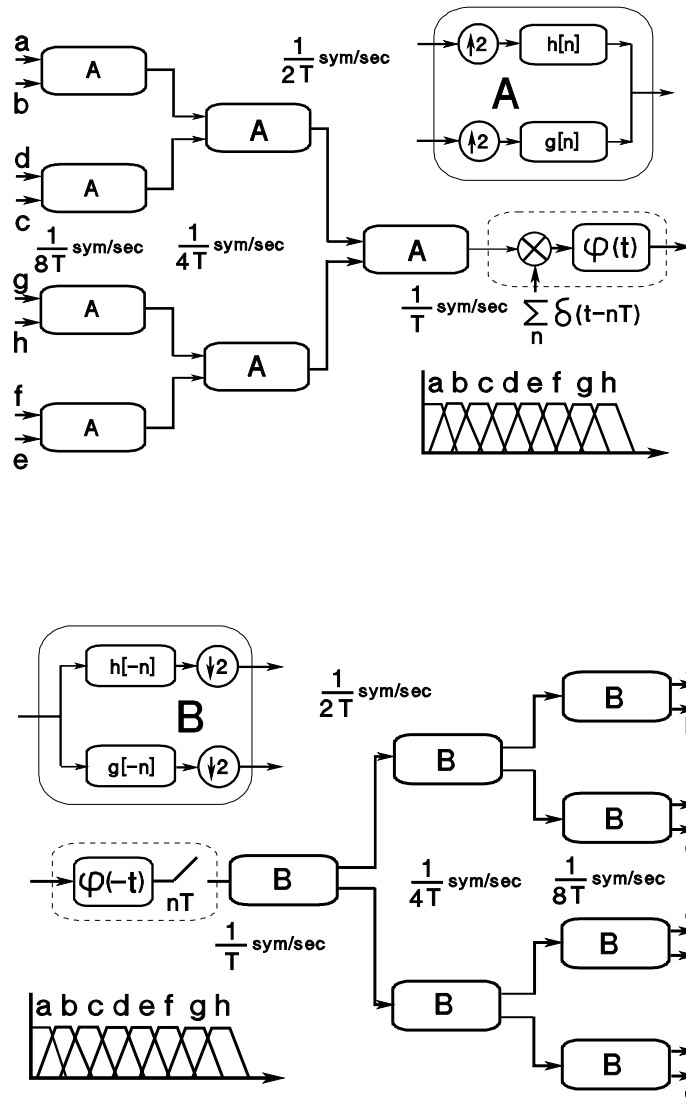
Figure 3.15.   The synthesis and analysis filter banks used at the transmitter and receiver respectively, for the WOFDM scheme of Case-study 7, based on order-8 Battle-Lemarié wavelet packets (T=Δ).

Chapter 4

Other communication applications

4.1 Introduction

In this chapter we present two particular applications of the wavelet based modulation. In the first example WOFDM and Trellis coded modulation are jointly used to shape the power spectrum of the overall transmitted signal in order to match it to the channel transfer function; such a technique is used to limit the distortion effect introduced on the received signal by deep frequency fading in the channel transfer function. In the second devised applications we exploit the filter bank structures of the wavelet mo-demodulator to efficiently implement a spread spectrum modulation system.

4.2 Power spectrum shaping using WOFDM and TCM codes

On linear filtering channels with side information, the transmitter may shape the power spectrum of the transmitted signal with the aim of increasing the data rate through the channel. Several possibilities have surfaced in the literature that address this problem. In Tomlinson-Harashima (TH) precoding [94], the channel symbols are precoded and transmitted across the known Inter-Symbol Interference (ISI) channel. The receiver employs a whitened matched filter followed by further processing. TH precoding eliminates the ISI due to the tail of the channel impulse response. Trellis precoding [95], may be viewed as a generalization of trellis shaping to ISI channels. This broad scheme encompasses TH precoding and can achieve spectral shaping

and shaping of the multidimensional constellation.

Another approach is based on Multicarrier Modulation (MM), a special case of which is the DFT-OFDM. In this approach the available spectrum is channelized into a large number of overlapping orthogonal frequency subchannels. In MM, after the frequency channelization, a loading algorithm can be used [98] to distribute the data rate and the available signal power in the available subchannels.

In trellis precoding, the whitened matched filter must exist and be causal and stable. For channels with nulls in their transfer function this cannot be assured. For such channels, instead of the zero forcing Decision Feedback Equalizer (DFE), one must employ the minimum mean squared error DFE which admits a limited amount of ISI at its output. In general, TH and trellis precoding may be characterized as techniques whereby the number of available orthogonal channels used at the transmitter is one, and the number of codes used is one as well. In contrast, the number of orthogonal subchannels used in DFT-OFDM is very large (e.g., 1024), and in many applications the number of codes used at the transmitter is one.

In this section, we propose a scheme that bridges the gap between these two extremes [6]. We employ a set of orthogonal subchannels generated at various nodes of a filter bank tree [28], whereby the total number of the frequency subchannels are much smaller than those used in DFT-OFDM, and employ one TCM code per subchannel selected wisely so that they may all be decoded in a *single decoder*. The main advantages of the proposed technique are: (1) dynamically adjustable power spectrum, provided channel state information is available; (2) relative ease in handling channels with nulls in their transfer function; (3) fast hardware and power efficient technique of generating the orthogonal frequency subchannels; (4) low complexity overhead at the receiver; and (5) ability to support unequal error protection of the data.

To provide a unifying framework, we shall focus on Geometrically Uniform TCM (GUTCM) codes, although the technique can be applied to general TCM codes. We refer the interested reader to references in [6] for the details on the GUTCM codes, their construction, and their canonical encoders. Observing the GUTCM encoder with k inputs and n outputs we have: (1) the input binary k-tuple can be divided into two segments. The first $\tilde{k}$-bits determine the state transitions and activate the label code. The second $(k-\tilde{k})$-bits address a particular element of a coset of the parallel transition subcode C_0, identified by the label code. C_0 itself is a block code; (2) the output is a signal vector in a typically $2L$-dimensional signal space. This space is often obtained as a Cartesian product of L two-dimensional subspaces; the $2L$-dimensional vector is transmitted by sending L two-dimensional vectors in

different time slots. From this description, the dynamics of the code are captured by the labeled state transition diagram. The process of generating the orthogonal frequency subchannels in MM can be viewed as one of *splitting* the spectrum of a root-Nyquist pulse $s(t)$, using a set of shift orthogonal splitting sequences as presented in Chapter 3. The resulting subchannels overlap in frequency, but maintain their orthogonality. It is instructive to think of the different subchannels as spanning different subspaces of the available signal space, and to think of a component GUTCM code as *acting on* a particular subchannel assigned to it.

4.2.1   GUTCM Coding of the Subchannels

Once the available frequency band has been channelized, it is important to choose which GUTCM code acts on a particular subchannel. All the subsequent discussion is based on the complex baseband equivalent model of the possibly narrowband communication system. The noise is assumed to be additive Gaussian.

Suppose the available frequency band is subdivided into N subchannels with symboling rates $R_j = (L_j \Delta)^{-1}$ for $j = 1,2,...,N$, where, L_j are positive integers. Let the GUTCM code acting on subchannel j be denoted by TCM(j) and have the rate k_j/m_j bits/(two-dimensional symbols), where, we assume m_j two-dimensional symbols are ejected by encoder per state transition. Each such sequence of m_j two-dimensional symbols represents a codeword of C_0 or one of its cosets. Let the average energy of the two-dimensional constellation used by TCM(j) be E_j. Then the average power level of subchannel j is $\frac{m_j E_j}{m_j L_j \Delta} = E_j R_j$, and the total average transmission power is $P = \sum_j E_j R_j$. The useful bit rate of the j-th subchannel is $R_{bj} = \frac{k_j/m_j}{L_j \Delta}$ bits/second, and the total bit rate is $R_b = \sum_j R_{bj}$. Assume the channel has a piecewise constant gain of C_j for subchannel j, and piecewise linear phase leading to group delay d_j of subchannel j. Adjusting for the group delays at the receiver, assume the subchannels can be aligned so that they remain orthogonal. Then the energy level of received signal for subchannel j is $E_j' = C_j^2 E_j$ (this is the effective energy level influencing the Bit Error Rate (BER)).

One objective of the system designer may be to maximize R_b subject to a constraint on P, while simultaneously satisfying the BER requirements. In the rest of the paper, we assume we are given a set of codes, with their respective rates and energy levels maximizing our objective function and satisfying our constraints. Note that from a complexity point of view, it is desirable to use the minimum number of subchannels while satisfying the spectrum

70

shaping, minimum interference (due to spectral overlap of the subchannels and linear filtering effect of the channel), and data rate maximization requirements, given our constraints.

4.2.2   Pipeline Mode Decoding of the Component Codes

Maximum Likelihood (ML) decoding of a GUTCM code can be performed in two steps: (1) ML decoding of the parallel transition subcode and all of its cosets; and (2) using the metrics generated in step 1 to decode the label code. The main complexity of the decoder is associated with decoding of the label code.
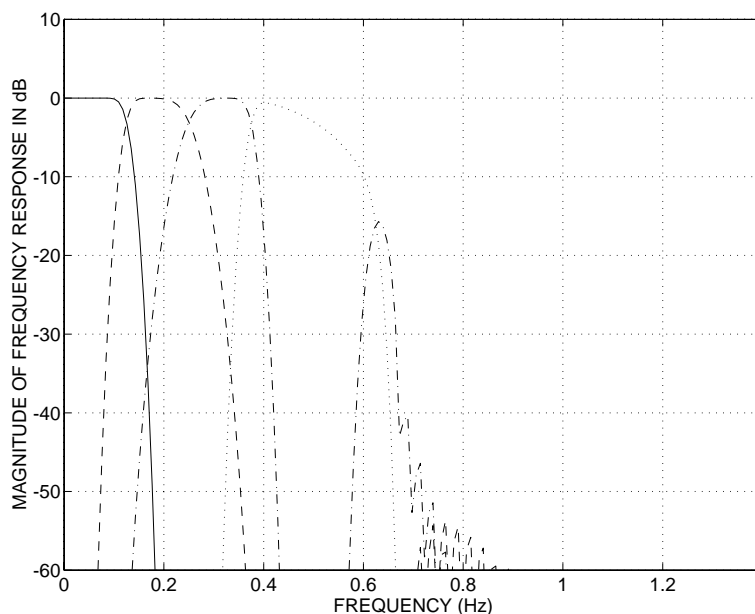
Figure 4.1.   Four channel splitting of the square-root raised cosine wave-form with Daubechies filters.

Decoding of the Label Codes:
Maximum likelihood decoding of the label code can be performed via usual Viterbi decoding [101]. In state-parallel Viterbi decoder, a single trellis section of the GUTCM code is mapped into hardware. The basic unit of a Viterbi Decoder (VD) is the Add-Compare-Select (ACS) unit. In a VD for

71
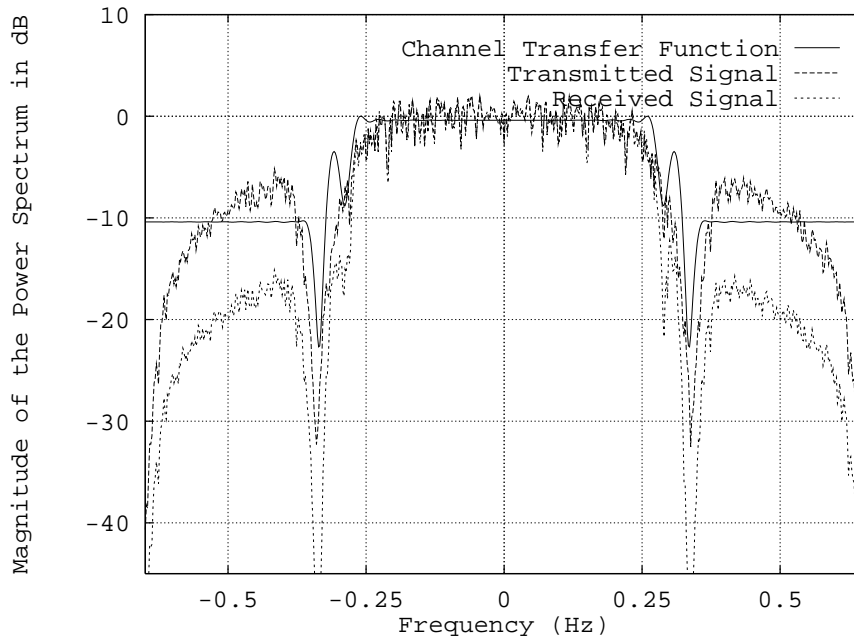
Figure 4.2. Power spectra of the shaped transmitted signal and of the received signal

a rate $\frac{\tilde{k}}{n}$ convolutional code, each ACS unit receives $2^{\tilde{k}}$ Accumulated path Metrics (AM), adds distinct Branch Metrics (BM) to each AM, selects the largest and presents the results of this selection in addition to the updated AM to other ACS units if they need it. The distribution of the updated AMs to the appropriate ACS units for the next decoding cycle can be done using a switching matrix [101]. This way label codes having the same number of states but different dynamics can be decoded in one decoder (see the discussion below on pipelining). From the outputs of the ACS units the decision vector is obtained and stored in the memory unit, that will be scanned by the trace-back unit in order to determine the decoded sequence.

Note that the orthogonal subchannels are synchronized relative to each other. Let $\Delta' = LCM(m_1 L_1,...,m_N L_N)\Delta$ where, LCM denotes the Least Common Multiple. Then the trellises of the component label codes align every Δ' seconds. In particular, every Δ' seconds we have $i_j = \Delta'/m_j L_j \Delta$ trellis sections for TCM(j), where i_j is an integer. Throughout the rest of the section, we assume that the label codes of different GUTCM codes have trellises with the same number of states. Since the decoder complexity is dominated by the code with the largest state space, it does not make sense

to use GUTCM codes with different number of states.

Given the trellis alignment noted above, we can simultaneously decode all of the label codes. The reason why this is possible is that *a Viterbi decoder can simultaneously decode independently encoded data streams in a pipeline mode with very little processing hardware overhead.* In particular, take a generic ACS unit operating on $2^{\tilde{k}}$ inputs at a time. Let the propagation delay of an ACS unit operating on $2^{\tilde{k}}$ inputs be $X(\tilde{k})$. Assuming the ACS data path is divisible by whatever amount desired, consider pipelining the ACS data path by $N' = \sum_{j=1}^{N} i_j$ stages [101]. Let the delay of each pipelining latch be τ_l. Using N'-stage pipelining the net propagation delay from the input to the output of the ACS units will be $X(\tilde{k}) + N'\tau_l$. Such pipelined ACS units can be used to sequentially operate on N' data streams, while the switching matrix takes care of the updated AM routing. Obviously, an ACS unit operating on 2^k inputs, can operate on $m \leq 2^{\tilde{k}}$ inputs. The price paid for this N-fold gain in processing power, is N' latches, and a reduced throughput due to propagation delay of the latches. Note that the power consumption of a decoder decoding the GUTCM codes acting on the subspaces of the signal space in a pipeline mode, is no more than the power consumption of a decoder for a single GUTCM code acting on the entire signal space. This is because the overall symboling rate for both cases are the same.

The hardware overhead for pipeline mode decoding of N label codes are: (1) N' pipelining latches inserted in the ACS hardware data path, and a switching matrix for updated AM routing (this unit is unnecessary if all the GUTCM codes have the same dynamics); (2) pipelining latches inserted in the trace-back unit(s) data path(s) (the number is highly design dependent); (3) multiplexers and demultiplexers for data flow regulation; and (4) N memory modules storing the decision vectors generated by the ACS units.

Decoding of the Parallel Transition Subcodes:

It can be demonstrated that owing to the algebraic structure of the GUTCM codes, *all* the parallel transitions connecting the states of the trellis at a given trellis section, can be simultaneously solved in a single hardware unit we denote GPTSU (see references in [6, 12]). What is true about the trellis diagrams of the label codes of the component GUTCM codes and their efficient decoding in one decoder, is certainly true about the trellis diagram associated with the parallel transition subcodes, their cosets, and their pipeline decoding in one GPTSU. In particular, if C_0 of different GUTCM codes are either identical, or are *subcodes* of each other, they can be efficiently decoded in one pipelined GPTSU unit. Note that the decoding trellis of C_0 and its cosets are often very short (these are essentially block codes). Hence, there is no need for trace-back units to store decision vectors, and the hardware overhead in pipelining the GPTSU is indeed minimal.

73

Example: We use the extensive tables of GUTCM codes over non-binary Abelian groups (Z_4 and Z_8) presented in [102]. We assume the channel has a null around 0.328 Hz for a normalized $\Delta = 1$. In this case, to place a null in signal spectrum, it suffices to consider two subchannels with unequal symboling rates. For TCM(1) acting on the lowpass subchannel $L_1 = 2$, and for TCM(2), $L_2 = 4$. For our example, TCM(1) has an effective rate of 3.5 bits/2Δ (Table LIII, entry $\nu = 3$, 2×16PSK, Partition I) and TCM(2) has an effective rate of 2.00 bits/4Δ (Table LI, entry $\nu = 3$, 4×8PSK, Partition I). Since the partition trees for the two codes are subsets of each other, the C_0 of the two codes are subcodes as desired. For a symbol error probability of 10^{-5} on both subchannels, TCM(1) requires 16.3 dB of Signal-to-Noise Ratio (SNR), while TCM(2) requires 10.2 dB of SNR, at the receiver. The ratio of average received power between the two subchannels P_1/P_2 is 9.1 dB. Fig. 4.2 depicts the power spectrum of the transmitted signal, squared magnitude of the channel transfer function, and the power spectrum of the received signal.

4.3 Permutation Spreading in Wavelet OFDM systems

Multicarrier modulation is an attractive technique for data transmission over bandlimited channels, particularly useful for audio [96] or video [97] broadcasting, with the potential of achieving the channel capacity via shaping the power spectrum of the transmitted signal to compensate for the linear filtering effect of the channel. In DFT-OFDM systems, a special case of Multicarrier Modulation (MM), the available spectrum is channelized into a large number of orthogonal frequency subchannels with a $sinc(.)$ transfer function (due to the use of a rectangular shaping pulse). In MM, after the different subchannels have been defined, a loading algorithm can be used [98] to distribute the data rate and the available signal power in the available subchannels. This scheme has found widespread use in broadcast applications over frequency selective slowly fading mobile radio channels. In this applications, if the channel transfer function varies slowly as a function of frequency, there is no significant cross-talk between adjacent subchannels due to channel filtering effect. A universal channel code for such applications can be designed based on the criteria of maximizing the product distance of the code [99].

Clearly, the splitting sequences used in MM, following the procedure described in Chapter 3, have a significant impact on the overall performance of the MM. In connection with the use of such sequences for MM we can make

the following comments:

1. in general, in order to minimize the spectral overlap among the adjacent frequency channels, the length of the splitting sequences must be very large. This has two negative side-effects:

   - the peak signal power may be large;

   - the elementary shaping pulses used for modulation spread in time.

   Hence, such waveform cannot be efficiently used for short frame and burst mode data transmission;

2. general spreading sequences are multilevel sequences. From an implementation point of view, it would be desirable to have very simple sequences, with an easy hardware implementation. Haar splitting sequences meet this requirement, with the disadvantage that they generate frequency subchannels with large sidelobes.

Regardless of the splitting sequences used for the generation of the frequency subchannels, MM systems are sensitive to timing errors. This inherent problem is due to the fact that, in order to maximize spectral efficiency, adjacent shift orthogonal subchannels overlap in the frequency domain. The permutation spreading technique proposed in this paper is indeed aimed at reducing the timing sensitivity problem.

More precisely, in this paper we propose the use of permutations for two purposes:

- generation of splitting sequences for multiple access communications;

- spreading of the frequency channels in a MM system for the purposes of achieving immunity to timing errors.

We provide an example of application of the concepts presented here to a MM system based on Haar splitting sequences, to indicate some of the possible advantages that may be derived from such an approach, in particular in connection with reducing the timing sensitivity and Adjacent Channel Interference (ACI) of the resulting system.

4.3.1 Permutations and group theory

Consider an indexed set of elements $x_1 x_2 x_3 ...$ which may be finite, or semi infinite in length. The set of elements noted above is well ordered and may be taken to represent the output of a discrete source that emits the symbol

chann. 1	chann. 2	chann. 3	chann. 4
0.06250	0.06250	0.06250	0.06250
0.06250	0.06250	0.06250	0.06250
0.12500	0.12500	0.00000	0.00000
0.12500	0.12500	0.00000	0.00000
0.12500	0.00000	0.00000	-0.12500
0.12500	0.00000	0.00000	-0.12500
0.12500	-0.12500	0.00000	0.00000
0.12500	-0.12500	0.00000	0.00000
0.06250	-0.06250	-0.06250	0.06250
0.06250	-0.06250	-0.06250	0.06250

Table 4.1.   Haar filter coefficients used to generate the four MM channels.

	$(S/I)_1$	$(S/I)_2$	$(S/I)_3$	$(S/I)_4$
no perm.	7 dB	2.8 dB	-18.8 dB	-7.1 dB
with perm.	26.5 dB	2.3 dB	-11.3 dB	7.5 dB

Table 4.2.   Signal-to Interference Ratios for the four MM channels.

x_n at the discrete time slot n. Henceforth, the notation $(x_i)\pi = x_j$ is used to mean that permutation π carries x_i to x_j. A *finite cycle* is a permutation on a finite set of letters $y_1 y_2 .. y_n$ (note that while the index in the set $x_1 x_2 ...$ implies a discrete time slot, the index associated with the elements $y_1 y_2 .. y_n$ is simply a place holder and does not necessarily have anything to do with time) such that $(y_1)\pi = y_2,...,(y_n)\pi = y_1$. A semi-infinite cycle on a set of letters $y_1 y_2 ...$ is similarly defined such that $(y_i)\pi = y_{i+1} \ \forall i = 1,2,....$ We write $(y_1, y_2, .., y_n)$ for a finite, and $(y_1, y_2, ...)$ for a semi-infinite cycle. Note that a finite cycle is invariant to cyclic shifts of its arguments so that for instance the cycles $(y_1, y_2, .., y_n)$ and $(y_2, y_3, .., y_n, y_1)$ are the same permutations.

Let us define an *interleaver* to be a device that implements a given permutation on a given input set of elements. We endow this device with a certain amount of memory where at each memory location an element of the input set can be stored. Given the sequential nature of data generated at the input of the interleaver, we envision this device to be a box that sequentially and at successive time slots receives an element of the input sequence $x_1 x_2 ...$, and correspondingly generates an element of the output sequence $z_1 z_2 ...$ where, z_1 is the first element that is produced at the output, z_2 the second, and so

on. Hence, the index of variable z implies an ordering in time, but it is *not the time slot* when an element is released.

It is a basic result in Group theory [104] that any permutation π on a set of elements S can be written as a product of disjoint cycles, and S may be divided into *disjoint subsets* such that each cycle operates on a different subset. By disjoint we mean that no two cycles move a common element. [1] Any permutation can essentially be written in only one way in this form. As an example, the permutation,

$$\Pi = \left(\begin{array}{cccccccccccc} 1 & 2 & 3 & 4 & 5 & 6 & 7 & 8 & 9 & 10 & 11 & 12 \\ 1 & 5 & 9 & 12 & 2 & 6 & 10 & 3 & 7 & 11 & 4 & 8 \end{array} \right)$$

can be easily written as the following product of cycles

$$\Pi = (1)(2,5)(3,9,7,10,11,4,12,8)(6).$$

Note that for simplicity we have omitted writing the variable x and used the index of the elements instead. Given this theorem, the study of realizations of a given permutation reduce to that of its constituent cycles.

A cycle of length two is called a *transposition*. It is easy to verify that any finite cycle can be written as a product of transpositions. For instance we have

$$(y_1, y_2, \dots y_n) = (y_1, y_2)(y_1, y_3) \dots (y_1, y_n).$$

Note that a permutation on a single element is a trivial permutation. Hence, in the expression for the cycle written as a product of transpositions we may include as many trivial permutations as we wish. For semi-infinite cycles we can extend this result by allowing the index n in the expression of the cycle as a product of transpositions to *run away* towards infinity. Notice that the representation of a cycle as a product of transpositions is *not unique*. This is evident in light of the fact that a finite cycle is invariant to cyclic shifts of its elements. Another important point is that it is implicitly assumed that the cycle is expressed as the *shortest* product of transpositions.

Having represented a cycle as a product of transpositions, we conclude that transpositions represent the elementary constituents of *any permutation*. Hence, we can envision our interleaver as a *sliding window transposition box* [103]. Instead of the data stream shifting into the interleaver while the output elements are ejected, we can assume that the input data stream is stationary, and a window of finite duration slides over it. At any given time slot, either a pair of elements in the sliding window are transposed and an output is generated, or an element is ejected without any transpositions performed (we

---

[1]this product is only a formal product when the set is infinite in size.

may represent such an event by a trivial permutation). With this set up, the delay of the interleaver is only due to the fact that during the initialization, it must store a certain number of elements of the input set in its local memory.
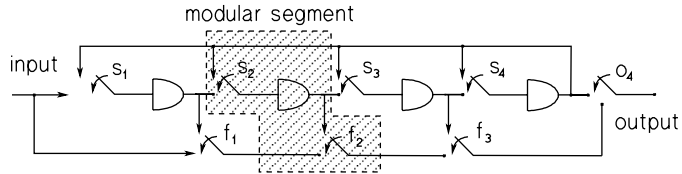
Figure 4.3.   The modular hardware realization of the FSP.

4.3.2   Hardware realization of the Finite State Permuter (FSP)

Based on our discussions thus far, the FSP is seen to be essentially a shift register with N memory locations whereby each memory cell is capable of storing an element of the input set, and additional hardware that allows the transposition of an element in the register with the output. A *modular* and hardware efficient realization can be obtained using a series of binary switches. An example of such a realization for a FSP of memory 4 is depicted in Fig. 4.3. It is evident that by properly positioning the switches in the structure it is possible to transpose any element stored in the register with the output. This structure is modular in the sense that it is sufficient to duplicate the segment shown in the dashed box to generate larger and larger FSPs. Note that the switches of Fig. 4.3 can be easily implemented using MOSFET transmission gates.

4.3.3   Example of application to Haar based MM system

The purpose of the example provided here is to show an application of permutations for spectrum spreading in a simple MM system with the goal of reducing the timing sensitivity of the overall modulation scheme. We considered a wavelet packet configuration with 4 channels with Haar filters of
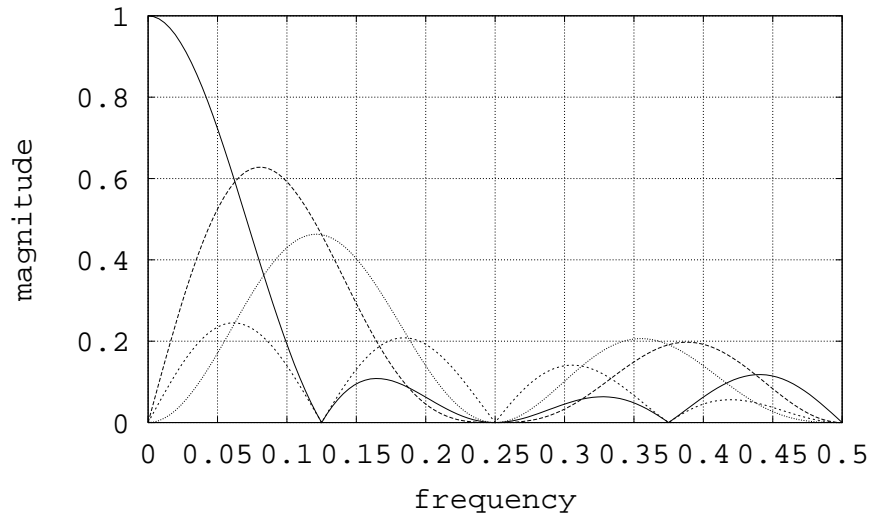
Figure 4.4.   The Haar wavelet packet channels.
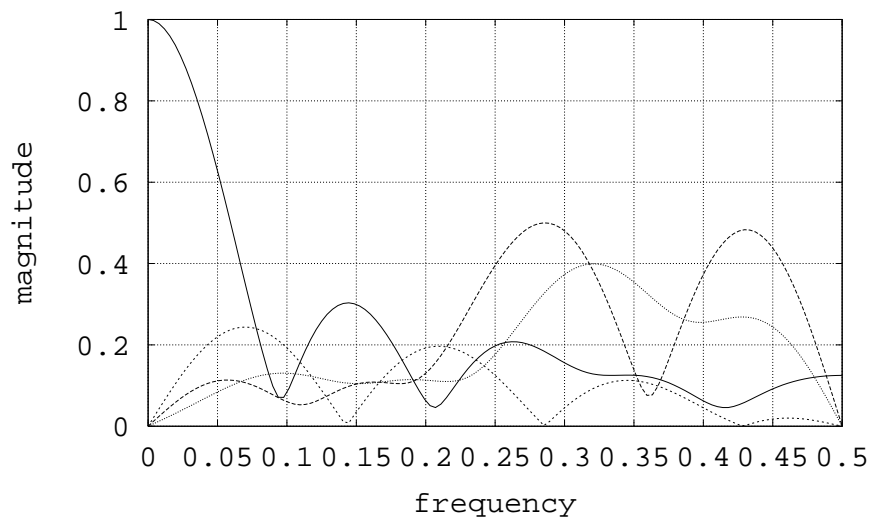
Figure 4.5.   The Haar wavelet packet spreaded channels.

length 10. The magnitude of the Fourier transform of the filters is depicted in Fig. 4.4. The Haar splitting sequences used for the purposes of generating the orthogonal frequency subchannels are tabulated in Table 4.1. The outputs of the four transmission filters are permuted with permutations belonging to the same cyclic group, generated by the following elementary permutation:

$$\Pi = \begin{pmatrix} 1 & 2 & 3 & 4 & 5 & 6 & 7 & 8 & 9 & 10 \\ 8 & 7 & 1 & 9 & 3 & 10 & 4 & 6 & 5 & 2 \end{pmatrix}$$

Permutation Π is used to spread the spectrum of the first channel, Π^2 is used for channel 2, Π^3 is used for channel 3, and Π^4 is used for channel 4. The applied permutations spread the power of the four transmission channels over all the available bandwidth. Note that not all the permutations are good, because not all of them spread the spectrum enough to achieve a gain in the Signal to Interference ratio (S/I) for *all* the channels, in comparison to the original un-spreaded channels. The magnitude of the Fourier transform of the transmission filters after spreading is depicted in Fig. 4.5.

The results are reported in Table 4.2, where we tabulate the values of the (S/I) ratios for all the four MM channels. The ratios in the first row of the table are evaluated as the ratio of the power of the useful despreaded channel to the total power of the other channels whose spectrum overlap the useful one. In this sense, the ratios represent a lowerbound for the Signal to Noise Ratio (SNR) achievable if the shift orthogonality between signals is lost due to timing errors.

From Table 4.2 it is possible to observe how the use of the permutation spreading and despreading in the four MM channels can significantly improve the signal to interference ratios. For the example provided here, three channels showed significant improvements in the lowerbounds on the values of the (S/I) ratios (one channel showed an improvement of 19 dB in the (S/I) ratio lowerbound), while there was a loss of 0.5 dB in (S/I) ratio for channel 2.

The results obtained experimentally indicate that the proposed technique has the potential to provide significant improvements in the (S/I) ratios.

Chapter 5

Symbol synchronization using wavelets

5.1 Introduction

The timing sensitivity of the multichannel modulation schemes plays an important role in the design and application of such systems for digital communications. The timing sensitivity is particularly important in multichannel modulation, since timing offsets can cause large Adjacent Channel Interference (ACI) due to the spectral overlap among adjacent channels. Most symbol synchronizers proposed in the literature for MM use pilot symbols for timing recovery [64]. We focus on an approximate Decision Directed (DD) Maximum Likelihood (ML) symbol synchronizer which derive the timing information from all the subchannels without the need for any pilot symbols.

We derive expressions for the jitter variance of the approximate DD ML symbol synchronizer for multichannel modulation over a baseband channel with arbitrary energy distribution in each subchannel, and for an arbitrary channel transfer function. We analytically study the effect of the splitting sequences used to generate the different channels, on the timing jitter variance, and provide criteria for the selection of suitable splitting sequences. We address the implementation issues of the approximate DD ML symbol synchronizer and propose a structure that can be used to combine the timing information from different subchannels. In effect, the timing information from subchannels with increasing center frequency is seen to provide successive refinements of the synchronizer S-curve leading to improved performance for each subchannel considered by the symbol synchronizer. We provide simulation results of the proposed scheme, validating its functionality and confirming the analytical results.

5.2 ML Timing Estimator and its Jitter Variance For The Two Channel Modulation

Let $s(t)$ be a Nyquist pulse with shift orthogonality period $\Delta/2$ whose spectrum is split to generate two Nyquist pulses with shift period Δ. When using scaling functions and wavelets for modulation $s(t) = \phi(2t)$ where $\phi(t)$ is the scaling function with shift period Δ. Otherwise, $s(t)$ can be any Nyquist pulse such as the square root raised-cosine pulse. Let the two Nyquist pulses obtained as a result of the split of the spectrum of $s(t)$ be denoted by $\phi(t)$ and $\psi(t)$ (this notation is used since if $s(t)$ is indeed a contracted scaling function, then the two Nyquist pulses obtained after the split of the spctrum of $s(t)$ would be the scaling function and wavelet respectively).

From the results of [4], if the composite rate of the two subchannels used for modulation is below the Nyquist rate, there is a pre-filter that produces zero crossings at the integer multiples of the correct timing instants. At high SNR, the output of this filter can be used to eliminate the pattern dependent jitter. Let us suppose that the excess BW associated with the simultaneous use of the two shaping pulses is low so that the sufficient statistic available at the output of the pre-filter eliminating the pattern dependent jitter has a negligible contribution to the estimation of the timing parameter at the operating SNR. Then the sufficient statistic for the estimation of the timing parameter τ is obtained from the projection of the received signal on the basis $\phi(t - k\Delta - \tau')$ and $\psi(t - k\Delta - \tau')$, where τ' is the locally generated timing estimate. The received signal in this case is $r(t) = \sum_n [a_n \phi(t - n\Delta - \tau) + b_n \psi(t - n\Delta - \tau)] + n(t - \tau)$, where a_n and b_n are independent white and real sequences, and $n(t)$ is a sample function of the AWGN. Note that here for simplicity we are assuming that the carrier recovery loop is operating perfectly and that the transmitted symbols are real (i.e., DSB PAM modulation).

Projection of the received signal on the locally generated basis yields

$$\langle r(t), \phi(t - k\Delta - \tau') \rangle = C_k + N_k^\phi = y_k^\phi$$

and

$$\langle r(t), \psi(t - k\Delta - \tau') \rangle = D_k + N_k^\psi = y_k^\psi,$$

where N_k^ϕ and N_k^ψ are independent Gaussian random variables with zero mean and variance $N_o/2$, and C_k and D_k are defined as

$$C_k = \sum_n a_n r_{\phi\phi}((n - k)\Delta + (\tau - \tau')) + b_n r_{\psi\phi}((n - k)\Delta + (\tau - \tau'))$$

83

and

$$D_k = \sum_n a_n r_{\phi\psi}((n-k)\Delta + (\tau - \tau')) + b_n r_{\psi\psi}((n-k)\Delta + (\tau - \tau')),$$

with $r_{x,y}(\alpha) = \langle x(t), y(t+\alpha) \rangle$, where $x(t)$ and $y(t)$ are two arbitrary time functions. The approximate decision directed ML estimate of τ is obtained from:

$$\tau^* = \arg\max_{\tau'} \sum_{k=0}^{K-1} (y_k^\phi \hat{a}_k + y_k^\psi \hat{b}_k), \tag{5.1}$$

where K denotes the length of the observation interval in number of symbols, and the receiver in the tracking mode is assumed to operate at low bit error rate so that the detected symbols $\hat{a}_k$ and $\hat{b}_k$ equal the actual symbols a_k and b_k respectively. To determine the variance of the timing jitter of the DD ML estimator, we need to make some assumptions about the statistics of the transmitted symbols. Hence, suppose we use BPSK signalling with $E[a_n^2] = E_a$ and $E[b_n^2] = E_b$ where $\{a_n\}_{n=-\infty}^{\infty}$ and $\{b_n\}_{n=-\infty}^{\infty}$ are two independent equiprobable WSS sequences.

When the timing error is small, we can use the Taylor series expansion of the derivative of the likelihood function $\Lambda(\tau')$ about $\tau = \tau'$ [66] for evaluation of the variance of the timing error. The parameter τ can be solved for by finding the zero of $\partial\Lambda/\partial\tau'$ using only the first two terms in the Taylor series expansion of this function. Using this method, and making the approximation that at moderate to high SNR levels $\partial^2\Lambda/\partial^2\tau'(\tau) \simeq E[\partial^2\Lambda/\partial^2\tau'(\tau)] \doteq A$ (here $E[.]$ denotes expectation), the variance of the timing jitter in the tracking mode can be expressed as $\sigma_\tau^2 = A^{-2}E[(\partial\Lambda/\partial\tau'(\tau))^2]$. Let us define $E[(\partial\Lambda/\partial\tau'(\tau))^2] \doteq (F_1 + F_2)$. Then it can be shown that (details of the derivation are presented in the appendix A):

$$
\begin{aligned}
F_1 &= -K(E_a r_{\phi\phi}^{(2)}(0) + E_b r_{\psi\psi}^{(2)}(0)), \tag{5.2}\\
F_2 &= K\sum_m [2E_a E_b (r_{\phi\psi}^{(1)}(m\Delta))^2 + (E_a r_{\phi\phi}^{(1)}(m\Delta))^2 + \\
&\quad (E_b r_{\psi\psi}^{(1)}(m\Delta))^2] - \sum_{k=0}^{K-1}\sum_{l=0}^{K-1} [2E_a E_b (r_{\phi\psi}^{(1)}(k\Delta - l\Delta))^2 \\
&\quad + (E_a r_{\phi\phi}^{(1)}(k\Delta - l\Delta))^2 + (E_b r_{\psi\psi}^{(1)}(k\Delta - l\Delta))^2], \tag{5.3}
\end{aligned}
$$

where, $r_{x,y}^{(1)}(\alpha)$ denotes the first and $r_{x,y}^{(2)}(\alpha)$ the second derivative of $r_{x,y}(\alpha)$ with respect to α respectively. Let us define

$$B = \sum_m [2E_a E_b (r_{\phi\psi}^{(1)}(m\Delta))^2 + (E_a r_{\phi\phi}^{(1)}(m\Delta))^2 + (E_b r_{\psi\psi}^{(1)}(m\Delta))^2] = 2B_1 + B_2 + B_3.$$
$$\tag{5.4}$$

Similarly, it can be shown that:

$$A = K(E_a r^{(2)}_{\phi\phi}(0) + E_b r^{(2)}_{\psi\psi}(0)). \tag{5.5}$$

This way, the variance of the timing jitter naturally breaks up into two parts $\sigma_\tau^2 = \sigma_\tau^2(noise) + \sigma_\tau^2(PDJ)$ where PDJ stands for Pattern Dependent Jitter:

$$\sigma_\tau^2(noise) = \frac{F_1}{A^2} = \frac{N_o/2}{-K(E_a r^{(2)}_{\phi\phi}(0) + E_b r^{(2)}_{\psi\psi}(0))}, \tag{5.6}$$

$$\sigma_\tau^2(PDJ) = \frac{F_2}{A^2} = \frac{B + G}{K(E_a r^{(2)}_{\phi\phi}(0) + E_b r^{(2)}_{\psi\psi}(0))^2}, \tag{5.7}$$

where,

$$G = -\frac{1}{K} \sum_{k=0}^{K-1} \sum_{l=0}^{K-1} [2E_a E_b (r^{(1)}_{\phi\psi}(k\Delta - l\Delta))^2 + (E_a r^{(1)}_{\phi\phi}(k\Delta - l\Delta))^2 + (E_b r^{(1)}_{\psi\psi}(k\Delta - l\Delta))^2]. \tag{5.8}$$

In the remainder of this section, we shall assume that $E_a = E_b = 1$ (i.e., equal energy distribution among the two subchannels). In the next section, we shall generalize the results by considering the effect of the channel and unequal energy distribution among different subchannels.

Let the splitting sequences be denoted by $(...,h_0,h_1,...)'$ (for example the scaling vector), and $(...,g_0,g_1,...)'$ (for example the wavelet vector). In the time domain we have $\phi(t) = \sum_n h_n s(t - 0.5n\Delta)$, and $\psi(t) = \sum_n g_n s(t - 0.5n\Delta)$. In the transform domain we have $\Phi(f) = H(e^{jw\Delta/2})S(f)$, $\Psi(f) = G(e^{jw\Delta/2})S(f)$ where, $S(f),\Phi(f),\Psi(f)$ are Fourier transforms of $s(t),\phi(t),\psi(t)$ respectively, and $H(e^{jw\Delta/2}),G(e^{jw\Delta/2})$ are the Discrete Fourier Transforms (DFT) of the lowpass and highpass splitting sequences respectively.

With this set up, it is now possible to obtain an equivalent expression for the variance of the timing jitter in the transform domain. Consider the equality:

$$r^{(2)}_{\phi\phi}(0) + r^{(2)}_{\psi\psi}(0) = -4\pi^2 \int_{-\infty}^{\infty} f^2 (|H(e^{jw\Delta/2})|^2 + |G(e^{jw\Delta/2})|^2)|S(f)|^2 df. \tag{5.9}$$

But, note that $(|H(e^{jw\Delta/2})|^2 + |G(e^{jw\Delta/2})|^2) = 2$ since the discrete filters with transfer functions $H(e^{jw\Delta/2})$ and $G(e^{jw\Delta/2})$ are a QMF pair [25, 28]. Hence, the above expression is *independent* of the choice of the splitting sequences used to split the spectrum of $s(t)$, and the variance of the timing jitter due to noise is given by:

$$\sigma_\tau^2(noise) = \frac{N_o/2}{8\pi^2 K \int_{-\infty}^{\infty} f^2 |S(f)|^2 df}. \tag{5.10}$$

Noting that $4\pi^2 \int_{-\infty}^{\infty} f^2 |S(f)|^2 df = -r_{ss}^{(2)}(0)$, we have an equivalent alternate expression:

$$\sigma_{\tau}^2(noise) = \frac{N_o/2}{-2Kr_{ss}^{(2)}(0)}, \tag{5.11}$$

where, $r_{ss}^{(2)}(0)$ is the second derivative of the autocorrelation function of the shaping pulse $s(t)$ evaluated at zero.

The Influence of Factor G:

Note that the analysis thus far indicates that in the case of equal energy distribution among the subchannels, *the only factor* that is dependent on the choice of the splitting sequences is the factor G appearing in the numerator of the expression for the PDJ. Using a shift of index we can write:

$$G = -\sum_{m=-(K-1)}^{(K-1)} (1 - \frac{|m|}{K})[2(r_{\phi\psi}^{(1)}(m\Delta))^2 + (r_{\phi\phi}^{(1)}(m\Delta))^2 + (r_{\psi\psi}^{(1)}(m\Delta))^2]. \tag{5.12}$$

Assuming that K is sufficiently large, the above sum contains most of the significant terms of the infinite sum. Hence, for large K the expression for the PDJ reduces to

$$\sigma_{\tau}^2(PDJ) \simeq \frac{\sum_{m=-(K-1)}^{(K-1)} \frac{|m|}{K}[2(r_{\phi\psi}^{(1)}(m\Delta))^2 + (r_{\phi\phi}^{(1)}(m\Delta))^2 + (r_{\psi\psi}^{(1)}(m\Delta))^2]}{2K(r_{ss}^{(2)}(0))^2}.$$

$$\tag{5.13}$$

It is evident that for large K, the jitter variance is a strong function of the derivative of the cross correlation between $\phi(t)$ and $\psi(t)$. The sharper is the filtering effect due to the splitting sequences, the smaller is the jitter variance of the PDJ for large K.

5.3 Generalization to Multichannel Modulation

In this section we shall generalize the results of the previous section in two directions simultaneously. The first, is the natural generalization to multichannel case where the number of subchannels $M > 2$; the second is the generalization to specific channels of practical interest.

5.3.1 Multichannel Modulation Over Baseband Telephone Channels

Typical telephone channels (e.g., twisted wire pair) introduce severe amplitude and phase distortion of the baseband signal used for data transmission.

The use of multichannel modulation in such applications is natural and can improve the effective data transmission rate significantly. In a typical set up, the channel spectrum is subdivided into a large number of equal bandwidth subchannels such that the transfer function of each subchannel has an almost constant amplitude and phase characteristic. Subsequently, the available signal power is distributed among the subchannels such that the overall data rate through the channel is maximized, subject to a fixed error rate performance for all the subchannels. This unequal power distribution is achieved by assigning a different size QAM constellation with different energy levels to each subchannel. Alternatively, for the same error performance in each subchannel, the available spectrum may be divided into a set of unequal bandwidth subchannels, and a fixed constellation size (e.g., QPSK) with different energy levels may be used for each subchannel.

When splitting the spectrum of a Nyquist pulse to generate the shaping pulses for multichannel modulation at baseband, it is no longer necessary to use quadrature modulation since the spectrum of the subchannels overlap and the excess bandwidth of the overall signalling scheme is due to the original shaping pulse whose spectrum is split. In light of this, we shall make the following assumptions for the analysis that follows:

1. the spectrum of the original shaping pulse is split into M orthogonal subchannels;

2. BPSK modulation is used in each subchannel whereby the data sequences are equiprobable iid and independent for different subchannels;

3. the binary sequence associated with l-th subchannel is denoted by $\{a_{l,n}\}_{-\infty}^{\infty}$ with $E[a_{l,n}^2] = E_l$;

4. the effect of the transmission channel in a given subband is an amplitude attenuation denoted by $\{g_l\}_{l=1}^{M}$ and a group delay $\{\tau_l\}_{l=1}^{M}$ both of which are assumed to be estimated accurately possibly via a training sequence so that we may consider them to be known quantities at the receiver (the difference in the group delay for adjacent subchannels is assumed to be small enough that the subchannels essentially maintain their relative orthogonality).

Under the above assumptions, the received signal is

$$r(t) = \sum_{l=1}^{M} \sum_{n} g_l a_{l,n} \phi_l(t - n\Delta - \tau - \tau_l) + n(t - \tau)$$

where, $\phi_l(t)$ is the l-th Nyquist pulse obtained as a result of splitting the spectrum of $s(t)$ with shift orthogonality period Δ/M, and τ is the timing

87

parameter to be estimated. Note that here we have assumed that all the subchannels have equal rates. Projection of $r(t)$ on the locally generated basis $\phi_i(t - k\Delta - \tau' - \tau_i)$ yields

$$y_{i,k} = \sum_{l=1}^{M} \sum_{n} g_l a_{l,n} r_{\phi_l \phi_i}((n-k)\Delta + (\tau - \tau')) + n_{i,k},$$

where as usual, $r_{\phi_l \phi_i}(.)$ denotes the correlation between the noted functions, and $n_{i,k}$ are iid Gaussian random variables $\mathcal{N}(0, N_o/2)$. Let us define

$$C_{i,k} = \sum_{l=1}^{M} \sum_{n} g_l a_{l,n} r_{\phi_l \phi_i}((n-k)\Delta + (\tau - \tau')).$$

The sufficient statistic for observation over K-symbols per subchannel (i.e., MK symbols in total) is the set of values $\{y_{i,k}\}_{i=1,k=0}^{i=M,k=(K-1)}$. The approximate decision directed ML estimate of τ is obtained from

$$\tau^* = \arg \max_{\tau'} \sum_{i=1}^{M} \sum_{k=0}^{K-1} y_{i,k} g_i \hat{a}_{i,k}, \tag{5.14}$$

where $\hat{a}_{i,k}$ is the k-th detected bit of the i-th subchannel. Assuming that the receiver is operating at low bit error rates, we may use $a_{i,k}$ instead of $\hat{a}_{i,k}$ for analytical evaluation of the jitter variance. Note that we may absorb the factor g_i in $a_{i,k}$ by defining $a'_{i,k} = g_i a_{i,k}$ so that $E[(a'_{i,k})^2] = g_i^2 E_i$. If we replace $M = 2$ in the above expression we obtain the expected result derived in section 5.2. Consequently, the analysis of the jitter variance follows exactly along the same lines as for the two channel modulation case presented in the appendix A. To present the results we follow the outline of the appendix but omit writing the intermediate derivations. Replacing $y_{l,k} = C_c + n_{l,k}$ in the likelihood function and collecting terms we have

$$\Lambda = \sum_{k=0}^{K-1} \sum_{l=1}^{M} g_l a_{l,k} C_{l,k} + \sum_{k=0}^{K-1} \sum_{l=1}^{M} g_l n_{l,k} a_{l,k} = \Lambda_1 + \Lambda_2.$$

Now, $E[(\partial \Lambda / \partial \tau)^2] = E[(\partial \Lambda_1 / \partial \tau)^2] + E[(\partial \Lambda_2 / \partial \tau)^2]$ since the cross product term has zero expectation (see the appendix A) and $E[\partial^2 \Lambda / \partial \tau^2] = E[\partial^2 \Lambda_1 / \partial \tau^2]$ since $E[\partial^2 \Lambda_2 / \partial \tau^2] = 0$ (see the appendix A). It can be verified that

$$E[(\partial \Lambda_2 / \partial \tau)^2] = -\frac{N_o}{2} K \sum_{l=1}^{M} g_l^2 E_l r_{\phi_l \phi_l}^{(2)}(0) \tag{5.15}$$

$$E[\partial^2 \Lambda_1 / \partial \tau^2] = K \sum_{l=1}^{M} g_l^2 E_l r_{\phi_l \phi_l}^{(2)}(0). \tag{5.16}$$

The derivation of $E[(\partial \Lambda_1 / \partial \tau)^2]$ is straight forward but tedius. We omit the details for brevity

$$
\begin{aligned}
E[(\partial \Lambda_1 / \partial \tau)^2] &= K \sum_{m=1}^{M} \sum_{i=1}^{M} g_m^2 g_i^2 E_m E_i \sum_n (r_{\phi_i \phi_m}^{(1)}(n\Delta))^2 - \\
&\quad \sum_{m=1}^{M} g_m^4 \sum_{k=0}^{K-1} \sum_{l=0}^{K-1} (E_m r_{\phi_m \phi_m}^{(1)}((k-l)\Delta))^2 - \\
&\quad \sum_{m=1}^{M} \sum_{n=1, n \neq m}^{M} g_m^2 g_n^2 E_m E_n \sum_{k=0}^{K-1} \sum_{l=0}^{K-1} (r_{\phi_n \phi_m}^{(1)}((l-k)\Delta))^2.
\end{aligned}
$$

$$(5.17)$$

Using the following equality

$$
\sum_{k=0}^{K-1} \sum_{l=0}^{K-1} (r_{\phi_n \phi_m}^{(1)}((l-k)\Delta))^2 = K \sum_{l=-(K-1)}^{(K-1)} (1 - \frac{|l|}{K})(r_{\phi_n \phi_m}^{(1)}(l\Delta))^2, \qquad (5.18)
$$

the above expression simplifies to

$$
E\left[\left(\frac{\partial \Lambda_1}{\partial \tau}\right)^2\right] = K \sum_{m=1}^{M} \sum_{i=1}^{M} g_m^2 g_i^2 E_m E_i [\sum_{|l| \geq K} (r_{\phi_i \phi_m}^{(1)}(l\Delta))^2 + \sum_{|l| \leq (K-1)} \frac{|l|}{K} (r_{\phi_i \phi_m}^{(1)}(l\Delta))^2].
$$

$$(5.19)$$

Putting the pieces together we have

$$
\sigma_\tau^2(noise) = -\frac{N_o/2}{K \sum_{l=1}^{M} g_l^2 E_l r_{\phi_l \phi_l}^{(2)}(0)} \qquad (5.20)
$$

$$
\sigma_\tau^2(PDJ) = \frac{E[(\partial \Lambda_1 / \partial \tau)^2]}{(K \sum_{l=1}^{M} g_l^2 E_l r_{\phi_l \phi_l}^{(2)}(0))^2} \qquad (5.21)
$$

Clearly the energy distribution and the channel gain in each subband has a major impact on the variance of the timing jitter and indeed the jitter variance may be optimized with respect to the energy distribution in the subchannels. As noted above, many times the energy distribution within the subbands is adjusted by the desire to maximize the data throughput of the overall scheme, and not based on considerations of the effect of this distribution on the timing jitter. However, a joint iterative optimization is indeed plausible whereby the energy distribution in the subbands is adjusted for throughput maximization but taking into account the deteriorating effect of the timing jitter.

For a given energy distribution in the subbands, there is yet another degree of freedom in system design and that is the choice of the splitting

sequences. Let us consider the effect of the splitting sequences under several cases of practical interest.

Case I: Low SNR and Large K

In this case the timing jitter variance due to noise dominates the component of the jitter variance due to PDJ. Consider expressing the denominator of equation (5.20) in the transform domain. The Fourier transform of $r^{(2)}_{\phi_l \phi_l}(\alpha)$ denoted $\mathcal{F}[r^{(2)}_{\phi_l \phi_l}(\alpha)]$ is $\mathcal{F}[r^{(2)}_{\phi_l \phi_l}(\alpha)] = -4\pi^2 f^2 |\Phi_l(f)|^2$, where $\Phi_l(f)$ denotes the Fourier transform of $\phi_l(t)$. Hence, we may write

$$
\begin{aligned}
\sum_{l=1}^{M} g_l^2 E_l r^{(2)}_{\phi_l \phi_l}(0) &= -\sum_{l=1}^{M} g_l^2 E_l \int_{-\infty}^{\infty} 4\pi^2 f^2 |\Phi_l(f)|^2 df \\
&= -\int_{-\infty}^{\infty} \{4\pi^2 f^2 \sum_{l=1}^{M} g_l^2 E_l |\Phi_l(f)|^2\} df. \qquad (5.22)
\end{aligned}
$$

Recalling that the individual shaping pulses $\phi_l(t)$ are obtained via splitting the spectrum of an elementary shaping pulse $s(t)$ we may write

$$
|\Phi_l(f)|^2 = |H_l(e^{j2\pi f \Delta/M})|^2 |S(f)|^2
$$

where $H_l(e^{j2\pi f \Delta/M})$ is the DFT of the splitting sequence associated with the l-th subchannel. Hence, we may write

$$
\sum_{l=1}^{M} g_l^2 E_l r^{(2)}_{\phi_l \phi_l}(0) = -\int_{-\infty}^{\infty} \{4\pi^2 f^2 \sum_{l=1}^{M} g_l^2 E_l |H_l(e^{j2\pi f \Delta/M})|^2\} |S(f)|^2 df. \quad (5.23)
$$

This equation captures the influence of the splitting sequences on the timing jitter variance. In particular, we would like to maximize the absolute value of the integral expression in equation (5.23) via an appropriate choice of the splitting sequences. Generally speaking short splitting sequences generate subchannels with larger bandwidths and reduced spectral height (since the signal energy is kept constant), in comparison to long splitting sequences that generate subchannels with smaller bandwidths and larger spectral heights. Naturally as the spectrum of the subchannels widen, there is more spectral overlap among adjacent subchannels. Interestingly enough, the integral expression in equation (5.23) suggests that in certain cases *short* splitting sequences leading to wider bandwidth subchannels may be preferred from a timing point of view. Note that short splitting sequences lead to wider subchannels and hence more ACI due to timing offsets. However, when the SNR is low and observation interval is large, the noise has the dominating effect on the jitter variance.

Case II: High SNR and Small K

In this case, the jitter variance due to noise is assumed to be negligible. The

impact of the splitting sequences on the denominator of expression of the jitter variance due to PDJ in equation (5.21) is already studied in case I and expressed in equation (5.23). Consider equation (5.19)and note that we have the upper bound

$$\left\{ \sum_{|l|\geq K} (r^{(1)}_{\phi_i \phi_m}(l\Delta))^2 + \sum_{|l|\leq(K-1)} \frac{|l|}{K}(r^{(1)}_{\phi_i \phi_m}(l\Delta))^2 \right\} < \sum_{l}(r^{(1)}_{\phi_i \phi_m}(l\Delta))^2. \qquad (5.24)$$

This upper bound should be tight for small K. To get more insights about the impact of the splitting sequences on the jitter variance, consider expressing $\sum_l (r^{(1)}_{\phi_i \phi_m}(l\Delta))^2$ in the transform domain

$$\sum_{l}(r^{(1)}_{\phi_i \phi_m}(l\Delta))^2 = 4\pi^2 \int_{-\infty}^{\infty}\int_{-\infty}^{\infty} f\eta \Phi_i(f)\Phi_i^*(\eta)\Phi_m^*(f)\Phi_m(\eta)\left(\sum_l e^{j2\pi(f-\eta)l\Delta}\right) df\, d\eta$$
$$(5.25)$$
$$= \frac{4\pi^2}{\Delta} \sum_l \int_{-\infty}^{\infty} f(f-\frac{l}{\Delta})\Phi_i(f)\Phi_i^*\left(f-\frac{l}{\Delta}\right)\Phi_m^*(f)\Phi_m\left(f-\frac{l}{\Delta}\right) df,$$
$$(5.26)$$

where, we have used the distributional equality

$$\sum_l e^{j2\pi(f-\eta)l\Delta} = \frac{1}{\Delta}\sum_l \delta\left(f-\eta-\frac{l}{\Delta}\right)$$

in equation (5.25) to get equation (5.26). Replacing this upper bound in equation (5.19) we get

$$E\left[\left(\frac{\partial \Lambda_1}{\partial \tau}\right)^2\right] < K\frac{4\pi^2}{\Delta}\sum_{m=1}^{M}\sum_{i=1}^{M} g_m^2 g_i^2 E_m E_i \cdot$$
$$\sum_l \left\{\int_{-\infty}^{\infty} f\left(f-\frac{l}{\Delta}\right)\Phi_i(f)\Phi_i^*\left(f-\frac{l}{\Delta}\right)\Phi_m^*(f)\Phi_m\left(f-\frac{l}{\Delta}\right) df\right\}$$
$$= K\frac{4\pi^2}{\Delta}\int_{-\infty}^{\infty} f^2 \left\{\sum_{i=1}^{M} g_i^2 E_i |H_i(e^{j2\pi f\Delta/M})|^2\}^2 |S(f)|^4 df\right\} +$$
$$K\frac{4\pi^2}{\Delta}\sum_{l\neq 0}\left\{\int_{-\infty}^{\infty} f(f-\frac{l}{\Delta})|\sum_{i=1}^{M} g_i^2 E_i \Phi_i(f)\Phi_i^*(f-\frac{l}{\Delta})|^2 df\right\}.$$
$$(5.27)$$

Generally speaking, the first half of equation (5.27), constitutes the most significant part of the upper bound on $E[(\partial \Lambda_1/\partial \tau)^2]$. When uniform bandwidth filterbanks are used for the split of the spectrum of $s(t)$, the center frequency

of the subchannel $\Phi_l(f)$ is $\frac{l}{\Delta}$. Note that the second half of equation (5.27) reduces to zero, if the subchannels $\Phi_l(f)$ for different l *do not overlap* in the frequency domain. Using the most significant part of equation (5.27) in the expression of the jitter variance, we may write

$$\sigma_\tau^2 \simeq \frac{\int_{-\infty}^{\infty} f^2 \{\sum_{i=1}^{M} g_i^2 E_i |H_i(e^{j2\pi f\Delta/M})|^2\}^2 |S(f)|^4 df}{K\Delta\{\int_{-\infty}^{\infty} f^2 \sum_{i=1}^{M} g_i^2 E_i |H_i(e^{j2\pi f\Delta/M})|^2 |S(f)|^2 df\}^2}. \qquad (5.28)$$

The impact of the splitting sequences on the variance of the timing jitter is essentially captured in equation (5.28). Note that now, it may be desirable to have splitting sequences that generate subchannels with sharp transitions and small amount of overlap in the frequency domain.

Case III: Intermediate Values of SNR and K

Looking at the two extreme cases considered above, it is evident that for intermediate values of SNR and K, the splitting sequences can be optimized to minimize the total expression for the jitter variance. We can make the following general observations:

1. the most significant subchannels in so far as the timing is concerned, are those for which the product $g_l^2 E_l$ is large. It is important that the splitting sequences for these subchannels be properly chosen to maximize the denominator term in the expressions of the jitter variance given above;

2. in a suboptimal (but reduced complexity) design, we may consider using the timing information from a *subset* of the subchannels. Once again, the derivations above provide guidelines for how to select the subchannels from which the timing information should be derived.

5.3.2   Multichannel SSB Transmission at RF

The multichannel modulation schemes employing a set of modulated elementary shaping pulses obtained via the splitting procedure presented in section 1, have two split sidebands around the carrier frequency f_0. This may be undesirable in application since the split sidebands of a given subchannel may experience different attenuations and phase shifts due to the linear filtering effect of the channel. However, the use of single sideband transmission eliminates this problem. In this subsection we shall assume as in the previous subsection, that the spectrum of a baseband Nyquist pulse is subdivided into a set of M possibly unequal width subchannels, and SSB-BPSK modulation with different energy levels for each subchannel is employed for data transmission. The receiver is assumed to operate coherently, and the effect of the

channel in each subband is essentially an attenuation and group delay. We use the same notation and definitions as above.

The received signal prior to mixing with the carrier at frequency f_0 is $z(t) = z_p(t) - z_q(t)$ with

$$z_p(t) = \left[\sum_{l=1}^{M}\sum_{n} g_l a_{l,n} \phi_l(t - n\Delta - \tau - \tau_l) + n_p(t - \tau)\right] \cos(\omega_0 t)$$

and

$$z_q(t) = \left[\sum_{l=1}^{M}\sum_{n} g_l a_{l,n} \hat{\phi}_l(t - n\Delta - \tau - \tau_l) + n_q(t - \tau)\right] \sin(\omega_0 t)$$

where $\hat{\phi}_l(.)$ is the Hilbert transform of $\phi_l(.)$ and $n_p(.)$ and $n_q(.)$ are the in-phase and quadrature components of the narrowband additive Gaussian noise with spectral density $N_o/2$ over a band of frequencies assumed to be significantly larger than the overall signal bandwidth. $n_p(.)$ and $n_q(.)$ are independent baseband Gaussian processes with spectral density level N_o. After carrier mixing we have the in-phase and quadrature components of the signal

$$r_p(t) = 0.5\left[\sum_{l=1}^{M}\sum_{n} g_l a_{l,n} \phi_l(t - n\Delta - \tau - \tau_l) + n_p(t - \tau)\right] + r_{ph}(t)$$

and

$$r_q(t) = 0.5\left[\sum_{l=1}^{M}\sum_{n} g_l a_{l,n} \hat{\phi}_l(t - n\Delta - \tau - \tau_l) + n_q(t - \tau)\right] + r_{qh}(t),$$

where $r_{ph}(t)$ and $r_{qh}(t)$ are high frequency terms which would be eliminated after matched filtering. The quadrature component $r_q(t)$ is passed through a Hilbert transformer and the resulting output is coherently combined with $r_p(t)$ to yield

$$r(t) = \sum_{l=1}^{M}\sum_{n} g_l a_{l,n} \phi_l(t - n\Delta - \tau - \tau_l) + 0.5(n_p(t - \tau) - \hat{n}_q(t - \tau)) + r_h(t)$$

where $\hat{n}_q(.)$ is the Hilbert transform of $n_q(.)$ and $r_h(t)$ is the high frequency term of $r(t)$ that would be eliminated by the matched filter. The resulting baseband noise component $n_1(t - \tau) = 0.5(n_p(t - \tau) - \hat{n}_q(t - \tau))$ is a baseband Gaussian noise process with spectral density $N_o/2$ over a band of frequencies assumed to be significantly larger than the signal bandwidth. From this point on the derivation of the jitter variance is identical to the baseband case considered above and identical results are obtained.

5.3.3 Multichannel Diversity Transmission Over a Slow-Fading Channel

Frequency diversity is a natural mean of combating the detrimental effects of fading. In such applications, the same data is transmitted over several orthogonal frequency subchannels, whereby each subchannel may introduce a random attenuation and a phase shift due to fading. Here, we consider the case where QPSK modulation is used in a multichannel modulation scheme, whereby the transmitted energy is the same in all the M subchannels and all the subchannels carry the same data, in order to achieve frequency diversity. We consider a coherent receiver and assume that we have perfect carrier recovery.

The in-phase component of the received signal after carrier mixing is

$$r_p(t) = \sum_{l=1}^{M} \sum_n g_{l,p} a_{n,p} \phi_l(t - n\Delta - \tau) + n_p(t - \tau)$$

and the quadrature component is

$$r_q(t) = \sum_{l=1}^{M} \sum_n g_{l,q} a_{n,q} \phi_l(t - n\Delta - \tau) + n_q(t - \tau)$$

where $(g_{l,p} + jg_{l,q})$ is the complex channel coefficient associated with the l-th subchannel, $(a_{n,p} + ja_{n,q})$ are the transmitted QPSK symbols, $\phi_l(t)$ is the shaping pulse of the l-th subchannel and $n_p(.)$ and $n_q(.)$ are components of a narrowband Gaussian noise process with power spectral density equal to $N_0/2$ on the signal bandwidth. We assume that $\{a_{n,p}\}_{-\infty}^{\infty}$ and $\{a_{n,q}\}_{-\infty}^{\infty}$ are two iid equiprobable BPSK sequences associated with the in-phase and quadrature components with $E[a_{n,p}^2] = E[a_{n,q}^2] = E_a$.

The approximate DD ML symbol timing estimator, whose structure is shown in Fig. 5.1 in the case $M = 2$, yields $\tau^* = \arg\max_{\tau'} \Lambda$, i.e.

$$\tau^* = \arg\max_{\tau'} \sum_{k=0}^{K-1} \sum_{i=1}^{M} (g_{i,p} \hat{a}_{k,p} y_{i,k,p} + g_{i,q} \hat{a}_{k,q} y_{i,k,q})$$

where, $y_{i,k,p} = C_{i,k,p} + n_{i,k,p}$, $C_{i,k,p} = \sum_{l=1}^{M} \sum_n g_{l,p} a_{n,p} r_{\phi_l \phi_i}((n-k)\Delta + (\tau - \tau'))$, $n_{i,k,p}$ is the projection of $n_p(.)$ on the k-th shift of the i-th shaping pulse associated with subchannel i, $r_{\phi_l \phi_i}(.)$ is the cross-correlation between $\phi_l(t)$ and $\phi_i(t)$ and $\hat{a}_{k,p}$ are the detected bits associated with the in-phase component of the received signal. The definitions for the quadrature components are totally analogous. As usual, assuming that the receiver is operating at low bit error rates, we shall use $a_{k,p}$ and $a_{k,q}$ in the above expression for the

derivation of the jitter variance. The derivation of the timing jitter variance is lengthy, but the procedure is conceptually straightforward. In the interest of brevity, we shall simply outline the procedure and present the main results without showing all the derivations.

Upon replacing $y_{i,k,p} = C_{i,k,p} + n_{i,k,p}$ and $y_{i,k,q} = C_{i,k,q} + n_{i,k,q}$ in the expression for Λ, the log-likelihood function breaks up into four parts

$$\Lambda = (\Lambda_{1,p} + \Lambda_{2,p}) + (\Lambda_{1,q} + \Lambda_{2,q})$$

where

$$\Lambda_{1,p} = \sum_{k=0}^{K-1} \sum_{i=1}^{M} g_{i,p} a_{k,p} C_{i,k,p},$$

$$\Lambda_{2,p} = \sum_{k=0}^{K-1} \sum_{i=1}^{M} g_{i,p} a_{k,p} n_{i,k,p},$$

and the expressions for $\Lambda_{1,q}$ and $\Lambda_{2,q}$ are analogous to $\Lambda_{1,p}$ and $\Lambda_{2,p}$, respectively. Clearly,

$$E\left(\frac{\partial \Lambda}{\partial \tau}\right)^2 = E\left(\frac{\partial \Lambda_{1,p}}{\partial \tau} + \frac{\partial \Lambda_{2,p}}{\partial \tau}\right)^2 + E\left(\frac{\partial \Lambda_{1,q}}{\partial \tau} + \frac{\partial \Lambda_{2,q}}{\partial \tau}\right)^2 +$$

$$2E\left(\frac{\partial \Lambda_{1,p}}{\partial \tau}\frac{\partial \Lambda_{1,q}}{\partial \tau} + \frac{\partial \Lambda_{1,p}}{\partial \tau}\frac{\partial \Lambda_{2,q}}{\partial \tau} + \frac{\partial \Lambda_{2,p}}{\partial \tau}\frac{\partial \Lambda_{2,q}}{\partial \tau}\right). \tag{5.29}$$

It can be shown that

$$E\left(\frac{\partial \Lambda_{1,p}}{\partial \tau}\frac{\partial \Lambda_{2,q}}{\partial \tau}\right) = 0 \tag{5.30}$$

$$E\left(\frac{\partial \Lambda_{2,p}}{\partial \tau}\frac{\partial \Lambda_{1,q}}{\partial \tau}\right) = 0 \tag{5.31}$$

$$E\left(\frac{\partial \Lambda_{2,p}}{\partial \tau}\frac{\partial \Lambda_{2,q}}{\partial \tau}\right) = 0 \tag{5.32}$$

$$E\left(\frac{\partial \Lambda_{1,p}}{\partial \tau}\frac{\partial \Lambda_{2,p}}{\partial \tau}\right) = 0 \tag{5.33}$$

$$E\left(\frac{\partial \Lambda_{1,q}}{\partial \tau}\frac{\partial \Lambda_{2,q}}{\partial \tau}\right) = 0. \tag{5.34}$$

Hence,

$$E\left(\frac{\partial \Lambda}{\partial \tau}\right)^2 = E\left(\frac{\partial \Lambda_{1,p}}{\partial \tau}\right)^2 + E\left(\frac{\partial \Lambda_{2,p}}{\partial \tau}\right)^2$$

$$+E\left(\frac{\partial \Lambda_{1,q}}{\partial \tau}\right)^2 + E\left(\frac{\partial \Lambda_{2,q}}{\partial \tau}\right)^2 + 2E\left(\frac{\partial \Lambda_{1,p}}{\partial \tau}\frac{\partial \Lambda_{1,q}}{\partial \tau}\right). \tag{5.35}$$

95

Evaluation of the components of the jitter variance above yields

$$E\left(\frac{\partial \Lambda_{1,p}}{\partial \tau}\frac{\partial \Lambda_{1,q}}{\partial \tau}\right) =$$

$$= K^2 E_a^2 \sum_{i=1}^{M}\sum_{l=1}^{M}\sum_{j=1}^{M}\sum_{u=1}^{M} g_{i,p}g_{l,p}g_{j,q}g_{u,q} r^{(1)}_{\phi_l\phi_i}(0)r^{(1)}_{\phi_u\phi_j}(0) \tag{5.36}$$

$$E\left(\frac{\partial \Lambda_{1,p}}{\partial \tau}\right)^2 = \left[KE_a \sum_{i=1}^{M}\sum_{l=1}^{M} g_{i,p}g_{l,p} r^{(1)}_{\phi_l\phi_i}(0)\right]^2 +$$

$$\sum_{i=1}^{M}\sum_{l=1}^{M}\sum_{j=1}^{M}\sum_{u=1}^{M} g_{i,p}g_{l,p}g_{j,p}g_{u,p}\left[\sum_{n\neq 0} K r^{(1)}_{\phi_l\phi_i}(n\Delta)r^{(1)}_{\phi_u\phi_j}(n\Delta)\right.$$

$$\left. + \sum_{k=0}^{K-1}\sum_{m=0,m\neq k}^{K-1} r^{(1)}_{\phi_l\phi_i}((m-k)\Delta)r^{(1)}_{\phi_u\phi_j}((k-m)\Delta)\right] E_a^2 \tag{5.37}$$

$$E\left(\frac{\partial \Lambda_{2,p}}{\partial \tau}\right)^2 = N_o E_a K \sum_{i=1}^{M}\sum_{j=1}^{M} g_{i,p}g_{j,p}\int_{-\infty}^{\infty}\phi_i^{(1)}(t)\phi_j^{(1)}(t)dt. \tag{5.38}$$

The expressions for $E(\partial \Lambda_{1,q}/\partial \tau)^2$ and $E(\partial \Lambda_{2,q}/\partial \tau)^2$ are identical to equations (5.37) and (5.38) with subscript p replaced by q. Note that expressing $\int_{-\infty}^{\infty}\phi_i^{(1)}(t)\phi_j^{(1)}(t)dt$ in the transform domain, it is easy to verify that this integral equals $-r^{(2)}_{\phi_i\phi_j}(0)$. Similarly, it can be shown that

$$E\left(\frac{\partial^2 \Lambda}{\partial \tau^2}\right) = KE_a \sum_{i=1}^{M}\sum_{l=1}^{M}(g_{i,p}g_{l,p} + g_{i,q}g_{l,q})r^{(2)}_{\phi_l\phi_i}(0). \tag{5.39}$$

Consider now equation (5.36), which can be written as

$$(KE_a)^2 \sum_{i=1}^{M}\sum_{l=1}^{M} g_{i,p}g_{l,p} r^{(1)}_{\phi_l\phi_i}(0) \sum_{i=n}^{M}\sum_{m=1}^{M} g_{n,q}g_{m,q} r^{(1)}_{\phi_m\phi_n}(0) \tag{5.40}$$

and take one of the expressions in the above product, say the first term. For $i = l$ we have $r^{(1)}_{\phi_i\phi_i}(0) = 0$ since the autocorrelation peaks at origin. Consider the off diagonal terms in the double summation and combine symmetric terms to generate expressions of the type $X_{l,i} = g_i g_l r^{(1)}_{\phi_l\phi_i}(0) + g_l g_i r^{(1)}_{\phi_i\phi_l}(0)$. Noting that $r^{(1)}_{\phi_l\phi_i}(\alpha) = -r^{(1)}_{\phi_i\phi_l}(-\alpha)$ we conclude that $X_{l,i}$ reduces to zero. Hence, the overall expression in equation (5.36) equals zero. For the same reason, the first part of equation (5.37) is also zero.

Putting the pieces together we have

$$\sigma_\tau^2(noise) = -\frac{N_o}{KE_a \sum_{i=1}^{M} \sum_{l=1}^{M} (g_{i,p}g_{l,p} + g_{i,q}g_{l,q})r_{\phi_l\phi_i}^{(2)}(0)} \tag{5.41}$$

$$\sigma_\tau^2(PDJ) = \frac{E(\partial\Lambda_{1,p}/\partial\tau)^2 + E(\partial\Lambda_{1,q}/\partial\tau)^2}{\left[KE_a \sum_{i=1}^{M} \sum_{l=1}^{M} (g_{i,p}g_{l,p} + g_{i,q}g_{l,q})r_{\phi_l\phi_i}^{(2)}(0) \right]^2}. \tag{5.42}$$

To proceed further, consider a component of the second part of equation (5.37) which can be written as

$$\sum_{k=0}^{K-1} \sum_{m=0,m\neq k}^{K-1} r_{\phi_l\phi_i}^{(1)}((m-k)\Delta)r_{\phi_u\phi_j}^{(1)}((k-m)\Delta) =$$

$$K \sum_{n=-(K-1),n\neq 0}^{(K-1)} \left(1 - \frac{|n|}{K}\right) r_{\phi_l\phi_i}^{(1)}(n\Delta)r_{\phi_u\phi_j}^{(1)}(-n\Delta). \tag{5.43}$$

If the shaping pulses $\{\phi_l\}_{l=1}^{M}$ are either all even or all odd, then $r_{\phi_u\phi_j}^{(1)}(-n\Delta) = -r_{\phi_u\phi_j}^{(1)}(n\Delta)$ and equation (5.37) reduces to

$$E(\partial\Lambda_{1,p}/\partial\tau)^2 = KE_a^2 \sum_{i=1}^{M} \sum_{l=1}^{M} g_{i,p}^2 g_{l,p}^2$$

$$\left[\sum_{|n|\geq K} (r_{\phi_l\phi_i}^{(1)}(n\Delta))^2 + \sum_{|n|\leq(K-1)} \frac{|n|}{K}(r_{\phi_l\phi_i}^{(1)}(n\Delta))^2 \right]. \tag{5.44}$$

The equation for $E(\partial\Lambda_{1,q}/\partial\tau)^2$ is identical to equation (5.44) with p replaced by q. Let us now consider the effect of the splitting sequences on the timing jitter variance under several different conditions.

Case I: Low SNR and Large K

In this case the component of the jitter variance due to noise dominates that of the Pattern Dependent Jitter (PDJ). The impact of the splitting sequences is essentially captured in the denominator of equation (5.41). Since a priori the channel attenuation coefficients are unknown ad time varying, the natural line of pursuit is to assume that they are all equal. We shall make this assumption and for simplicity we shall set these coefficients to be equal to one. With this set up, the denominator of equation (5.41) reduces to $-2KE_a \sum_{i=1}^{M} \sum_{l=1}^{M} r_{\phi_l\phi_i}^{(2)}(0)$. Consider expressing this quantity in the transform domain

$$-\sum_{i=1}^{M} \sum_{l=1}^{M} r_{\phi_l\phi_i}^{(2)}(0) = \sum_{i=1}^{M} \sum_{l=1}^{M} \int_{-\infty}^{\infty} (2\pi f)^2 \Phi_l(f)\Phi_i^*(f)df$$

97
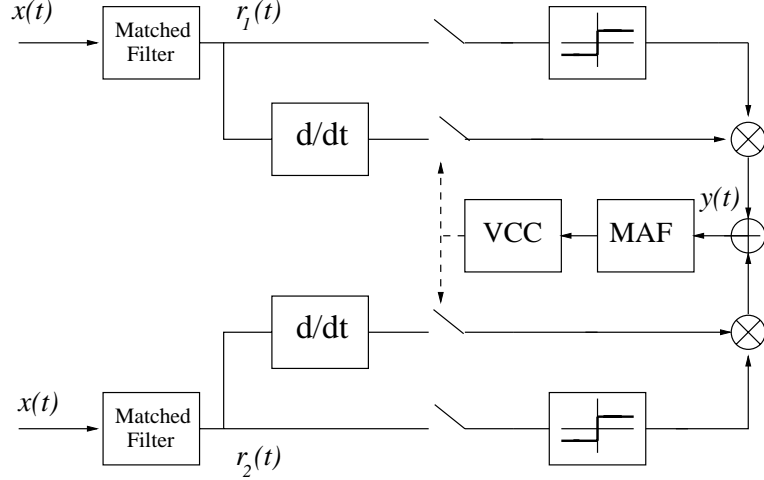
Figure 5.1. The proposed approximate DD ML two channel synchronizer.

$$= \int_{-\infty}^{+\infty} 4\pi^2 f^2 \left[\sum_{i=1}^{M} \sum_{l=1}^{M} \Phi_l(f) \Phi_i^*(f) \right] df$$

$$= \int_{-\infty}^{\infty} (2\pi f)^2 \left| \sum_{i=1}^{M} \Phi_i(f) \right|^2 df$$

$$= \int_{-\infty}^{\infty} (2\pi f)^2 \left| \sum_{i=1}^{M} H_i(e^{j2\pi f\Delta/M}) \right|^2 |S(f)|^2 df, \tag{5.45}$$

where, the last equality arises since $S(F)$ is the Fourier transform of the shaping pulse $s(t)$ that is originally split, $\Phi_i(f) = H_i(e^{j2\pi f\Delta/M})S(f)$ and $H_i(e^{j2\pi f\Delta/M})$ is the DFT of the splitting sequence for the i-th subchannel. Equation (5.45) captures the effect of the splitting sequences on the variance of the timing jitter. Note that the *phase characteristic* of the splitting sequences has impact on the jitter variance. Since the splitting sequences are assumed to be generated using QMF filterbanks, we have that

$$\left| \sum_{i=1}^{M} H_i(e^{j2\pi f\Delta/M}) \right|^2 \leq \sum_{i=1}^{M} |H_i(e^{j2\pi f\Delta/M})|^2 = M. \tag{5.46}$$

The inequality of equation (5.46) becomes an equality if indeed the individual transfer functions $H_i(e^{j2\pi f\Delta/M})$ for different i have disjoint frequency supports so that at any given frequency, only one term in the summation

$\sum_{i=1}^{M} H_i(e^{j2\pi f\Delta/M})$ is nonzero. The bound in equation (5.46) allows us to write

$$\sigma_\tau^2 \geq \frac{N_o}{-2KE_aMr_{ss}^{(2)}(0)}. \tag{5.47}$$

Figure 5.2. Normalized timing variance due to noise: average over 500 fading channels (-) and over flat frequency channel (- -) as a function of the Battle-Lemarié filters order.

Equation (5.47) shows that the jitter variance due to noise in this multichannel modulation is *always higher* than the case when a single shaping pulse is used. Note however that the present result is obtained assuming that the channel gain coefficients are all equal. In practice, this is never the case, and indeed the reason multichannel modulation was used in the present example, was to combat the detrimental effects of fading. Fig. 5.2 shows the average over five hundred fading channels of the normalized variance of the timing jitter due to noise as a function of the Battle-Lemarié filter order N for eight subchannels generated splitting a square root raised cosine pulse with 30 % excess BW. The bound for the flat channel, which is independent on the splitting sequences, is also shown for comparison. We can observe that, for the most part, the jitter variance due to noise is weakly dependent on N and, as in the case of the baseband channel of section5.3.1 , is primarily a function of the original shaping pulse whose spectrum is split.

Case II: Large SNR and Small K

In this case the component of the jitter variance due to noise is assumed to be

negligible. Note that equation (5.44) is identical to the expression that can be found in the case of transmission over a baseband channel [13]. Using the same procedure applied in case of multichannel modulation over a baseband channel, we have the following upper bound which should be tight for small K

$$E[(\partial\Lambda_{1,p}/\partial\tau)^2] + E[(\partial\Lambda_{1,q}/\partial\tau)^2] <$$

$$\frac{8KE_a^2\pi^2}{\Delta} \int_{-\infty}^{\infty} f^2 \left[\sum_{i=1}^{M} |H_i(e^{j2\pi f\Delta/M})|^2\right]^2 |S(f)|^4 df +$$

$$\frac{8KE_a^2\pi^2}{\Delta}\sum_{l\neq 0} \left[\int_{-\infty}^{\infty} f\left(f - \frac{l}{\Delta}\right) \left|\sum_{i=1}^{M} \Phi_i(f)\Phi_i^*\left(f - \frac{l}{\Delta}\right)\right|^2 df\right]. \qquad (5.48)$$

In the above expression, generally the most significant term is the first half of equation (5.48), since the adjacent subchannels do not have significant overlap in the frequency domain. Recalling that $\sum_{i=1}^{M} |H_i(e^{j2\pi f\Delta/M})|^2 = M$, the first half of equation (5.48) is in fact independent of the splitting sequences. Hence, we have the following approximate expression for $\sigma_\tau^2(PDJ)$

$$\sigma_\tau^2(PDJ) \simeq \frac{M^2 \int_{-\infty}^{\infty} f^2 |S(f)|^4 df}{8\pi^2 K\Delta \left[\int_{-\infty}^{\infty} f^2 \left|\sum_{i=1}^{M} H_i(e^{j2\pi f\Delta/M})\right|^2 |S(f)|^2 df\right]^2}. \qquad (5.49)$$

Equation (5.49) captures the impact of the splitting sequences on the timing jitter variance. The bound that can be obtained for the flat channel and the average of the of the PDJ variance over five hundred fading channels are shown in Fig. 5.3 as a function of the Battle-Lemarié filter order N. The PDJ variance depends on the choice of the splitting sequences and this dependence is stronger than in the case of transmission over baseband channel [13]. In fact, as noted before, in this case the phase characteristic of the splitting sequences is also important. It is also possible to observe that, as in the case of the baseband channel, less selective splitting sequences associated with small values of N produce the best results.

Case III: Intermediate Values of SNR and K

For intermediate values of SNR and K, the second half of equation (5.48) (note that this term could have a negative contribution) and the denominator term appearing in the expression for both $\sigma_\tau^2(noise)$ and $\sigma_\tau^2(PDJ)$, are the only terms impacted by the choice of the splitting sequences. Clearly, the splitting sequences can be optimized considering their effect on the overall jitter variance.
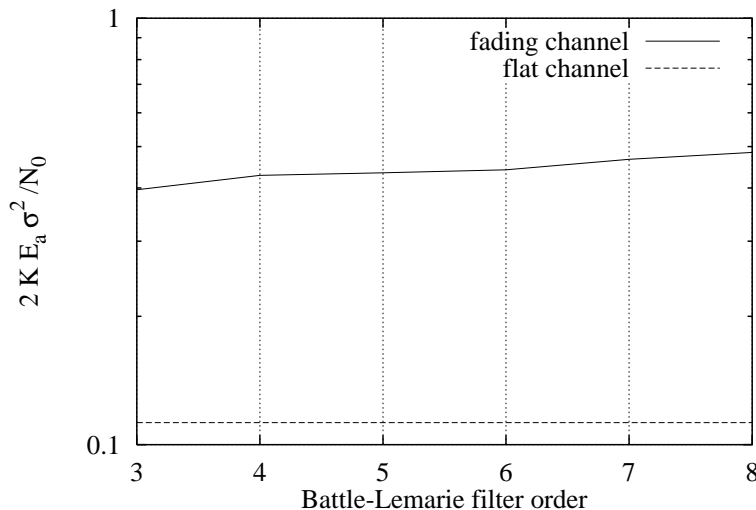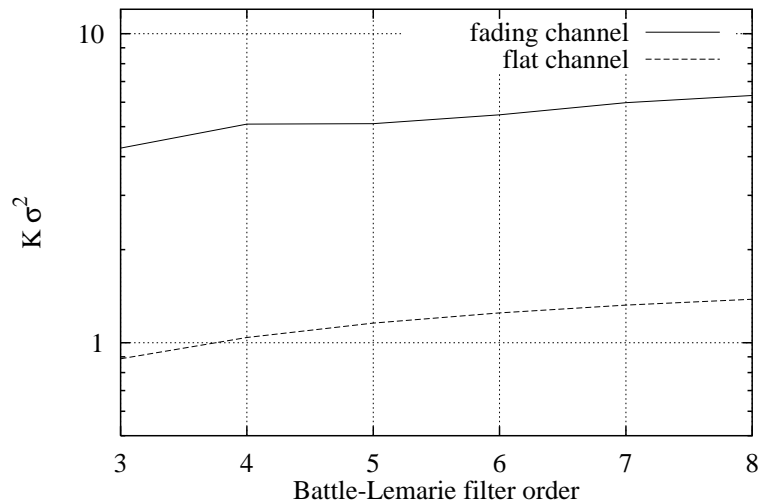
Figure 5.3. Normalized timing PDJ variance: average over 500 fading channels (-) and over flat frequency channel (- -) as a function of the Battle-Lemarié filters order.

5.4   Implementation issues

The actual implementation of the approximate DD ML two-channel synchronizer is reported in Figure 5.1. The scheme can be considered an extension to multichannel modulation of the one presented in [42], and can be generalized for a generic number of channels M. In the following we will give some considerations about the actual functionality of the proposed scheme.

5.4.1   Tracking phase analysis

In this section we analyze the timing synchronizer behavior in tracking mode, when the information extracted form each branch is combined to recover the clock signal.

As an example, we will consider in the following a two channel scheme in which the signal spanning the low-pass channel is denoted as $\phi_1(t) = s(t)$, while the signal spanning the high-pass channel is denoted as $\phi_2(t) = w(t)$.

The transmitted signal has the form

$$x(t) = \sum_{n=-\infty}^{+\infty} \alpha_{s,n} s(t - n\Delta) + \alpha_{w,n} w(t - n\Delta)$$

101

where $\{\alpha_{s,n}\}_{n=-\infty}^{+\infty}$ and $\{\alpha_{w,n}\}_{n=-\infty}^{+\infty}$ are i.i.d symbols sequences and Δ is the signaling period. Considering the upper branch of the scheme and denoting as $r_1(t)$ the signal obtained after the matched filter, we have:

$$r_1(t) = \sum_{n=-\infty}^{+\infty} \alpha_{s,n} r_{ss}(t) + \alpha_{w,n} r_{sw}(t)$$

while on the lower branch we have:

$$r_2(t) = \sum_{n=-\infty}^{+\infty} \alpha_{s,n} r_{ws}(t) + \alpha_{w,n} r_{ww}(t).$$

Assuming that the correct symbol is decided, and denoting as $y(t)$ the signal at the input of the Moving Average Filter (MAF), we have

$$y(l\Delta) = \alpha_s^2 r_{ss}^{(1)}(l\Delta) + \alpha_s \alpha_w r_{sw}^{(1)}(l\Delta) +$$

$$\alpha_w^2 r_{ww}^{(1)}(l\Delta) + \alpha_s \alpha_w r_{ws}^{(1)}(l\Delta) \tag{5.50}$$

It has to be noted that the terms depending on the cross-correlations in equation (5.50) are undesired terms; in case of misalignment of the reconstructed clock with respect to the correct sampling instant, only the derivative of the auto-correlations, $r_{ss}^{(1)}(t)$ and $r_{ww}^{(1)}(t)$, give the correct information needed to move the clock towards the correct sampling instant. Hence, conditions have to be found to assure the cancellation of the undesired terms. A sufficient condition is

$$r_{sw}^{(1)}(t) = -r_{ws}^{(1)}(t). \tag{5.51}$$

In the transform domain equation (5.51) becomes:

$$j2\pi f S(f)W(-f) = -j2\pi W(f)S(-f) \tag{5.52}$$

Writing the Fourier transforms as

$$S(f) = |S(f)|e^{j\varphi_s(f)}$$

and

$$W(f) = |W(f)|e^{j\varphi_w(f)},$$

and remembering that for a real signal the phase is an odd function, it is possible to show that equation (5.51) is satisfied if the following condition on $\varphi_s(f)$ and $\varphi_w(f)$ holds:

$$\varphi_s(f) - \varphi_w(f) = k\pi + \frac{\pi}{2} \quad k = 0,1,2,\dots \tag{5.53}$$

If $s(t)$ is an even function and $w(t)$ is an odd function with respect to the same symmetry point, condition (5.53) is automatically satisfied. In our example we have selected $s(t)$ and $w(t)$ equal to the Battle-Lemarié scaling function and wavelet, respectively, which satisfy condition (5.53). When $M > 2$ shaping pulses $\{\Phi_i(t)\}_{i=1}^{M}$ are used, condition (5.51) can be properly generalized, requiring all the shaping pulses to be either even or odd around the same symmetry point.
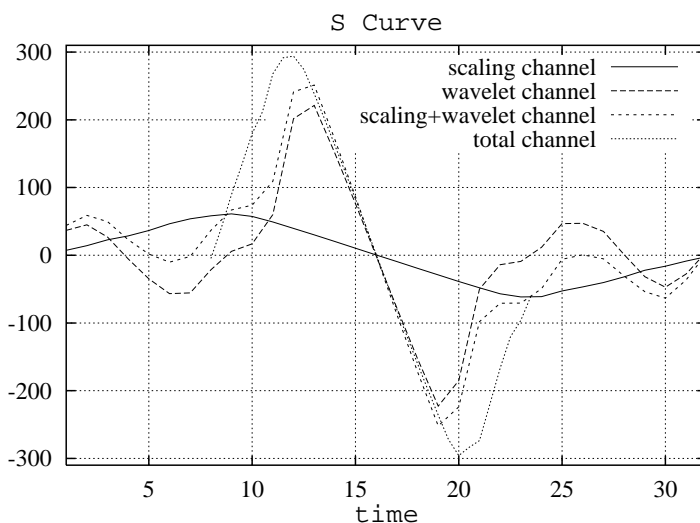
Figure 5.4. S-curves for the two-channel synchronizer of Fig 5.1 using Battle-Lemarié waveforms.

5.4.2 Acquisition phase analysis

The essence of equation (5.28) is that, in case of high SNR and on AWGN channel, if we are able to recover the timing information from each subchannel, we can achieve the same performance obtainable using the original shaping pulse $q(t)$ spanning the overall bandwidth [13]. In Figure 5.4 the S-curves of the synchronizer of Figure 5.1 for a Battle-Lemarié based transmission system are reported. The curves are obtained considering the signal only on the low-pass (upper) branch, and on the high-pass (lower) branch respectively, assuming that both $s(t)$ and $w(t)$ are transmitted. The S-curve obtainable in case of transmission of the single pulse $q(t)$ is also reported. It has to be reminded that the shift-orthogonality period of $q(t)$ is $\Delta/2$. Furthermore we are assuming the same overall transmitted power and that the

103
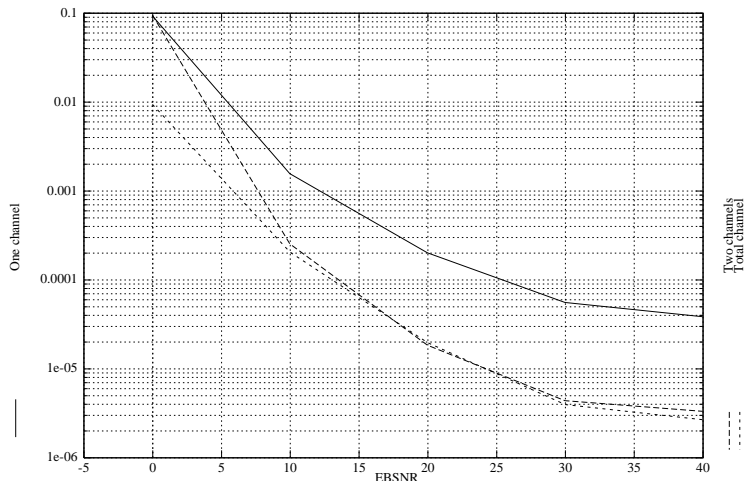
Figure 5.5.   The non-normalized jitter variance of the proposed symbol synchronizer obtained via simulation. The solid line is obtained using ch.-1 timing information only, the upper dashed line is obtained using ch.-1 and ch.-2 simultaneously for timing estimation, and the lower dashed line is obtained using the Battle-Lemarié scaling function at twice the rate (i.e., spanning the original frequency channel prior to splitting). In all the cases, the loop BW is kept constant and equal to $B_L = 0.05$.

closed-loop equivalent bandwidth is the same in both cases.

As it is well known, the synchronization information lies on the high frequencies of the signal spectrum. In fact, it can be easily observed that the slope in the linear zone of the S-curve of the high-pass channel branch is much higher than the one for the low-pass channel, and stronger is also its contribution to the overall S-curve characteristic. Unfortunately this curve presents false lock points (i.e. zero crossings with the right slope that can make the system lock on incorrect sampling instants). This is never true for the low-pass channel branch that provides a S-curve with a unique lock point. The following strategy can be used to avoid locks in stable false points.

1. For a number of symbols intervals larger than the system transient, only the low-pass channel employing the pulse $s(t)$ is transmitted, and only the low-pass channel branch is used to reconstruct the recovered clock signal. During this phase we are using the low-pass channel S-curve, which has no false lock points

2. The high-pass channel employing the pulse $w(t)$ is then added at the

104

transmitter and at the same time also the corresponding high-pass channel branch of the synchronizer is activated. Since the sampling instant is already close to the correct zero-crossing point of the over-all S-curve, the timing information provided by the second (high-pass) channel will increase the synchronizer sensitivity without generating false locks.

3. If $M > 2$ other channels spanning higher frequency intervals are added one by one following the same strategy.

The increased complexity of the synchronizer training phase is justified by the relevant gain that can be obtained on the sensitivity of the overall S-curve. In fact, the major impact of the added high-pass channel can be easily observed comparing the slopes of the S-curves in the linear zone. From Figure 5.4 we can observe how the use of multichannel timing synchronization schemes allows us to achieve the same slope of the overall S-curve as in the case of a single channel synchronizer based on the original shaping pulse $q(t)$.

As seen before, an example of the symbol synchronizer for a two channel modulation scheme employing the Battle-Lemarié wavelet and scaling functions to span the orthogonal subchannels is depicted in Figure 5.1. The simulation results showing the jitter variances for this scheme are reported in Figure 5.5, demonstrating the significant gains achievable from combining the timing information from both subchannels in order to achieve timing estimation.

Chapter 6

Conclusions

In this thesis we have tied together several results in the areas of modulation theory, perfect reconstruction filter bank theory, and the theory of wavelets, to show that wavelets and discrete orthonormal sequences, provide a general framework for the design of multichannel communication systems. Suitability of such systems for modulation has been shown through the investigation of several examples of practical significance.

The connection provided here between the envelope functions for bandwidth efficient modulation and discrete filter banks and wavelets, opens the door to a whole range of possibilities in the area of modulation theory in a formal context of the filter bank and wavelet theories.

The most important results achieved can be summarized as follows:

High efficiency multichannel system design
The *splitting procedure* exploiting properties of digital filterbanks is a flexible toolbox to design multichannel communication systems (WOFDM). We showed in chapter 3 that it is possible to devise double channel communication schemes with high spectral efficiency close to the theoretical bound. As far as multichannel modulation schemes are concerned, the important theoretical result achieved is that wavelet based systems can be more efficient that classical OFDM if there is no need for a splitting of the available bandwidth in a large number of subchannel. Joint use of WOFDM and trellis coded modulation lends to a powerful technique for shaping the power spectrum in order to match the channel transfer function and limiting distortions of the received signal induced by the channel.

Performance over non-linear channel
While over linear channels, wavelets behave like any other Nyquist pulse, we have shown that over non-linear channels, some gain can be achieved using wavelet shaping pulses for digital modulation, expecially in critical

transmission condtions. A novel wavelet, properly designed to be suitable for modulation, namely, the Modified Gaussian, has competitive performance with respect to the square-root raised cosine pulse over non-linear satellite channels. Over multipath fading channel in addition to the gain embedded in the use of multichannel schemes, the digital nature of the modulator allows for an efficient implementation of a spread spectrum system.

Pattern dependent timing jitter

In multichannel schemes designed via the splitting procedure, we have theoretically demonstrated that the jitter variance of the ML symbol synchronizer for a multichannel (multicarrier) modulation scheme to a first order approximation is independent of how the available spectrum is channelized into orthogonal subchannels. The extension of the results to arbitrary channelization of the available spectrum based on a binary decomposition follows by induction on the decomposition tree associated with such constructions. We have validated this results through simulations. In addition, we have provided a complete performance analysis over fading channels and we have proposed a scheme for the implementation of a multichannel maximum likelihood synchronizer that exploits information of all the subchannels for reconstruction the timing signal.

Great interest has arisen towards wavelet for modulation, and nowadays pulse shaping and multichannel modulation are frequently among the interesting applications of wavelets. The work presented, gives an original contribution in the field of digital modulation, collecting many results from the mathematical theory of wavelets and digital signal processing. While eversince theri inception, the theory of wavelets has been considered a powerful tool for signal analysis, our vision has been one of viewing this theory as a powerful tool for signal sinthesis. As demonstrated in this thesis, the reversal of the role of this theory in signal processing which is the crux of contribution of this thesis, can have many benefits in design of digital communication systems.

Appendix A

Derivation of the variance of the timing jitter

In this appendix we shall provide the derivation of the variance of the timing jitter for the two channel modulation case. The ideal data feedback, approximate decision directed ML symbol synchronizer generates the timing estimate

$$\tau^* = \arg\max_{\tau'} \sum_{k=0}^{K-1} (y_k^\phi a_k + y_k^\psi b_k) = \arg\max_{\tau'} \Lambda(\tau), \tag{A.1}$$

where, K is the observation interval in number of symbols. The timing jitter variance is given by

$$\sigma_\tau^2 = A^{-2} E[(\frac{\partial \Lambda}{\partial \tau}|_{\tau=\tau'})^2], \tag{A.2}$$

where, $A = E[\partial^2 \Lambda / \partial \tau^2|_{\tau=\tau'}]$. Making the substitution

$$y_k^\phi = C_k + n_k^\phi$$

and

$$y_k^\psi = D_k + n_k^\psi$$

where

$$C_k = \sum_n [a_n r_{\phi\phi}((n-k)\Delta + (\tau - \tau')) + b_n r_{\psi\phi}((n-k)\Delta + (\tau - \tau'))]$$

and

$$D_k = \sum_n [a_n r_{\phi\psi}((n-k)\Delta + (\tau - \tau')) + b_n r_{\psi\psi}((n-k)\Delta + (\tau - \tau'))]$$

and collecting terms we get

$$\Lambda = \sum_{k=0}^{K-1} (a_k C_k + b_k D_k) + \sum_{k=0}^{K-1} (n_k^\phi a_k + n_k^\psi b_k) = \Lambda_1 + \Lambda_2. \tag{A.3}$$

In the rest of the derivations we my at times omit writing repeatedly that the noted partial derivatives should be evaluated at $\tau = \tau'$. Clearly,

$$E[(\partial\Lambda/\partial\tau)^2] = E[(\partial\Lambda_1/\partial\tau)^2] + E[(\partial\Lambda_2/\partial\tau)^2] + 2E[(\partial\Lambda_1/\partial\tau)(\partial\Lambda_2/\partial\tau)]$$

where the expectation is over both the data symbols and noise. Since the noise process is zero mean it can be easily verified that

$$E[(\partial\Lambda_1/\partial\tau)(\partial\Lambda_2/\partial\tau)] = 0.$$

The term $(\partial\Lambda_1/\partial\tau)^2$ is completely independent of the noise and leads to $\sigma_\tau^2(PDJ)$, while $E[(\partial\Lambda_2/\partial\tau)^2]$ leads to $\sigma_\tau^2(noise)$. Hence, we have $\sigma_\tau^2(noise) = A^{-2}E[(\partial\Lambda_2/\partial\tau|_{\tau=\tau'})^2]$ and $\sigma_\tau^2(PDJ) = A^{-2}E[(\partial\Lambda_1/\partial\tau|_{\tau=\tau'})^2]$.

Evaluation of $E[(\partial\Lambda_2/\partial\tau)^2]$:
Below when possible, we shall change the order of expectation and evaluattion of the argument at a fixed point $\tau = \tau'$ in order to simplify the analysis. Note that the expectations below are with respect to both noise and the data sequences.

$$E\left[\left(\frac{\partial\Lambda_2}{\partial\tau}\right)^2\right] = \sum_{k=0}^{K-1}\sum_{l=0}^{K-1} E\{(a_k a_l \frac{\partial n_k^\phi}{\partial\tau}\frac{\partial n_l^\phi}{\partial\tau} + a_k b_l \frac{\partial n_k^\phi}{\partial\tau}\frac{\partial n_l^\psi}{\partial\tau} + b_k a_l \frac{\partial n_k^\psi}{\partial\tau}\frac{\partial n_l^\phi}{\partial\tau} + b_k b_l \frac{\partial n_k^\psi}{\partial\tau}\frac{\partial n_l^\psi}{\partial\tau})\}.$$

(A.4)

Since the data sequences are iid equiprobable, binary and independent of noise, the above expression simplifies to

$$E[(\partial\Lambda_2/\partial\tau)^2] = \sum_{k=0}^{K-1}\left(E[a_k^2]E\left[\left(\frac{\partial n_k^\phi}{\partial\tau}\right)^2\right] + E[b_k^2]E\left[\left(\frac{\partial n_k^\psi}{\partial\tau}\right)^2\right]\right). \quad (A.5)$$

Let $E[a_k^2] = E_a$ and $E[b_k^2] = E_b$ and note that

$$\begin{aligned}
E\left[\left(\frac{\partial n_k^\phi}{\partial\tau}\right)^2\right] &= \int\int_{-\infty}^{\infty} E[n(t)n(u)]\phi^{(1)}(t-k\Delta+(\tau-\tau'))\phi^{(1)}(u-k\Delta+(\tau-\tau'))dtdu \\
&= \frac{N_o}{2}\int_{-\infty}^{\infty}(\phi^{(1)}(t))^2 dt \\
&= -\frac{N_o}{2}r_{\phi\phi}^{(2)}(0).
\end{aligned} \quad (A.6)$$

Similarly it can be shown that

$$E[(\frac{\partial n_k^\psi}{\partial\tau})^2] = -\frac{N_o}{2}r_{\psi\psi}^{(2)}(0). \quad (A.7)$$

109

Hence, we have

$$E[(\partial\Lambda_2/\partial\tau)^2] = -\frac{N_o}{2}K\left(E_a r_{\phi\phi}^{(2)}(0) + E_b r_{\psi\psi}^{(2)}(0)\right). \qquad (A.8)$$

Evaluation of $E[\partial^2\Lambda/\partial\tau^2]$:
Now consider, $E[\partial^2\Lambda/\partial\tau^2] = E[\partial^2\Lambda_1/\partial\tau^2] + E[\partial^2\Lambda_2/\partial\tau^2]$ and note that

$$E[\partial^2\Lambda_2/\partial\tau^2] = \sum_{k=0}^{K-1}\left(E[a_k]E[\partial^2 n_k^\phi/\partial\tau^2] + E[b_k]E[\partial^2 n_k^\psi/\partial\tau^2]\right) = 0, \quad (A.9)$$

since both the data sequence and noise are zero mean. Consider the evaluation of

$$E[\partial^2\Lambda_1/\partial\tau^2] = \sum_{k=0}^{K-1}\left(E[a_k\partial^2 C_k/\partial\tau^2] + E[b_k\partial^2 D_k/\partial\tau^2]\right). \qquad (A.10)$$

We can write

$$
\begin{aligned}
E[a_k\partial^2 C_k/\partial\tau^2|_{\tau=\tau'}] &= \sum_{k=0}^{K-1}\sum_{l} E[a_k a_l]r_{\phi\phi}^{(2)}((l-k)\Delta) + E[a_k b_l]r_{\psi\phi}^{(2)}((l-k)\Delta) \\
&= \sum_{k=0}^{K-1} E_a \delta_{k,l} r_{\phi\phi}^{(2)}((l-k)\Delta) \\
&= E_a K r_{\phi\phi}^{(2)}(0), \qquad (A.11)
\end{aligned}
$$

where, $\delta_{k,l}$ is the Kronecker delta function. Similarly, $E[b_k\partial^2 D_k/\partial\tau^2|_{\tau=\tau'}] = E_b K r_{\psi\psi}^{(2)}(0)$. Hence, we have

$$E[\partial^2\Lambda/\partial\tau^2] = K(E_a r_{\phi\phi}^{(2)}(0) + E_b r_{\psi\psi}^{(2)}(0)) = A. \qquad (A.12)$$

Evaluation of $E[(\partial\Lambda_1/\partial\tau)^2]$:

$$
\begin{aligned}
E\left[\left(\frac{\partial\Lambda_1}{\partial\tau}\right)^2\right] &= E\{\sum_{k=0}^{K-1}\sum_{l=0}^{K-1}[a_k a_l \frac{\partial C_k}{\partial\tau}\frac{\partial C_l}{\partial\tau} + a_k b_l \frac{\partial C_k}{\partial\tau}\frac{\partial D_k}{\partial\tau} + b_k a_l \frac{\partial D_k}{\partial\tau}\frac{\partial C_l}{\partial\tau} + b_k b_l \frac{\partial D_k}{\partial\tau}\frac{\partial D_l}{\partial\tau}]\} \\
&= P_1 + P_2 + P_3 + P_4, \qquad (A.13)
\end{aligned}
$$

where, P_1,P_2,P_3, and P_4 are different parts of the above expectation. Consider evaluation of P_1

$$P_1 = E\sum_{k=0}^{K-1}\sum_{l=0}^{K-1} a_k a_l \frac{\partial C_k}{\partial\tau}\frac{\partial C_l}{\partial\tau}|_{\tau=\tau'}$$

110

$$= E \sum_{k=0}^{K-1} \sum_{l=0}^{K-1} a_k a_l \sum_m \sum_n [a_m r_{\phi\phi}^{(1)}((m-k)\Delta) + b_m r_{\psi\phi}^{(1)}((m-k)\Delta)] \times [a_n r_{\phi\phi}^{(1)}((n-l)\Delta) + b_n r_{\psi\phi}^{(1)}((n-l)\Delta)].$$

(A.14)

Using the equalities

$$[a_k a_l a_m b_n] = 0,$$

$$E[a_k a_l b_m a_n] = 0,$$

$$E[a_k a_l b_m b_n] = E[a_k a_l]E[b_m b_n] = E_a \delta_{k,l} E_b \delta_{m,n}$$

we get

$$P_1 = \sum_{k=0}^{K-1} \sum_m \sum_{l=0}^{K-1} \sum_n E[a_k a_l a_m a_n] r_{\phi\phi}^{(1)}((m-k)\Delta) r_{\phi\phi}^{(1)}((n-l)\Delta) + K E_a E_b \sum_m r_{\psi\phi}^{(1)}(m\Delta).$$

(A.15)

Now, consider the equality

$$P_{1a} = \sum_{k=0}^{K-1} \sum_m \sum_{l=0}^{K-1} \sum_n \quad E[a_k a_l a_m a_n] r_{\phi\phi}^{(1)}((m-k)\Delta) r_{\phi\phi}^{(1)}((n-l)\Delta) =$$

$$\sum_{k=0}^{K-1} \sum_m \sum_{l=0}^{K-1} E a_k a_m a_l [a_l r_{\phi\phi}^{(1)}((m-k)\Delta) r_{\phi\phi}^{(1)}(0) +$$

$$\sum_{n \neq l} a_n r_{\phi\phi}^{(1)}((m-k)\Delta) r_{\phi\phi}^{(1)}((n-l)\Delta)]. \qquad \text{(A.16)}$$

For BPSK signalling $a_l^2 = E_a$ and note that $r_{\phi\phi}^{(1)}(0) = 0$ since the assumed center of symmetry of the autocorrelation is at origin. Hence, we can write

$$P_{1a} = \sum_{k=0}^{K-1} \sum_m \sum_{l=0}^{K-1} \sum_{n \neq l} E[a_k a_m a_l a_n] r_{\phi\phi}^{(1)}((m-k)\Delta) r_{\phi\phi}^{(1)}((n-l)\Delta).$$

(A.17)

Iterating on the above simplification we have

$$P_{1a} = \sum_{k=0}^{K-1} \sum_m \sum_{l=0}^{K-1} E[a_k a_m a_l a_m] r_{\phi\phi}^{(1)}((m-k)\Delta) r_{\phi\phi}^{(1)}((m-l)\Delta) + P_{1b}$$

$$P_{1b} = \sum_{k=0}^{K-1} \sum_m \sum_{l=0}^{K-1} \sum_{n \neq l, n \neq m} E[a_k a_m a_l a_n] r_{\phi\phi}^{(1)}((m-k)\Delta) r_{\phi\phi}^{(1)}((n-l)\Delta)$$

(A.18)

$$P_{1a} = E_a^2 K \sum_m (r_{\phi\phi}^{(1)}(m\Delta))^2 + P_{1b}. \qquad \text{(A.19)}$$

Iterating once more we have

$$
\begin{aligned}
P_{1b} &= \sum_{k=0}^{K-1} \sum_{m} \sum_{l=0}^{K-1} E[a_k a_m a_l a_k] r_{\phi\phi}^{(1)}((m-k)\Delta) r_{\phi\phi}^{(1)}((k-l)\Delta) + P_{1c} \\
P_{1c} &= \sum_{k=0}^{K-1} \sum_{m} \sum_{l=0}^{K-1} \sum_{n\neq l, n\neq m, n\neq k} E[a_k a_m a_l a_n] r_{\phi\phi}^{(1)}((m-k)\Delta) r_{\phi\phi}^{(1)}((n-l)\Delta)
\end{aligned}
$$

$$
\text{(A.20)}
$$

$$
P_{1b} = E_a^2 \sum_{k=0}^{K-1} \sum_{l=0}^{K-1} r_{\phi\phi}^{(1)}((l-k)\Delta) r_{\phi\phi}^{(1)}((k-l)\Delta) + P_{1c}. \tag{A.21}
$$

Since $n \neq k, n \neq l, n \neq m$, $E[a_k a_l a_m a_n] = E[a_n] E[a_k a_l a_m] = 0$ and $P_{1c} = 0$. Putting the pieces together and noting that $r_{\phi\phi}^{(1)}(-\alpha) = -r_{\phi\phi}^{(1)}(\alpha)$ we have

$$
P_1 = K \sum_{m} [(E_a r_{\phi\phi}^{(1)}(m\Delta))^2 + E_a E_b (r_{\psi\phi}^{(1)}(m\Delta))^2] - E_a^2 \sum_{k=0}^{K-1} \sum_{l=0}^{K-1} (r_{\phi\phi}^{(1)}((k-l)\Delta))^2. \tag{A.22}
$$

In a totally analogous fashion we obtain

$$
\begin{aligned}
P_4 &= E \sum_{k=0}^{K-1} \sum_{l=0}^{K-1} b_k b_l \frac{\partial D_k}{\partial \tau} \frac{\partial D_l}{\partial \tau} \Big|_{\tau=\tau'} \\
&= K \sum_{m} [(E_b r_{\psi\psi}^{(1)}(m\Delta))^2 + E_a E_b (r_{\phi\psi}^{(1)}(m\Delta))^2] - \\
&\quad E_b^2 \sum_{k=0}^{K-1} \sum_{l=0}^{K-1} (r_{\psi\psi}^{(1)}((k-l)\Delta))^2. \tag{A.23}
\end{aligned}
$$

To find P_2 and P_3 we use the equalities

$$
E[a_k b_l a_m a_n] = E[a_k b_l b_m b_n] = 0,
$$

$$
E[a_k b_l a_m b_n] = E_a \delta_{k,m} E_b \delta_{l,n},
$$

$$
E[a_k b_l a_n b_m] = E_a \delta_{k,n} E_b \delta_{l,m},
$$

$$
r_{\phi\psi}(\alpha) = r_{\psi\phi}(-\alpha),
$$

$$
r_{\phi\psi}^{(1)}(-\alpha) = -r_{\psi\phi}^{(1)}(\alpha)
$$

to obtain

$$
P_2 = -E_a E_b \sum_{k=0}^{K-1} \sum_{l=0}^{K-1} (r_{\phi\psi}^{(1)}((k-l)\Delta))^2 \tag{A.24}
$$

$$
P_3 = -E_a E_b \sum_{k=0}^{K-1} \sum_{l=0}^{K-1} (r_{\phi\psi}^{(1)}((l-k)\Delta))^2. \tag{A.25}
$$

Collecting terms and simplyfying we obtain

$$E\left[\left(\frac{\partial \Lambda_1}{\partial \tau}\right)^2\right] = K \sum_m [2 E_a E_b (r_{\phi\psi}^{(1)}(m\Delta))^2 + (E_a r_{\phi\phi}^{(1)}(m\Delta))^2 + (E_b r_{\psi\psi}^{(1)}(m\Delta))^2] +$$

(A.26)

$$- \sum_{k=0}^{K-1} \sum_{l=0}^{K-1} [2 E_a E_b (r_{\phi\psi}^{(1)}((k-l)\Delta))^2 + (E_a r_{\phi\phi}^{(1)}((k-l)\Delta))^2 + (E_b r_{\psi\psi}^{(1)}((k-l)\Delta))^2].$$

Bibliography

[1] F. Daneshgaran and M. Mondin, "Bandwidth Efficient Modulation With Wavelets," *Electronics Letters*, Vol.30, No.15, pp.1200-1202, July 1994.

[2] F. Daneshgaran and M. Mondin, "Coherent Frequency-Hopped CDMA and Orthogonal Frequency Division Multiplexing With Wavelets," *Electronics Letters*, Vol.31, Issue 6, March 1995.

[3] F. Daneshgaran and M. Mondin, "Shaping the Power Spectrum of Geometrically Uniform TCM Codes Using Wavelet Packet Modulation," *Proc. of CISS'96*, Princeton (NJ), USA, March 1996.

[4] F. Daneshgaran and M. Mondin, "Clock Synchronization Using Wavelets,"*Proc. of Globecom'95*, pp.1287-1291, Singapore, Nov. 1995.

[5] F. Daneshgaran, M. Mondin, "Jitter-Free Wavelet-Based Clock Synchronization ", *IEEE Trans. on Communications*, December 1997.

[6] F. Daneshgaran and M. Mondin, "Shaping the Power Spectrum of Geometrically Uniform TCM Codes Using Wavelet Packet Modulation," *Proc. of MILCOM'96*, McLean VA, October 1996.

[7] F. Daneshgaran and M. Mondin, "Clock Synchronization Without Self Noise Using Wavelets," *Electronics Letters*, Vol.31, No.10, pp.775-776, May 1995.

[8] F. Daneshgaran and M. Mondin, "Multidimensional Signaling With Wavelets," *Proc. Conf. on Info. Sci. and Sys. CISS'95*, pp.756-761, March 22-24, 1995.

[9] F. Dovis, M. Mondin and F. Daneshgaran, "The Modified Gaussian waveform: a Novel Wavelet with Low Sidelobes with Applications to Digital Communications", *IEEE Communications Letters*, Aug. 1998

[10] F. Daneshgaran, M.Mondin, F. Dovis, "Shaping The Power Spectrum of TCM Codes Using Wavelet Packet Modulation," *IEE Electronics Letters*, Vol.35, No.17, Aug. 1999

[11] F. Dovis, M.Mondin, F. Daneshgaran, "Permutation Spreading in Wavelet OFDM Systems," Proc. EUSIPCO '98, European Signal Processing Conference, Sept. 1998, Rhodes Island, Greece.

[12] F. Daneshgaran, M. Mondin, F. Dovis "Shaping the Power Spectrum of TCM codes Using Wavelet Packets Modulation," *Electronics Letters*, Vol.35, No.17, Aug. 1999.

[13] F. Daneshgaran, M.Mondin, F. Dovis, "Symbol Synchronization for Multicarrier Modulation," Proc. Conf. on Inform. Sciences and Syst. CISS '98, Mar. '98, Princeton Univ., Princeton NJ, USA

[14] F. Daneshgaran, M.Mondin, F. Dovis, "Performance of Wavelet-Based Shaping Pulses on Linear and Non-Linear Channels," Proc. Conf. on Inform. Sciences and Syst. CISS '99, The Johns Hopkins Univ., 17-19 Mar. 1999, Baltimore MA, USA.

[15] F. Daneshgaran, M.Mondin, F. Dovis, "ML Symbol Synchronization for Multichannel Modulation: Analysis and Implementation," Proc. Conf. on Inform. Sciences and Syst. CISS '99, The Johns Hopkins Univ., 17-19 Mar. 1999, Baltimore MA, USA.

[16] F. Daneshgaran, M.Mondin, F. Dovis, "Symbol Synchronization for Multichannel Frequency Diversity Transmission Over Fading Channels", Proc. of Vehicular Technology Conference (VTC'99), May '99, Houston TX, USA.

[17] F. Daneshgaran, M. Mondin, F. Dovis, "Performance of Wavelet Based Shaping Pulses," SPIE International Symposium '99, 18-23 July 1999, Denver CO, USA.

[18] F. Daneshgaran, M. Mondin, F. Dovis, "Permutation Spreading in Wavelet OFDM Systems," SPIE International Symposium '99, 18-23 July 1999, Denver CO, USA.

[19] F. Dovis, M. Mondin, F. Daneshgaran, "Wavelet Based Multichannel Modulation," European Conference on Circuit Theory and Design (EC-CTD), 29 August - 2 Sept. Stresa, Italy

115

[20] F. Daneshgaran, M.Mondin, F. Dovis, "Wavelet Waveforms for Modulation Over Linear and Non-Linear Channels," IEEE Wireless Communication and Networking Conference, Sept. 1999, New Orleans LO, USA.

[21] S. Benedetto, E. Biglieri, and V. Castellani, *Digital Transmission Theory*, Prentice-Hall, 1987.

[22] J. G. Proakis, *Digital Communications,*, Mc Graw-Hill, New York, 1995.

[23] Battle G., "A block spin construction of ondelettes, Part I: Lemarié functions", *Comm. Math. Phys.*, v. 110, 1987

[24] Ajmone Marsan M. et al., "Digital simulation of communication systems with TOPSIM III", *IEEE Jou. on Sel. Areas in Comm.*, v. SAC-2, n. 1, 1984

[25] I. Daubechies, *Ten Lectures on Wavelets*, Society for Industrial and Applied Mathematics, CBMS-NSF 61 Regional conference series in applied mathematics, 1992.

[26] Chui C. K., *An introduction to wavelets*, Prentice Hall, Inc., 1987

[27] C. K. Chui, *Wavelets: A Tutorial in Theory and Applications*, Vol. 2, Academic Press, 1992.

[28] P.P.Vaidyanathan, *Multirate Systems and Filter Banks*, Prentice-Hall, 1993.

[29] M. Vetterli and J. Kovacevic, *Wavelets and Subband Coding*, Prentice Hall, 1995.

[30] Coifman R.R., Meyer Y., "Orthonormal wave packet bases" preprint Numerical algorithms research group, Yale University, 1989

[31] Cohen A., Daubechies I., Feauveau J.C., "Biorthogonal bases of compactly supported wavelets", *Comm. Pure Appl. Math.*, v. 45, 1992

[32] Meyer Y. *Wavelets Algorithms and Applications* Society for Industrial and Applied Mathematics, Philadelphia, 1993

[33] Daubechies I.,"Orthonormal bases of compactly supported wavelets", *Comm. Pure Appl. Math.*, v. 41, 1988

[34] Franks L. E., "Carrier and bit syncronisation in data communication", *IEEE Trans. on Commun.*, v. COM-28, pp. 1107-1129, 1980

[35] Grossman A. e Morlet J., "Decomposition of Hardy functions into square integrable wavelets of constant shape." *SIAM J. Math.* ,v. 15

[36] Lemarié P.-G., "Ondelettes à localisation exponentielle", *J. Math. pures Appl.*, v. 67, 1988

[37] Mallat S., "A theory for multiresolution signal decomposition: the wavelet rapresentation", *IEEE Trans. Patt. Anal. Mach. Intell.*, v. 11, 1989

[38] Mallat S. Zhong S., "Characterization of signal from multiscale edges" *IEEE Trans. Patt. Anal. Mach. Intel.*, v. 14, n. 7, 1992

[39] Meyer Y., "Ondelettes et function splines", Séminaire EDP, Ecole Politechnique, Paris France, 1986

[40] Meyers M. H., Franks L. E., "Joint carrier phase and symbol timing recovery for PAM system", *IEEE Trans. on Commun.*, v. COM-28, 1980

[41] Meyers M. H., Franks L. E., "Joint carrier phase and symbol timing recovery for PAM systems", *IEEE Trans. on Commun.*, v. COM-28, pp. 1121-1129, 1980

[42] Moeneclaey M., "A comparison of two types of symbol synchronizers for wich self-noise is absent", *IEEE Trans on Commun.*, v. COM-31, pp. 329-333, 1983

[43] Rioul O. e Vetterli M., "Wavelets and signal processing",*IEEE Signal proc. mag.*, 1991

[44] Vaidyanathan P.P., "Improved technique for design of perfect reconstruction FIR QMF banks with lossless polyphase matrices", *IEEE Trans. on Acou. Speech and Signal proc.*, v. ASSP-37, pp. 1049-1056, 1989

[45] M. Vetterli, "Perfect Transmultiplexers," *Proc. IEEE Int. Conf. Acoust. Speech and Signal Proc.*, pp.2567-2570, Tokyo, Japan, April 1986.

[46] G. W. Wornell and A. V. Oppenheim, "Wavelet-Based Representations for a Class of Self Similar Signals with Application to Fractal Modulation," *IEEE Trans. on Inform. Theory*, Vol.38, pp.785-800, March 1992.

[47] M. A. Tzannes and M. C. Tzannes, "Bit-by-Bit Channel Coding of Digital Communication Signals," *Proc. of Globecom'92*, Vol.2, Orlando (FL), USA, Dec. 1992.

[48] P.P.Gandhi, S.S.Rao, and R.S.Pappu, "On Waveform Coding using Wavelets," *Proc. of 27th Asilomar Conf. on Sig., Sys.,and Comput.,* Vol.2, pp.901-905, Pacific Grove (CA), USA, Nov. 1993.

[49] D.Cochran and C.Wei, "Bandlimited Orthogonal Wavelet Symbols," *Proc. of the 27th Asilomar Conf. on Sig., Sys.,and Comput.,* Vol.2, pp.528-532, Pacific Grove (CA), USA, Nov. 1993.

[50] W.W.Jones, "Multi-Scale Wavelet Modulation," *Proc. of the 26th Southeastern Symp. on System Theory,* pp.590-594, Athens (OH), USA, March 1994.

[51] A. R. Lindsey, "Supersymbol Tuning Algorithms for Wavelet Packet Modulation," *Proc. of the 29-th Annual Conf. on Info. Sciences and Systems, CISS'95,* pp.737-743, Johns Hopkins Univ., Baltimore MD, March 1995.

[52] A.R Lindsey, "Wavelet Packet Modulation for Orthogonally Multiplexed Communication," *IEEE Trans. on Sign. Proc.,* Vo.45 No.5, May 1997, pp.1336-1339.

[53] A.R. Lindsey, "Multi-dimensional Signaling via Wavelet Packets," *SPIE Conference: Wavelet Applications for Dual Use,* Orlando, Florida, Apr. 17-21, 1995.

[54] A.R. Lindsey, M.J. Medley, "Wavelet Transform and Filter Banks in Digital Communication," *SPIE Conference: Wavelet Applications for Dual Use,* Orlando, Florida, Apr. 8-12, 1996.

[55] J.N.Livingston and C.C.Tung, "Wavelet Basis for Multichannel Modulation," *Proc. 29th Conf. on Info. Sci. and Syst., CISS'95,* Baltimore (MA), USA, March 1995.

[56] C.C. Tung and J.N. Linvingston,"Biorthogonal Raised-Cosine Wavelets," *IEE Electronics Letters,* Vol.31, No.6, Mar. 1995

[57] K. M. Wong, J. Wu, T. N. Davidson and Q. Jin, "Wavelet Packet Division Multiplexing and Wavelet Packet Design Under Timing Error Effects," *IEEE Trans. on Signal Processing,* Vol.45, No.12, pp.2877-2890, Dec. 1997.

[58] T.N. Davidson, A.J. Schott, K.M. Wong, "Branch Hopped Wavelet Packet Division Multiplexing," *Proc. IEEE ICASSP'98,* May. 12-15 1998, Seattle, Washington, USA.

118

[59] K. H. Chang, X.D. Lin, M. G. Kyeong, "Performance Analysis of Wavelet-based MC-CDMA for FPLMTS/IMT-2000," *Proc. of IEEE 4th Int. Symp on Spread Spec. Tech. and Appl.*, Vol.3, 1996, pp.1356-1360.

[60] S. Srinidhi, J.C. Proakis, M. Stojanovic "Wavelet Based Modulation for Frequency Hopped Spread Spectrum Communications," *Proc. of IEEE 49th Veh. Tech. Conf.*, May '99, Houston TX, USA.

[61] F.Y. Kuo, G. Ma, "On Performance of the Wavelet Domain Multirate Transmission for Wireless Multimedia," *Proc. of IEEE 1st Work. on Mult. Sig. Proc.*, 1997.

[62] W. Yang, G. Bi, T.S.P. Yum "A Multirate Wireless Transmission System Using Wavelet Packet Modulation," *Proc. of IEEE 47th Veh. Tech. Conf.*, May 1997.

[63] T. Olson, D. Healy, U. Osterberg "Wavelets in Optical Communications," *Computing in Science and Engineering*, Vo.1, No.1, Jan.-Feb. 1999, pp.51-57.

[64] M. Alard, R. Lassalle, "Principles of Modulation and Channel Coding for Digital Broadcasting for Mobile Receivers", *EBU Technical Review*, n. 224, pp. 168-190, August 1987.

[65] M. Moeneclaey, "Two Maximum Likelihood Symbol Synchronizers with Superior Tracking Performance," *IEEE Trans. on Communications*, Vol.32, No.11, November 1984.

[66] W. C. Lindsey, *Synchronization systems in communication and control*, Englewood Cliffs; Prentice-Hall, 1972.

[67] P.P.Vaidyanathan, T.Q.Nguyen, Z.Doù ganata, and T. Saramäki, "Improved Technique for Design of Perfect Reconstruction FIR QMF Banks with Lossless Polyphase Matrices," *IEEE Trans. on Acou., Speech and Signal Proc.*, Vol.ASSP-37, pp.1042-1056, July 1989.

[68] A.D. Rizos, J.G. Proakis, T.Q. Nguyen, "Comparison of DFT and Cosine Modulated Filter Banks in Multicarrier Modulation", *Proc. Globecom '94*, pp.687-691, San Francisco (CA), November 1994.

[69] D. Slepian and H.O. Pollak, "Prolate Spheroidal Wave Functions, Fourier Analysis and Uncertainty-I," *Bell System Technical Journal*, No.40, pp.43-63, Jan. 1961.

119

[70] H. J. Landau and H.O. Pollak, "Prolate Spheroidal Wave Functions, Fourier Analysis and Uncertainty-II," *Bell System Technical Journal*, No.40, pp.65-84, Jan. 1961.

[71] H. J. Landau and H.O. Pollak, "Prolate Spheroidal Wave Functions, Fourier Analysis and Uncertainty-III: The Dimension of the Space of Essentially Time- and Band-Limited Signals," *Bell System Technical Journal*, No.41, pp.1295-1336, July 1962.

[72] D. Slepian, "On Bandwidth," *Proc. of IEEE*, Vol.64, No.3, pp.292-300, Mar. 1976.

[73] Special issue on Transmultiplexers, *IEEE Trans. on Comm.*, Vol.COMM-30, July 1982.

[74] R. W. Chang, "Synthesis of Band-Limited Orthogonal Signals for Multichannel Data Transmission," *Bell Syst. Tech. J.*, Vol.45, pp.1775-1796, Dec. 1966.

[75] N. J. Fliege, "Orthogonal Multiple Carrier Data Transmission," *Euro. Trans. on Telecomm.*, Vol.3, No.3, pp.225-253, May 1992.

[76] I. Kalet, "The Multitone Channel," *IEEE Trans. on comm.*, Vol.37, No.2, pp.119-124, Feb. 1989.

[77] S. B. Weinstein and P. M. Ebert, "Data Transmission by Frequency Division Multiplexing Using Discrete Fourier Transform," *IEEE Trans. on comm.*, Vol comm-19, pp.628-634, Oct. 1971.

[78] dTTb/WP3.1/179, *"Mathematical models of the terrestrial channel for fixed and portable reception of digital television broadcasting"*, Final report, June 1994.

[79] S. D. Sandberg and M. A. Tzannes, "Overlapped Discrete Multitone Modulation for High Speed Copper Wire Communications," *IEEE j. on Selected Areas in Comm.*, Vol.13, pp.1571-1585, Dec. 1995.

[80] R. E. Learned, H. Krim, B. Claus, A. S. Willsky, and W. C. Karl, "Wavelet-packet-based Multiple Access Communication," *Proc. of SPIE International Sympo. on Optics, Imaging and Instrumentation-mathematical Imaging: Wavelet Applications in Signal and Image Processing*, Vol.2303, pp.246-259, San Diego CA, July 1994.

[81] G. W. Wornell, "Spread-signature CDMA: Efficient Multiuser Communication in the Presence of Fading," *IEEE Trans. on info. Theory*, Vol.IT-41, pp.1418-1438, Sept. 1995.

[82] D. Cochran and C. Wei, "Scale Based Coding of Digital Communication Signals," *Proc. IEEE-SP International Sympo. on Time-Frequency and Time-Scale Analysis*, pp.455-458, Victoria B.C. Canada, Oct. 1992.

[83] D. Cochran and C. Wei, "A Wavelet Based Multiple Access Spread Spectrum Modulation Scheme," *Proc. 13th IEEE Ann. Int. Phoenix Conf. on Comp. and Comm.*, Apr. 12-15 1994, Phoenix, AZ, USA.

[84] T.K. Adhikary, V.U. Reddy, "Complex Wavelet Packets for Multicarrirer Modulation," *Proc. IEEE ICASSP'98*, May 12-15 1998, Seattle, Washington, USA.

[85] K. Hetling, M. Medley, G. Saulnier and P. Das, "A PR-QMF (Wavelet) Based Spread Spectrum Communication System," *Proc. of the Military Comm. Conf., MILCOM'94*, pp.760-764, Long Branch NJ, Oct. 1994.

[86] M. V. Tazebay, A. N. Akansu and M. J. Sherman, "A Novel Adaptive Time Frequency Excision Technique for Direct Sequence Spread Spectrum Communications," *Proc. IEEE-SP International Sympo. on Time-Frequency and Time-Scale Analysis*, Philadelphia, Pennsylvania, pp.492-495, Oct 1994.

[87] S. Heidari and C. L. Nikias, "A New Method for the Design of High Performance Receivers in the Presence of co-channel Interference," *Proc. IEEE-SP International Sympo. on Time-Frequency and Time-Scale Analysis*, Philadelphia, Pennsylvania, pp.496-499, Oct 1994.

[88] R. S. Orr, C. Pike, M Tzannes, S. Sandberg, and M. Bates, "Covert Communications Employing Wavelet Technology," *Proc. of the 27-th ASILOMAR Conf. on Signals, Systems, and Computers*, Vol.1, pp.523-527, Pacific Grove CA, Nov. 1993.

[89] M. Visintin, E. Biglieri, and V. Castellani, "Four Dimensional Signaling for Bandlimited Channels," *IEEE Trans. on Comm.* Vo.42, No.2, pp.403-409, Feb. 1994.

[90] D. Saha and T. G. Birdsall, "Quadrature-quadrature Phase-Shift Keying," *IEEE Trans. on Comm.* Vol.37, No.5, pp.437-448, May 1989.

121

[91] M. Sablatash, J. H. Lodge, and C. J. Zarowski, "Theory and Design of Communication Systems Based on Scaling Functions, Wavelets, Wavelet Packets and Filter Banks," *Proc. 8-th International Conf. on Wireless Commun., Wireless'96,* Vol.2, pp.640-659, Calgary, Alberta, Canada, July 1996.

[92] M. Sablatash and J. H. Lodge, "The Design of Filter Banks With Specified Minimum Stopband Attenuation for Wavelet Packet-Based Multiple Access Communications," *Proc. 18-th Bien. Sympos. on Comm.,* pp.53-56, Kingston, Ontario, Canada, June 1996.

[93] E. Biglieri, "Ungerboeck Codes Do Not Shape the Signal Power Spectrum," *IEEE Trans. on Inf. Th.,* Vol.IT-32, No.4, July 1986.

[94] M. Tomlinson, "New Automatic Equalizer Employing Modulo Arithmetic," *Electronics Letters,* Vol.7, pp.138-139, Mar. 1971.

[95] M. V. Eyuboğlu and G.D. Forney, "Trellis Precoding: Combined Coding, Precoding and Shaping for Intersymbol Interference Channels,"*IEEE Trans. on Inf. Th.,* Vol.IT-38, No.2, pp.301-313, Mar. 1992.

[96] B. LeFloch, R. Halbert-Lassalle, and D. Castelain, "Digital Sound Broadcasting to Mobile Receivers," *IEEE Trans. Consum. Elec.,* Vol.35, No.3, pp.493-503, Aug. 1989.

[97] P. J. Tourtier, R. Monnier, and P. Lopez, "Multicarrier Modem for Digital HDTV Terrestrial Broadcasting," *Signal Processing: Image Commun.,* Vol.5, pp.379-403, 1993.

[98] P. S. Chow, J. M. Cioffi, and A. C. Bingham, "A Practical Discrete Multitone Transceiver Loading Algorithm for Data Transmission Over Spectrally Shaped Channels,"*IEEE Trans. on Comm.,* Vol.COM-43, No.2-4, pp.773-775, Feb. 1995.

[99] R. D. Wesel and J. M. Cioffi, "Fundamentals of Coding for Broadcast OFDM," *Proc. 29th Asilomar Conf. on Sig. Syst. & Comput.,* 1995.

[100] K. Cheong, J.M. Cioffi, "Discrete Wavelet Transforms in Multi-carrier Modulation," *Proc. IEEE Globecom '98,* Sydney, Australia, Nov. 8-12, 1998.

[101] F. Daneshgaran and K. Yao, "The Iterative Collapse Algorithm: A Novel Approach for the Design of Long Constraint Length Viterbi Decoders Part-I, -II," *IEEE Trans. on Comm.,* Vol.COM-43, No.2-4, pp.1409-1428, Feb. 1995.

[102] S. Benedetto, R. Garello, M. Mondin, and G. Montorsi, "Geometrically Uniform TCM Codes Over Groups Based on L×MPSK Constellations," *IEEE Trans. on Inf. Th.,* Vol.IT-40, pp.137-152, Jan. 1994.

[103] F. Daneshgaran and M. Mondin, "Minimal Delay Realization of Permutations With Application to Turbo Coding," *Proc. ISITA 96,* Victoria, Canada, Sept. 1996.

[104] Marshall Hall, Jr., *The Theory of Groups,* Chelsea publishing company, 2nd edition, 1976.